Cracking of the PCC Layer in Composite Pavement

A DISSERTATION
SUBMITTED TO THE FACULTY OF THE GRADUATE SCHOOL
OF THE UNIVERSITY OF MINNESOTA
BY

PRIYAM SAXENA

IN PARTIAL FULFILLMENT OF THE REQUIREMENTS
FOR THE DEGREE OF
DOCTOR OF PHILOSOPHY

Lev Khazanovich, Advisor

December 2011

ACKNOWLEDGEMENTS

I wish to express my sincere thanks to my advisor Dr. Lev Khazanovich for the guidance, cooperation, and continuous support that he provided during my stay at the University of Minnesota. I greatly appreciate his patience and the encouragement he provided to help me focus on the work. I would also like to thank my thesis committee members Dr. Mihai Marasteanu, Dr. Henryk K. Stolarski, and Dr. Douglas M. Hawkins for their help and valuable feedback on this dissertation.

The financial support provided by the Minnesota Department of Transportation and the Federal Highway Administration (FHWA) Transportation Pooled Fund Study TPF-5(149) "Design and Construction Guidelines for Thermally Insulated Concrete Pavements" is deeply acknowledged. Special thanks to all my fellow students for making memories that I will cherish forever.

Last but not the least, I am most grateful to my husband, Amit for his love and support during this time. I am forever thankful to my loving family.

To my parents

ABSTRACT

An asphalt concrete (AC) overlay of a jointed plain concrete pavement (JPCP) is intended to extend the service life of the existing pavement structure. Also known as composite pavements, such pavements exhibit features of both rigid and flexible pavements. While behavior of rigid pavements is mainly elastic, behavior of asphalt layer is load-duration dependent. At the same time, temperature curling causes non-linear interaction with the foundation. The available models of composite pavement ignore the behavior of the load duration dependent asphalt layer when the composite pavement is subjected to a combination of temperature curling and traffic loads.

This research concentrates on the improvement of structural modeling of composite pavements subjected to slow developing temperature curling and instantaneous traffic loads. A finite element (FE)-based model accounting for the viscoelastic behavior of the asphalt layer in composite pavements is developed and verified using comparisons with semi-analytical solutions obtained in this study. In order to maintain compatibility with the Mechanistic-Empirical Pavement Design Guide (MEPDG) framework, a simplified procedure is developed. The procedure uses a different asphalt modulus for curling than for axle loading and determines the total stresses in the pavement as a combination of the stresses from solutions of three elastic boundary value problems. The simplified procedure is compared with the existing MEPDG model for fatigue cracking in AC overlaid JPCP. A framework for the implementation of the proposed model into the MEPDG is also developed.

TABLE OF CONTENTS

List of Tables

List of Figures

CHAPTER 1. INTRODUCTION

Properly designed pavements are crucial for the sustenance of highway systems in any country. Until recently, pavements were designed and rehabilitated using primarily the American Association of State Highway and Transportation Officials (AASHTO) Guide for Design of Pavement Structures, last modified in 1993. Commonly known as the 1993 AASHTO Guide, it provides design procedures based on equations that are empirical in nature and were developed using the AASHO Road Test data collected in the late 1950's. In addition to being empirical, the 1993 AASHTO Guide extrapolates heavily for conditions (traffic, materials, climate, etc.) other than those at the AASHO Road Test site.

In the later 1990s, the AASHTO Joint Task Force on Pavements along with the National Cooperative Highway Research Program (NCHRP) and the Federal Highway Administration (FHWA) mandated the development of mechanistic-empirical (M-E) based pavement design guidelines. As a result, NCHRP Project 1-37A, *Development of the 2002 Guide for Design of New and Rehabilitated Pavement Structures: Phase II* was initiated in 1996 and the Mechanistic-Empirical Pavement Design Guide (MEPDG) was released in 2004 (*AASHTO 2008*). The MEPDG contains distress prediction models that are derived mechanistically, empirically, or as a combination of these methods.

Pavements are generally classified as flexible or rigid depending on the type of material used for the surface course. Rigid pavements have a portland cement concrete (PCC) surface layer and are advantageous in terms of better structural load bearing

capacity (Figure 1.1.a). Flexible pavements have an asphalt concrete (AC) surface course and provide a smooth riding surface, a reduction in tire-pavement noise, and an easily renewable wearing course (Figure 1.1.b). A third category of pavement consists of composite pavements that are usually designed and constructed as a combination of the above mentioned materials. This includes, but is not limited to, PCC over PCC, AC over AC, and AC over PCC pavements. For the purpose of this research, the term "composite pavement" is used solely for a newly constructed, structural PCC layer overlaid with a high quality AC surface layer as soon as the concrete cures (Figure 1.1.c). This kind of composite pavements are also referred to "as-built AC over PCC pavements."

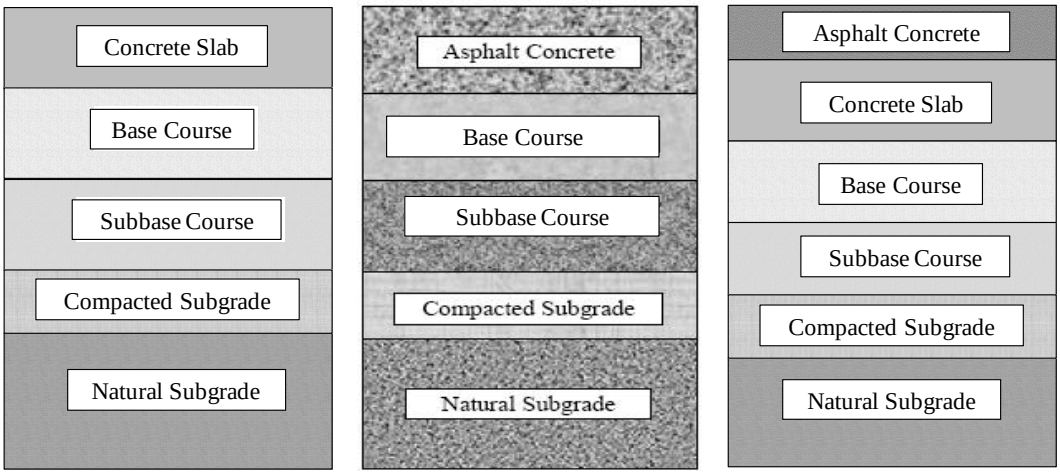

Figure 1.1 Structure of (a) rigid pavement, (b) flexible pavement, and (c) composite pavement (adopted from *AASHTO 2008*).

Composite pavements provide a combination of the advantageous characteristics of both flexible and rigid pavements. They are considered an extremely promising choice for providing strong, durable, safe, smooth, and quiet pavements that need minimal

maintenance (*Darter et al. 2008*). The PCC layer of a composite pavement is generally sound structurally and does not exhibit any distress history. The AC layer is provided primarily for non-structural benefits such as noise reduction or improved ride quality but it can also act as an insulating layer in reducing the extremities of temperature in the PCC layer.

The MEPDG contains distress prediction models corresponding to various distresses in a pavement which can be used to predict the design life. One such distress model for predicting the PCC cracking in a composite pavement was adopted directly from the fatigue cracking model of a new jointed plain concrete pavement (JPCP). JPCP is a class of rigid pavements that do not contain distributed steel to control random cracking and may or may not contain transverse joint load transfer devices (i.e. dowels) (*AASHTO 2008*).

The MEPDG cracking model for composite pavements computes the critical bending stresses in the PCC layer based on the assumption that the AC layer behavior is elastic and its modulus changes on a monthly basis. However, this adaptation is an over-simplification of the actual cracking process as it does not account for the key material property of composite pavements i.e. the viscoelastic behavior of asphalt and its high sensitivity to temperature and loading duration. The major goal of this research is to address this limitation of the MEPDG cracking model in the PCC layer of a composite pavement.

Furthermore, an additional challenge in developing modifications for the MEPDG is the need for computational efficiency. The MEPDG calculates the stress in the PCC

layer for every hour of the pavement design life (ex. each hour over 20 years). In this regard, the MEPDG is comprehensive and, as a result, computationally demanding. A secondary goal for this research is to develop a computationally efficient process to account for the cracking behavior in the PCC layer.

This dissertation is divided into six chapters as follows:

- Chapter 1 introduces the research statement and objectives.
- Chapter 2 reviews existing literature on the MEPDG fatigue cracking model for JPCP, characterization of the asphalt layer using the viscoelastic constitutive relationship, adoption of the JPCP fatigue cracking model for composite pavements, and the limitations identified in this research
- Chapter 3 presents the finite element (FE) model developed to analyze a composite pavement which incorporates both elastic and viscoelastic layers and is subjected to a combination of traffic loads and temperature distributions.
- Chapter 4 introduces a *2-moduli approach* for structural analysis of composite pavements. The composite pavement response is characterized using two separate AC dynamic moduli based on traffic load duration and temperature load duration. The combined stress obtained using the *2-moduli approach* is verified against the stress solution from the viscoelastic FE model.
- Chapter 5 presents a framework for the implementation of the stresses computed using the *2-moduli approach* into the MEPDG.
- Chapter 6 summarizes the research findings and recommendations for future research.

CHAPTER 2. LITERATURE REVIEW

A review of the structural modeling of composite pavements has been conducted. Since the Mechanistic-Empirical Pavement Design Guide (MEPDG) utilizes the state-of-the-art methodology of pavement analysis, a substantial portion of this review is dedicated to MEPDG procedures. This chapter is divided into seven sections. The first section provides a brief overview of the MEPDG fatigue cracking distress prediction model, originally developed for a new jointed plain concrete pavement (JPCP). The second section discusses the JPCP curling analysis. The third section extends the review to the stress computation procedure employed by MEPDG for efficiently predicting the critical PCC surface stresses. The fourth section examines the adoption of the JPCP fatigue cracking model for composite pavements in MEPDG. The fifth section presents the characterization of asphalt commonly adopted in literature and in the MEPDG. The sixth section documents the limitations in the adoption of the JPCP fatigue cracking model for composite pavements, identified under this research. Finally, the seventh section presents a comparison of existing pavement analysis packages with a focus on their ability to perform linear viscoelastic analysis.

2.1 MEPDG Fatigue Cracking Model

MEPDG states that under typical service conditions the potential for either bottom-up or top-down cracking is present in all JPCP slabs, and a slab may crack either from bottom-up or top-down, but not both (*AASHTO 2008*). As the name suggests, bottom-up

cracking initiates at the bottom of the PCC layer as a hairline crack at the center of the slab away from the transverse joint. The crack then propagates upwards through the PCC layer as shown in Figure 2.1. Cracking is caused by tensile stresses at the bottom of the PCC layer that exceed the tensile capacity of the PCC slab due to repeated mid-slab traffic loading at or near the edge of the slab, day-time positive temperature gradient, or their combination.

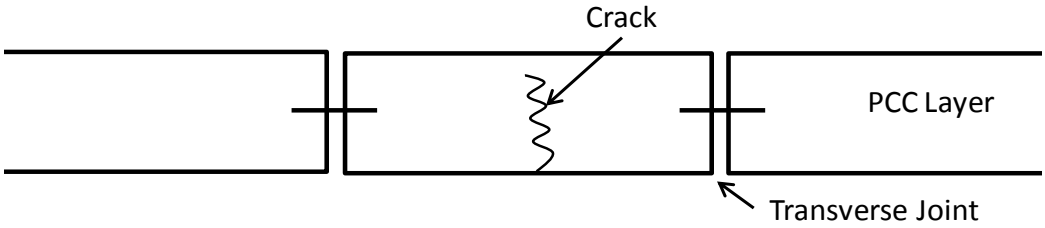

Figure 2.1 Bottom-up fatigue cracking in JPCP.

The critical region for top-down crack initiation is at the top, middle area of the PCC slab. The crack eventually propagates to the bottom of the PCC layer over time as shown in Figure 2.2. Top-down cracking is caused by tensile stresses at the top of the PCC layer that exceed the tensile capacity of the PCC slab. Cracking initiates under repeated traffic loading at the transverse joint, nighttime negative thermal gradients, or their combination.

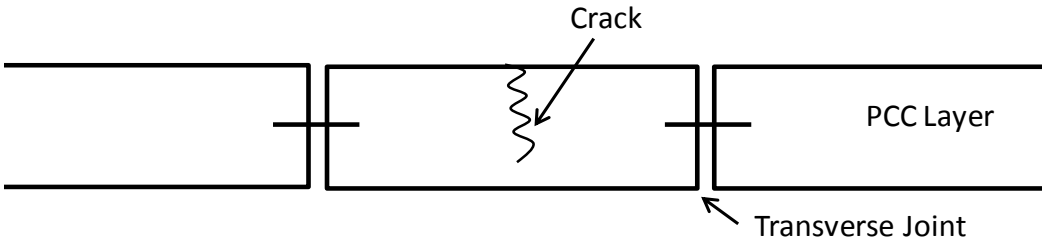

Figure 2.2 Top-down fatigue cracking in JPCP.

In the case of composite pavements, bottom-up cracks in the PCC layer propagates through the AC layer over time. Figure 2.3 shows the propagation of a crack from the bottom of the PCC layer to the top of the AC layer. The crack in the AC layer exposes the pavement to ingress of water, thereby, causing further deterioration.

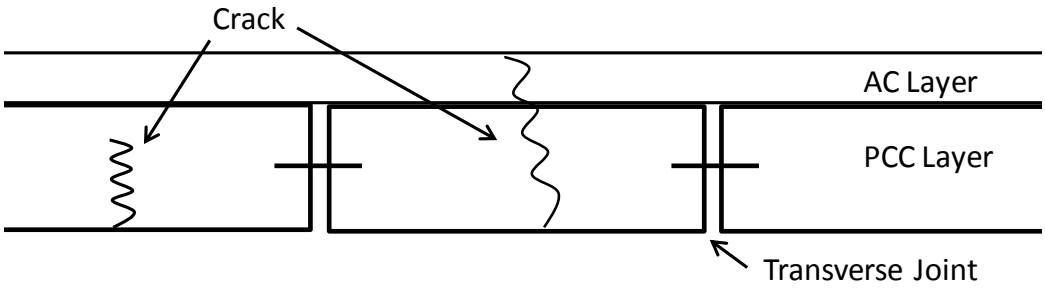

Figure 2.3 Propagation of fatigue cracking in a composite pavement.

In the MEPDG total fatigue cracking is estimated by excluding the possibility that both bottom-up and top-down cracking occur simultaneously on the same slab. The cracking in the PCC layer is computed as follows:

$$TCRACK = \left(CRK_{Bottom-up} + CRK_{Top-down} - CRK_{Bottom-up} \cdot CRK_{Top-down}\right) \cdot 100\% \quad (2.1)$$

$$CRK = \frac{100}{1 + FD^{-1.68}} \quad (2.2)$$

$$FD = \sum \frac{n_{t,j,k,l,m,p}}{N_{t,j,k,l,m,p}} \quad (2.3)$$

$$\log(N_{t,j,k,l,m,p}) = C_1 \cdot \left(\frac{MR}{\sigma_{t,j,k,l,m,p}}\right)^{C_2} + 0.4371 \quad (2.4)$$

where

TCRACK is the total transverse cracking (percent, all severities),

CRK is the percentage of bottom-up or top-down PCC cracking,

FD is the fatigue damage,

n is the applied number of load applications at conditions *t, j, k, l, m, p,*

N is the allowable number of load applications at conditions *t, j, k, l, m, p,*

t, j, k, l, m, p are conditions relating to the age, month, axle type, load level, temperature difference, and traffic path, respectively,

MR is the modulus of rupture of the PCC,

σ is the applied stress at conditions *t, j, k, l, m, p,* and

C_1, C_2 are calibration constants (C_1 = 2.0, C_2 = 1.22).

It implies from equation 2.4 that cracking in the PCC layer is a function of the applied stress and thus depends on traffic loads and temperature gradients. Accurate computation of the stress at the critical location in the PCC layer is an important step in the calculation of fatigue cracking. The next section provides an overview of the components of stress due to traffic loading and temperature curling.

2.2 Components of Stress under Temperature Curling

Pavements are subjected to bending stresses under temperature gradients and traffic loads. During the daytime the pavement slab is under a positive thermal gradient (i.e., the temperature at the top of a layer is greater than the temperature at the bottom of the layer) and during nighttime the slab is under negative thermal gradient (i.e., temperature at the bottom of a layer is greater than the temperature at the top of the layer).

Khazanovich (*1994*) demonstrated the existence of an additional stress attributed to the temperature distribution that acts on single or multi-layered pavement systems so as to produce stresses that are self-equilibrating in nature. Consider a slab on an elastic foundation subjected to an arbitrary temperature distribution. The arbitrary temperature distribution may be linear or non-linear through the thickness of the slab but does not vary in the plane of the slab. Also, the slab is free to contract or expand in the horizontal directions. According to Thomlinson (*1940*) any arbitrary temperature distribution, $T(z)$ can be divided into three components, namely:

1. The constant-strain-causing temperature component, T_C
2. The linear-strain-causing temperature component, T_L, and
3. The nonlinear-strain-causing temperature component, T_{NL}.

Since the arbitrary temperature distribution may vary along the depth of the slab, it must be noted that each of these three components may also vary along the depth of the slab. The constant-strain-causing temperature component, T_C, produces horizontal strains that are constant through the depth of the slab. These strains do not produce stress when the slab is unrestrained in the horizontal directions. Khazanovich (1994) defined the constant-strain-causing temperature component, T_C as follows:

$$T_c(z) = T_o + \frac{\sum_{i=1}^{l} \int_h \alpha(z)E(z)[T(z) - T_o]dz}{\alpha(z)\sum_{i=1}^{l} \int_h E(z)dz} \tag{2.5}$$

where

z is the distance to the point of interest from the neutral axis,

T_0 is the reference temperature of the layer at which there are no temperature-related stresses or strains in the layer,

l is the total number of layers in the multi-layered system,

E is the Young's modulus,

α is the coefficient of thermal expansion, and

$T(z)$ is the arbitrary temperature distribution.

It implies from equation (2.5) that if the coefficient of thermal expansion is constant through the depth of the slab then the constant-strain-causing temperature component will also be constant.

The linear-strain-causing temperature component, T_L, produces horizontal strains that are linearly distributed along the depth of the slab. Due to the linear distribution of strains, T_L produces bending stresses that can be solved for by using any finite element (FE)-based method. The temperature component, T_L, is defined as follows:

$$T_L(z) = T_o + \frac{z}{\alpha(z)} \frac{\sum_{i=1}^{l} \int_h \alpha(z) E(z) [T(z) - T_o] z dz}{\sum_{i=1}^{l} \int_h E(z) z^2 dz} \tag{2.6}$$

As before, equation (2.6) implies that if the coefficient of thermal expansion is constant through the depth of the slab then the linear-strain-causing temperature component will be linear through the depth of the slab. The difference between the total temperature distribution and the reference temperature is equal to the sum of the

differences of the individual temperature components and the reference temperature defined as follows:

$$T(z)-T_o=\left[T_c(z)-T_o\right]+\left[T_L(z)-T_o\right]+\left[T_{NL}(z)-T_o\right] \tag{2.7}$$

Knowing the constant- and linear-strain-causing temperature components, T_C and T_L, the nonlinear-strain-causing temperature component, T_{NL}, can be written as:

$$T_{NL}(z)-T_o=T(z)-\left[T_c(z)-T_o\right]-\left[T_L(z)-T_o\right]-T_o \tag{2.8}$$

For slabs modeled using linear elastic material models, the corresponding stress at any depth *z* according to Hooke's law is given as:

$$\sigma_{NL}(z)=-\frac{E(z)\alpha(z)}{(1-\mu)}\left(T_{NL}(z)-T_o\right) \tag{2.9}$$

where

μ is Poisson's ratio of the layer.

Appendix A provides the analytical solution for calculating the self equilibrating stress, σ_{NL}.

Traffic loads are generally modeled as either concentrated or distributed pressure loads that cause bending stresses. Therefore, the total stress at any point in the slab due to combined traffic loading and temperature curling is given as:

$$\sigma_{Total}(z)=\sigma_{bending}(z)+\sigma_{NL}(z) \tag{2.10}$$

The bending stresses include stress due to traffic loads and stress due to the linear-strain-causing temperature component T_L. The following section documents the procedure adopted by MEPDG to compute the bending stresses.

2.3 MEPDG Rapid Solutions for Predicting Critical PCC Bottom Surface Stresses

The MEPDG identifies 30 input parameters to evaluate the JPCP fatigue cracking model. Some of these factors include slab geometry and material properties, interface conditions between different layers, joint spacing, lane width, shoulder type, temperature distribution, load properties, etc. The MEPDG states that "… an attempt to run all combinations of all 30 input parameters would require analysis of more than $2x10^{14}$ cases if each parameter is allowed to have just 3 values" (*AASHTO 2008*). For the analysis of a composite pavement, the independent number of input parameters will be even higher due to additional AC properties, and this will further increase the total number of cases to be analyzed. Therefore, a need was identified for developing rapid solutions for calculating PCC stresses in the MEPDG. As a result, a method was developed to compute rigorous yet efficient solutions. The method is based on the following concepts:

1. Slab equivalency concept, and
2. Development of artificial neural networks (NNs).

2.3.1 Slab Equivalency Concept

The concept of slab equivalency was adopted by the MEPDG to reduce the number of independent parameters affecting PCC stresses without introducing any additional error. According to this concept, a multi-layered pavement system could be simplified by using an equivalent transformed section in the form of a single layer slab (*Ioannides et al. 1992*). The solution of a multi-layered system could be developed from the solution for the equivalent single layer slab is known.

The equivalent single layer slab must exhibit the same deflection profile as the multi-layered slab if the load and the foundation properties (k-value) are the same. This concept employs three equivalency conditions namely, 1) equivalent thickness, 2) equivalent temperature gradient, and 3) equivalent slab. The following equations (2.11 to 2.19) demonstrate the equivalency concept for a bonded PCC-base composite system. Similar equations are also provided in the MEPDG documentation for an unbonded PCC-base system.

2.3.1.1 Equivalent Thickness

Ioannides et al. (*1992*) presented an equivalent thickness solution for a multi-layered pavement system. The transformation involved flexural stiffness *D*, with an assumption that the Poisson's ratio of all the layers and that of the equivalent layer were equal, i.e.

$$D_{eqn} = D_{PCC} + D_{Base} \tag{2.11}$$

if, $$\mu_{eqn} = \mu_{PCC} = \mu_{Base} \tag{2.12}$$

where:

D is the flexural stiffness given as:

$$D = \frac{E\ h^3}{12(1-\mu^2)} \tag{2.13}$$

E is the Young's modulus,

h is the layer thickness, and

μ is the Poisson's ratio.

According to Khazanovich (*1994*) the governing equation of the transformation (equation 2.11) can also be written in terms of moment in each plate *M*, as follows:

$$M_{eqn} = M_{PCC} + M_{Base} \tag{2.14}$$

For a fully bonded PCC-base system, the neutral axis of the bonded system, assuming the origin is at the top of the PCC layer, is given as follows:

$$x = \frac{\int_0^h E(z) z dz}{\int_0^h E(z) dz} = \frac{E_{PCC} h_{PCC} \left(\frac{h_{PCC}}{2} \right) + E_{Base} h_{Base} \left(h_{PCC} + \frac{h_{Base}}{2} \right)}{E_{PCC} h_{PCC} + E_{Base} h_{Base}} \tag{2.15}$$

where *x* is the location of the neutral axis from the top of PCC layer. The thickness and modulus of the equivalent single layer slab can be established in terms of the thicknesses and moduli of the corresponding multi-layered slab by combining equations (2.11) to (2.15) as follows:

$$E_{eff} h_{eff}^3 = E_{PCC} h_{PCC}^3 + E_{Base} h_{Base}^3 + 12 \left[E_{PCC} h_{PCC} \left(\frac{h_{PCC}}{2} - x \right)^2 + E_{Base} h_{Base} \left(h_{PCC} + \frac{h_{Base}}{2} - x \right)^2 \right] \tag{2.16}$$

Since the properties of the equivalent slab depend on the product of its Young's modulus (E) and thickness cubed (h^3), either of the two parameters can be assumed to be equal to a reasonable value. The other parameter can then be expressed in terms of the assumed parameter and properties of the multi-layered slab system. For example, the thickness of the equivalent single-layer slab that has the same modulus of elasticity and Poisson's ratio as the PCC layer of the composite slab is given as:

$$h_{eff} = \sqrt[3]{h_{PCC}^3 + \frac{E_{Base}}{E_{PCC}} h_{Base}^3 + 12 \left[h_{PCC} \left(\frac{h_{PCC}}{2} - x \right)^2 + \frac{E_{Base}}{E_{PCC}} h_{Base} \left(h_{PCC} + \frac{h_{Base}}{2} - x \right)^2 \right]} \tag{2.17}$$

Equation (2.17) represents the equivalent thickness of the single-layer slab that can replace the multi-layered slab while maintaining the same deflection profile and modulus of subgrade reaction (k-value) under the applied loads.

2.3.1.2 Equivalent Linear Temperature Gradient

Thomlinson (*1940*) introduced the concept of equivalent temperature gradient for a single-layer slab. Khazanovich (*1994*) and Ioannides and Khazanovich (*1998*) later generalized the concept for a non-uniform, multi-layered slab. The MEPDG documentation states that (*AASHTO 2008*)

> "if two slabs have the same plane-view geometry, flexural stiffness, self-weight, boundary conditions, and applied pressure, and rest on the same foundation, then these slabs have the same deflection and bending moment distributions if their through-the-thickness temperature distributions satisfy the following condition:

$$\int_{h_A} E_A(z)\alpha_A(z)(T_A(z)-T_{0,A})zdz = \int_{h_B} E_B(z)\alpha_B(z)(T_B(z)-T_{0,B})zdz \quad (2.18)$$

where

A and *B* are subscripts denoting the two slabs,

z is the distance from the neutral axis,

T_0 is the temperature at which theses slabs are assumed to be flat,

α is the coefficient of thermal expansion,

E is the modulus of elasticity, and

h is the slab thickness."

Khazanovich (*1994*) also states that "[A]s a corollary, two temperature distributions are equivalent only if their respective linear strain components are identical." If the temperature distribution in the single-layer equivalent slab is chosen to be a linear function of depth then the difference between the top and bottom surface temperatures of the equivalent slab can be expressed in terms of temperature distributions of the PCC and base layers of the fully bonded PCC-base system slab as follows:

$$\Delta T_{L,eff} = \frac{-12}{h_{eff}^2}\left(\int_{-x}^{h_{PCC}-x} [T(z)-T_o]zdz + \frac{\alpha_{Base}E_{Base}}{\alpha_{PCC}E_{PCC}} \int_{h_{PCC}-x}^{h_{PCC}+h_{Base}-x} [T(z)-T_o]zdz \right) \quad (2.19)$$

where

$\Delta T_{L,eff}$ is the difference between the top and bottom surface temperatures of the equivalent slab,

$T(z)$ and T_o are the temperature distributions and reference temperature respectively,

α_{PCC} and α_{Base} are coefficients of thermal expansion of the PCC and base layers, respectively.

2.3.1.3 Korenev's Equivalent Slab

Korenev and Chernigovskaya (*1962*) proposed an equivalency concept for circular slabs resting on a Winkler foundation and subjected to traffic loads and temperature curling. According to this concept, the stresses in a slab of known dimensions, properties, loading conditions, and temperature distribution are related to the stresses in another slab by equation (2.20), if the following are the same (*Khazanovich et al. 2001*):

- Ratio of the slab characteristic dimension to the radius of relative stiffness (L/l),
- The total applied load to the slab self-weight (P/Q), and
- Korenev's non-dimensional temperature gradient ϕ.

$$\sigma_1 = \frac{h_2 \gamma_1 l_1^2}{h_1 \gamma_2 l_2^2} \sigma_2 \tag{2.20}$$

where

σ, h, γ, and l are the temperature stress, thickness, unit-weight, and radius of relative stiffness of a given slab, respectively.

MEPDG adopts the Korenev's non-dimensional temperature gradient to combine many factors that affect curling stresses into one parameter (*Khazanovich et al. 2001, AASHTO 2008*). It is defined as:

$$\phi = \frac{2\alpha(1+\mu)l^2}{h^2} \frac{k}{\gamma} \Delta T_L \tag{2.21}$$

where

α, μ, l, γ, h are the coefficient of thermal expansion, Poisson's ratio, radius of relative stiffness, unit-weight, and thickness of the slab respectively,

k is the modulus of subgrade reaction, and

ΔT_L is the linear temperature difference between the top and bottom surface of the slab.

Korenev's slab equivalency concept was modified for the analysis of rectangular slabs. It was found that if the following conditions are fulfilled, then the concept holds true for rectangular slab as well (*AASHTO 2008*).

$$
\begin{aligned}
&l_1 = l_2 \\
&L_1 = L_2 \\
&\phi_1 = \phi_2 \\
&\frac{AGG_1}{k_1 l_1} = \frac{AGG_2}{k_2 l_2} \\
&\frac{P_1}{\gamma_1 h_1} = \frac{P_2}{\gamma_2 h_2} \\
&s_1 = s_2
\end{aligned}
\tag{2.22}
$$

where

l is the radius of relative stiffness,

L is the joint spacing,

ϕ is the Korenev's nondimensional temperature gradient,

AGG is the aggregate interlock between the main lane and the shoulder,

P is the axle weight,

γ is the PCC slab unit weight,

h is the PCC thickness, and

s is the distance between slab edge and outer wheel edge

Khazanovich et al. (*2001*) states that if these conditions hold true for the top surface of continuously reinforced concrete pavements (CRCP), then Korenev's slab equivalency concept can be applied to CRCP.

In summary, the number of independent parameters affecting PCC stresses in a multi-layered system can be reduced by using an equivalent single layer slab and equivalent linear temperature gradient. Once the stresses in the equivalent system are solved for, the stresses in the multi-layered system can be computed using Korenev's equivalent slab method.

2.3.2 MEPDG Neural Networks for Computing PCC Stresses

The purpose of building and training artificial neural networks (NNs) is to essentially create an exhaustive database corresponding to a variety of combinations of design and loading parameters. This database can then be referred quickly for an almost instantaneous prediction of responses. Several NN models were proposed for predicting responses in airfield jointed concrete pavements (*Haussmann et al. 1997*; *Ceylan et al. 1998, 1999, 2000*) that basically eliminated the need for using FE based programs such as ILLI-SLAB (*Tabatabie and Barenberg 1980*).

MEPDG uses a modified MS-HARP neural network architecture (*Banan and Hjelmstad 1994*, *Khazanovich and Roesler 1997*) to further reduce the computational time while computing the PCC stresses. An analysis of three loading scenarios, namely *i*) traffic loading only, *ii*) temperature loading only, and *iii*) combined traffic and temperature loading found that "there is a certain interaction between traffic and temperature loadings such that stresses from traffic loading and temperature gradient cannot be simply superimposed" (*AASHTO 2008*). In light of this observation, MEPDG substituted the original multi-slab system by a combination of two simpler systems as follows:

- A single slab (system A)
- A two-slab system (system B)

Schematics for the original system, system A, and system B are presented in Figure 2.4.

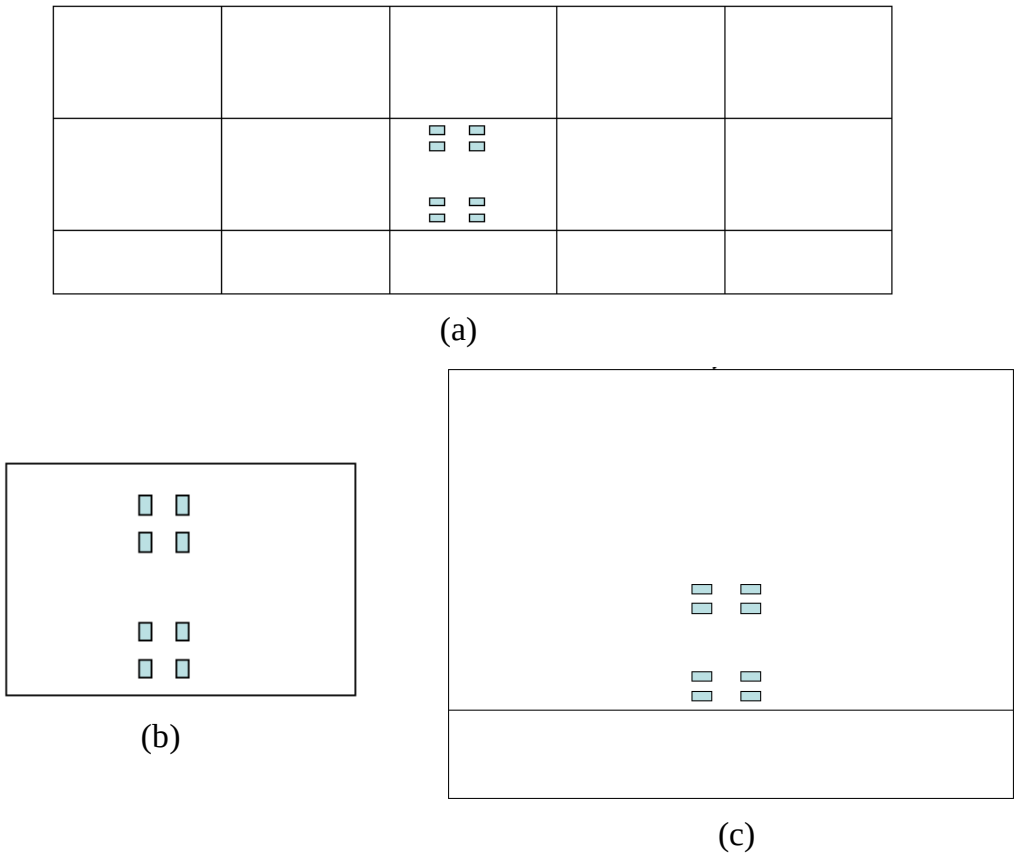

Figure 2.4 Schematics for (a) original multi-layered system, (b) single slab system A, and (c) two-slab system B (*AASHTO 2008*).

2.3.2.1 Neural Network NNA Based on System A

The length of single slab system A is equal to the transverse joint spacing of the original system, its width equals the truck lane width of the original system, and its thickness equals the slab thickness of the original system. Two neural networks NNA1 and NNA2 were trained each using a factorial of 14175 ISLAB2000 runs to compute stresses

corresponding to temperature curling and single axle loading, and temperature curling and tandem axle loading, respectively. Figure 2.5 presents the structural model for NNA1 and NNA2.

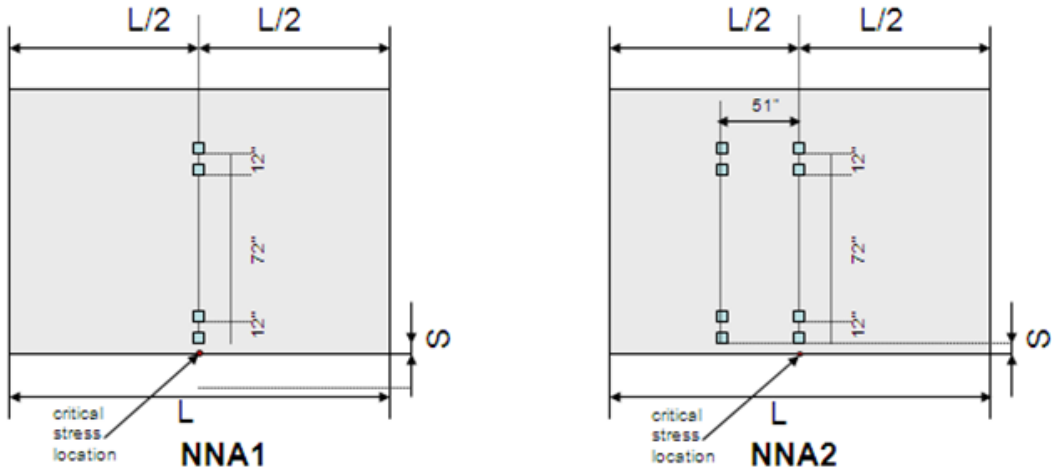

Figure 2.5 Structural model for (a) NNA1 (corresponding to single axle load) and (b) NNA2 (corresponding to tandem axle load) (*AASHTO 2008*).

Neural networks NNA1 and NNA2 were trained to calculate the stresses in system A for three (3) loading conditions, namely:

- Stress due to axle loading, *P* only, $\sigma^A(P,0)$,
- Curling stress due to equivalent linear temperature loading only (expressed in terms of Korenev's nondimensional temperature gradient ϕ), $\sigma^A(0,\phi)$, and
- Stress due to combined axle and linear temperature loading, $\sigma^A(P,\phi)$.

It should be noted that NNA1 and NNA2 account for neither the tire-footprint geometry nor the shoulder load transfer efficiency (LTE). The stress due to the linear temperature loading $\sigma^A(0,\phi)$ is equal to the curling component of the bending stress, i.e., when no axle load is present (*AASHTO 2008*).

2.3.2.2 Neural Network NNB Based on System B

System B is a two-slab system (i.e., single slab with shoulder) that has a sufficiently large slab length to ignore slab size effects, its width equals the truck lane width of the original system, and its thickness equals the slab thickness of the original system. NNs based on system B account for the tire-footprint geometry and the effect of shoulder support. These NNs consider traffic loading but not temperature curling. The stresses in the system B were computed for two (2) conditions, namely:

- No load transfer between the slabs in the system B $\sigma^B(0)$, and
- The LTE between the slabs in the system B is equal to shoulder LTE $\sigma^B(LTE_{sh})$.

For single axle loading, all the wheels in the axle are used for computing the stress using neural network NNB1. In case of tandem or tridem axle loading, an additional neural network NNB2 computes the stresses from the remaining wheels (four for a tandem axle and eight for a tridem). The final stress is obtained by superimposing stresses from NNB1 and NNB2 for the given LTE (either 0 or LTE_{sh}).

Neural networks NNB1 and NNB2 were trained using a factorial of 24300 ISLAB2000 runs and 910 ISLAB2000 runs, respectively. Figure 2.6 presents the structural model for NNB1 and NNB2.

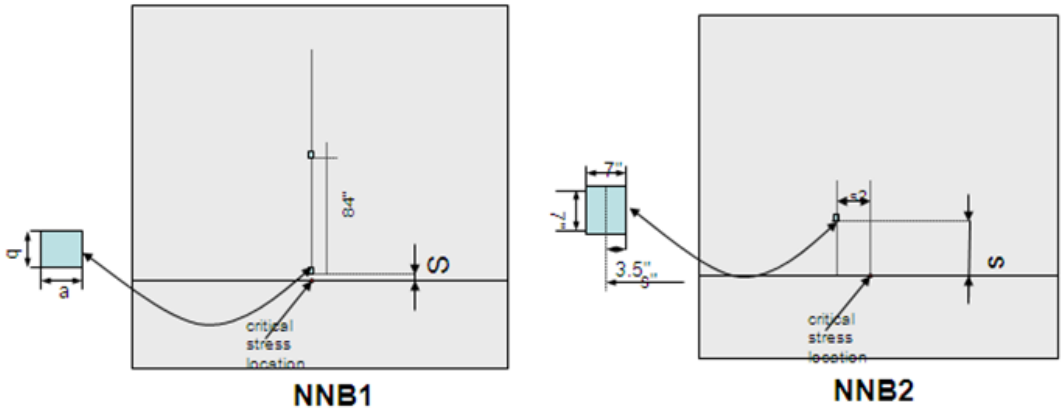

(a) (b)

Figure 2.6 Structural model for (a) NNB1 (corresponding to single axle single wheel load) and (b) NNB2 (corresponding to single wheel load) (*AASHTO 2008*).

The total stress in the equivalent slab is then expressed as a combination of stresses from NNA and NNB as follows:

$$\sigma_{comb} = \left[\left(\sigma^{A}(P,\phi) - \sigma^{A}(0,\phi) - \sigma^{A}(P,0) + \sigma^{B}(0) \right) \times \frac{\sigma^{B}(LTE_{sh})}{\sigma^{B}(0)} \right] + \sigma^{A}(0,\phi) \tag{2.23}$$

Finally, the stress at the bottom of the PCC layer in the composite pavement is calculated as follows:

$$\sigma_{PCC,bend} = \frac{2*(h_{PCC} - x)}{h_{eff}} \sigma_{comb} \tag{2.24}$$

$$\sigma_{PCC} = \sigma_{PCC,bend} + \sigma_{NL,PCC,bot} \tag{2.25}$$

where

σ_{PCC} is the total stress at the bottom of the PCC slab,

$\sigma_{PCC,bend}$ is the bending stress at the bottom of the PCC slab, and

$\sigma_{NL,PCC,bot}$ is the stress at the bottom of the PCC layer caused by the nonlinear-strain-causing temperature component, T_{NL}, of the temperature distribution.

So far in this chapter a review of the MEPDG fatigue cracking model for JPCP was presented. A comprehensive appraisal of the PCC surface stresses due to traffic and temperature loading was performed. And finally, the method adopted by MEPDG to derive rapid solutions through the use of neural networks was discussed. With this as the underlying theory, the focus of discussion now shifts to the adoption of the JPCP fatigue cracking model for composite pavements, presented below.

2.4 Adoption of the Fatigue Cracking Model for Composite Pavements in MEPDG

The adoption of the JPCP fatigue cracking model for composite pavements was evaluated by two criteria:

1. Does the physical transformation of the multi-layered composite system to an equivalent system satisfy all the conditions of equivalency previously discussed?
2. Does the stress-strain analysis under traffic loads and temperature curling change due to the inclusion of viscoelastic material properties of the AC layer?

MEPDG adopts the transformed sections concept to convert the composite pavement to an equivalent single layer PCC slab placed directly on the same subgrade as

the composite pavement. A representation of the MEPDG composite pavement transformation is shown in Figure 2.7.

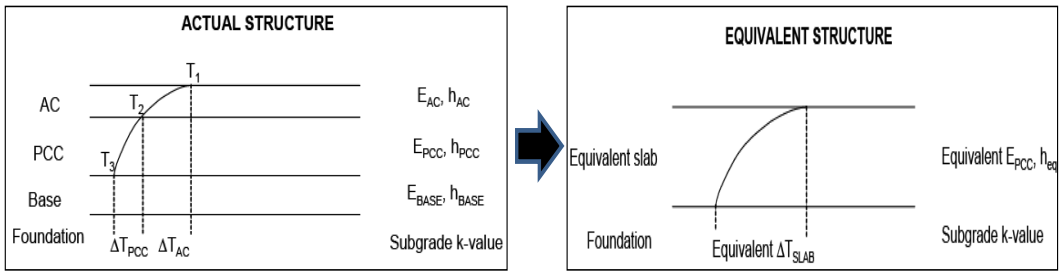

Figure 2.7 Conversion of a composite pavement to an equivalent PCC structure (adopted from *AASHTO 2008*).

Equations for equivalent thickness (2.17) and equivalent linear temperature gradient (2.19) were employed such that the thicknesses, moduli, and temperature distributions of the AC and PCC layers were expressed in terms of the thickness, modulus, and the linear temperature gradient of the equivalent structure. The following assumptions were made to define the equivalent structure (*AASHTO 2008*):

1. The deflection basin of the equivalent structure is same as the original composite structure under the same conditions of traffic and temperature loading, and
2. The equivalent temperature gradient must induce the same magnitude of moments in the equivalent structure as that in the PCC slab of the original composite structure.

In the case of JPCP, the material response of the constituent layers (PCC and base) is assumed to be elastic. However, due to the introduction of AC layer, the material

response for composite pavements is not purely elastic anymore. Asphalt is a viscoelastic material with a load-deflection response dependent on both the elastic and the viscous components of the material property. Asphalt undergoes creep or relaxation depending upon the loading criterion. Under constant strain, the stress in asphalt dissipates with time. However, the rate of dissipation, also referred to as stress relaxation, is dependent on the temperature at which the asphalt is kept. At high temperatures, stress relaxation occurs quickly whereas at low temperatures, stress relaxation may take several hours or days (*Nesnas and Nunn, 2004*). MEPDG simplifies the representation of asphalt through the use of a single time-temperature dependent AC dynamic modulus.

It was identified under this research that the use of a single dynamic modulus may introduce certain limitations in the stress computation process and eventually fatigue cracking computations. In order to better understand the limitations due to the use of a single dynamic modulus, a brief review of computation of AC dynamic modulus under MEPDG framework is presented next.

2.5 Asphalt Characterization

2.5.1 Viscoelastic Behavior of Asphalt Concrete

Several researchers have demonstrated that the constitutive equation (relationship between stresses and strains) of asphalt is dependent on time (*Saal et al. 1950, 1958*; *Van der Poel 1958*; *Sayegh 1967*; *Monismith et al. 1962, 1992*; *Marasteanu and Anderson 2000*). The viscoelastic behavior of asphalt is represented by physical models such as the Maxwell model, the Kelvin-Voigt model, and their generalized forms that are

combinations of elastic springs and viscous dashpots. The Maxwell model is a combination of spring and dashpot in series; while the Kelvin-Voigt model is a combination of springs and dashpots in parallel. By themselves, the simple Maxwell or Kelvin-Voigt models do not represent the linear viscoelastic behavior of AC adequately. Therefore, more complex models consisting of a combination of several Maxwell and/or Kelvin-Voigt models provide greater flexibility in modeling the response of the viscoelastic material (*Mase 1970*).

If a material is modeled using several Kevin-Voigt models connected in series the creep compliance of that material has the form of a Prony series which will be defined in Chapter 3. The Prony series coefficients are generally used as input parameters in finite element based programs such as ABAQUS (*ABAQUS 1997*), ANSYS (*ANSYS 2004*), and NIKE3D (*Maker et al. 1995*). The Prony series has been used by many researchers to characterize AC behavior (*Soussou et al. 1970*; *Daniel 1998*; *Park et al. 1999, 2001*; *Di Bendetto et al. 2004, 2007*; *Elseifi et al. 2006*; *Zofka 2007*, *Wang 2007, Zofka et al. 2008*, *Marasteanu et al. 2009*).

The viscoelastic behavior of AC is highly sensitive to the temperature and the rate of loading of the AC material. With an increase in temperature, the stiffness of the AC layer reduces. Similar behavior is observed when the AC layer is subjected to low frequency loads (i.e. long loading rates). The stiffness of the AC layer increases with a decrease in temperature or when subjected to high frequency loads. Or, in other words, the stiffness of the AC layer under a certain loading frequency can be "shifted" to replicate the stiffness under another frequency by "shifting" the temperature of the

analysis. This behavior of asphalt concrete is termed as the time-temperature superposition. The effect of temperature and loading frequency is most commonly represented by asphalt master curves that are based on the time-temperature superposition principles (*Bahia et al. 1992, Christensen and Anderson 1992, Gordon and Shaw 1994, Marasteanu and Anderson 1999, Rowe 2001, Pellinen and Witczak 2002, Ping and Xiao 2007*).

Di Bendetto et al. (*2004*) proposed a 15-element generalized Kevin-Voigt model using Prony series to represent the creep compliance of asphalt. The high number of Kevin-Voigt elements was adopted to cover the entire range of AC behavior under various temperatures and loading frequencies.

2.5.2 Characterization of Asphalt in the MEPDG

The MEPDG characterizes the viscoelastic behavior of the AC layer using a load duration dependent dynamic modulus. The dynamic modulus of asphalt is computed using a master curve of sigmoidal shape, at a reference temperature of 70°F, as shown by the following equations (*Pellinen and Witczak 2002*):

$$\log(E_{AC}) = \delta + \frac{\alpha}{1 + \exp(\beta + \gamma \log(t_r))} \tag{2.26}$$

where

E_{AC} is the dynamic modulus of asphalt,

δ, α, β, and γ are parameters based on the volumetric property of the asphalt mix, and

t_r is the reduced time, which accounts for the effects of temperature and the rate of

loading. It is given as:

$$\log(t_r) = \log(t) - c*(\log(\eta) - \log(\eta_{TR})) \tag{2.27}$$

where

t is the actual loading time,

c = 1.255882, and

η and η_{TR} are viscosities at temperature T and reference temperature T_R, respectively.

The MEPDG utilizes Odemark's method of equivalent thickness (MET) to calculate the actual loading time t. According to this method, any layer of a pavement system can be transformed into an equivalent layer. The transformation is valid as long as both the layers (original and equivalent) have the same flexural stiffness. Maintaining the flexural stiffness ensures that the transformation does not influence the stresses and strains below the transformed layer.

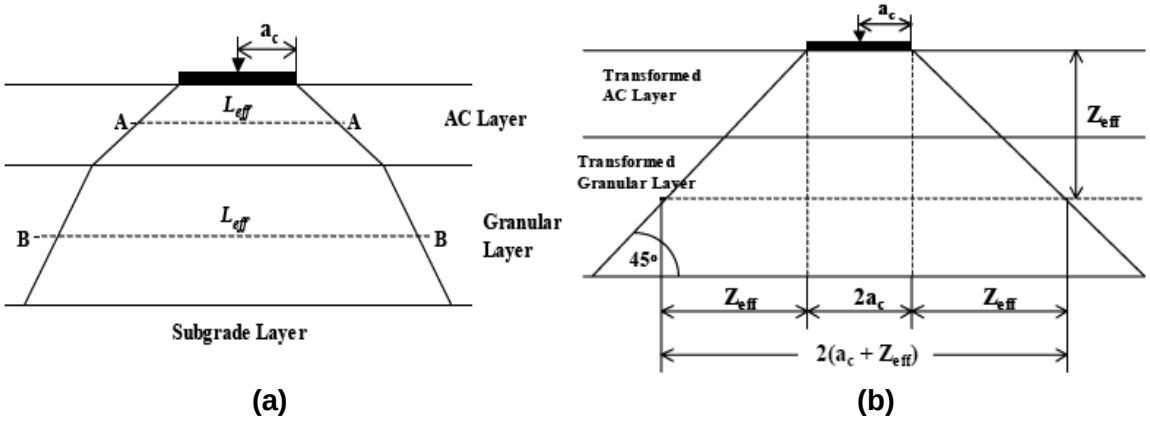

Figure 2.8 (a) Effective length and (b) effective depth for single axle in a conventional flexible pavement (adopted from *AASHTO 2008*).

Using Odemark's MET, both the AC and base layers are transformed into equivalent subgrade layers, i.e., the moduli of the transformed AC and the transformed base layers are equal to the subgrade modulus (Figure 2.8). For simplicity, the stress distribution for a typical subgrade soil is assumed to be at 45° (*AASHTO 2008*). The effective depth (Z_{eff}), effective length (L_{eff}), and loading time (t) at the mid-depth of the transformed layer are given as:

$$Z_{eff} = \sum_{i=1}^{n-1}\left(h_i * \sqrt[3]{\frac{E_i}{E_{SG}}} \right) + \frac{h_n}{2} * \sqrt[3]{\frac{E_n}{E_{SG}}} \tag{2.28}$$

$$L_{eff} = 2*(a_c + Z_{eff}) \tag{2.29}$$

$$t = \frac{L_{eff}}{17.6 * V_s} \tag{2.30}$$

where

n is the layer to be transformed,

h is the thickness of a layer,

E is the modulus of the layer,

E_{SG} is the modulus of the subgrade layer,

a_c is the radius of contact area, and

V_s is the speed of the vehicle.

Equations (2.27) to (2.30) demonstrate that the asphalt behavior is dependent on the duration of the loads. A traffic load is nearly instantaneous; the duration at highway speeds ranges between 0.01 sec. to 0.05 sec. Under traffic loads asphalt behaves practically as an elastic material as it does not undergo relaxation. On the other hand, the temperature gradient functions like a long-term load, which is applied over the duration

of few hours. The long-term load response could be termed as quasi-elastic as the modulus increases to the asymptote of the long-term asphalt modulus. From Figure 2.9 it can be inferred that the instantaneous modulus of asphalt is significantly different than the long-term modulus.

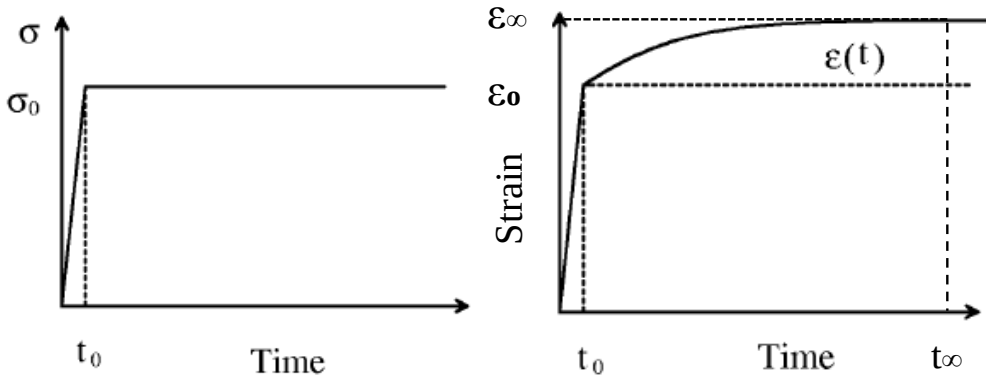

Figure 2.9 Stress-strain response under different load durations (adopted from *Chen 2000*).

Since the MEPDG considers only one value of the AC modulus (the dynamic modulus), the distress computation process due to traffic loads and temperature gradients is over-simplified. There is a need to re-evaluate the characterization of AC layer to account for stress computation under a combination of traffic loads and temperature gradients.

2.6 Limitations of the Structural Modeling of Composite Pavements in the MEPDG

As stated before, the adopted fatigue cracking model seems reasonable in its approach towards computing the stress in the PCC layer of a composite pavement. However, an analysis of the AC modulus confirms that there are limitations that need to be considered

in this study. These limitations are addressed in the following sections.

2.6.1 Use of a Single Dynamic Modulus of Asphalt

The viscoelastic behavior of AC is dependent on the duration of the loads. As described in the preceding section, asphalt behaves practically as an elastic material under instantaneous traffic loads, whereas under temperature gradients, the long-term load response of AC is quasi-elastic. The instantaneous modulus of asphalt is significantly different than the long-term modulus. Therefore, a single dynamic modulus is not representative of the combination of traffic load and temperature curling that causes cracking in the PCC layer of a composite pavement.

2.6.2 Assumption that the AC Modulus Changes on a Monthly Basis

The fatigue cracking model for composite pavements is based on the assumption that the AC modulus changes on a monthly basis. Pavements experience changes in temperature, and correspondingly, stresses, throughout a 24-hour cycle. Since AC is highly sensitive to temperature, its modulus should also change depending on the magnitude of the temperature change. However, as the modulus of asphalt is assumed to change on a monthly basis, the computed stresses in the PCC layer do not reflect the actual stresses due to the changes in the stiffness of the AC layer throughout the month. In order to improve the accuracy of predicted PCC stresses and corresponding fatigue cracking, it is of utmost importance to address the limitations identified in this section.

2.7 Existing Computer Programs for Pavement Analysis

Finite-element (FE) based programs are extremely efficient in analyzing pavement stresses for multi-layered pavements (with cracks and joints) that are subjected to traffic loading, temperature curling, or their combination. These include both general purpose FE programs (such as ABAQUS [*ABAQUS 1997*], ANSYS [*ANSYS 2004*]) and those developed specifically for the analysis of pavements (such as ISLAB2000 (*Khazanovich et al. 2000*), KENSLAB [Huang 1993], and EVERFE [*Davids et al. 1998*], etc).

The general purpose FE programs provide a universal framework where a three-dimensional (3D) analysis can be performed for a variety of conditions such as static or dynamic loads, elastic or viscoelastic material properties, and homogenous or non-homogenous layers. However, general purpose FE programs are inefficient in analyzing continuous damage accumulation that occurs due to repeated loading over time (*AASHTO 2008*). Programs developed specifically for the analysis of pavements include ILLI-SLAB (*Tabatabie and Barenberg 1980*), J-SLAB (*Tayabji and Colley 1983*), KENSLAB (*Huang 1993*), EVERFE (*Davids et al. 1998*), and ISLAB2000 (*Khazanovich et al. 2000*). Each of these programs has its own advantages and disadvantages.

ILLI-SLAB, specifically designed for the analysis of rigid pavements, underwent several revisions between 1977 and 1994. During these years, various researchers improved the program by adding functionality to analyze pavement stresses under several subgrade models, linear temperature gradients, nonlinear temperature distributions, and separation between the pavement layers, among others. The ERES Division of Applied

Research Associates (ARA) revised ILSL2 (the latest version of ILLI-SLAB) and released it as a propriety version called ISLAB2000 (*Khazanovich et al. 2000*).

ISLAB2000 is an efficient program with the capabilities to perform batch mode analysis for a large factorial of cases. This lets a user save significant pre-processing time. The MEPDG employs artificial neural networks (ANNs) that were trained using a database of several thousand ISLAB2000 cases. The use of ANNs ensures efficient computation of pavement stresses, thereby, substantially reducing the processing time for rigid pavement design.

As ISLAB2000 was developed for analyzing rigid pavements only, it has natural limitations when layers that are not purely elastic are a part of the pavement structure. The current framework of ISLAB2000 cannot capture the creep or relaxation behavior of viscoelastic materials such as AC. Under this research, a FE code is developed similar to the existing framework of ISLAB2000 but with the capability to analyze multi-layered pavements that incorporate viscoelastic as well as elastic layers.

CHAPTER 3. FINITE ELEMENT ANALYSIS OF COMPOSITE PAVEMENT INCORPORATING A VISCOELASTIC LAYER

In this chapter, a finite element (FE)-based model of a multi-layered composite pavement structure is presented. The asphalt concrete (AC) layer is considered to be viscoelastic while all other constructed layers (primarily portland cement concrete [PCC] and base) are elastic. The developed FE model is a generalization of ISLAB2000 (*Khazanovich et al. 2000*), a widely used computer program for the analysis of rigid pavements. The rationale for selecting ISLAB2000 was based on the fact that the Mechanistic Empirical Pavement Design Guide (MEPDG) uses the ISLAB2000 framework for structural modeling of concrete pavements and asphalt overlays, and the results of this study could be incorporated into the next versions of the MEPDG.

This chapter details the viscoelastic material representation of AC, formulation of a FE slab-on-grade model incorporating viscoelastic layers, validation of the FE model using simple examples, and sensitivity of the FE model to internal parameters.

3.1 Viscoelastic Material Representation of Asphalt Concrete

The stress or strain at a given time in a viscoelastic material depends on the history of the stress or strain at all times preceding the time of interest. The constitutive equation for linear viscoelastic materials is described by Boltzman's superposition principle.

According to this principle, the strain (or stress) in a viscoelastic material is the sum or superposition of all strains (or stresses) acting on the material at different times as shown in Figure 3.1 (*Osswald and Menges, 2003*).

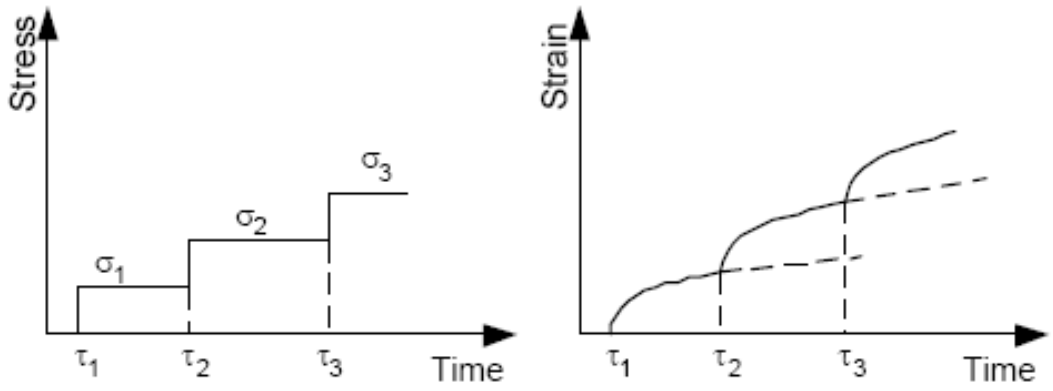

Figure 3.1 Schematic representation of Boltzman's superposition principle (adopted from *UMN Online Lecture 2011*).

The strain at any time *t* can be expressed mathematically as:

$$\varepsilon(t) = J(t-\tau_1)\sigma_1 + J(t-\tau_2)(\sigma_2 - \sigma_1) + ... + J(t-\tau_i)(\sigma_i - \sigma_{i-1}) \tag{3.1}$$

where

$\varepsilon(t)$ is the strain at time *t*,

σ_i is the applied stress at time τ_i, and

$J(t)$ is the creep compliance of the material defined as the strain under unit stress at any time *t*, written as follows:

$$J(t) = \frac{\varepsilon(t)}{\sigma_0} \tag{3.2}$$

Equation (3.1) can also be written in the Volterra integral equation form as:

$$\varepsilon(t) = \int_{-\infty}^{t} J(t-\tau) d\sigma(\tau) = \int_{-\infty}^{t} J(t-\tau) \dot{\sigma}(\tau) d\tau \tag{3.3}$$

It can be deduced from equation (3.3) that the creep compliance function characterizes the viscoelastic behavior. Under constant stress, the strain time history can be measured in a laboratory creep test. One of the ways to determine the creep compliance function is by fitting the laboratory measured strain data into a functional form. Several researchers have used linear or non-linear optimization techniques to minimize the least square error between a linear or non-linear model, used to fit the creep compliance function, and the measured test data (*Schapery 1974*, *Johnson and Quigley 1992*, *Hill 1993*, *Chen 2000*).

Of the many available functional forms, a commonly adopted method uses the Prony series [i.e. $\sum_{i=1}^{N} \alpha_i (e^{-\lambda_i t})$] to represent the creep compliance. The advantage of using the Prony series is two-fold. First, the Prony series has a very simple physical interpretation in the form of a physical model composed of springs and dashpots. Second, the viscoelastic constitutive equation can be expressed in differential form instead of the integral form given by equation (3.3). The differential form of the viscoelastic constitutive equation can be effectively incorporated into numerical techniques and finite element algorithms (*Zienkiewicz and Taylor 1967*, *Lesieutre and Govindswamy 1996*, *Johnson et al. 1997*, *Johnson 1999*, *Chen 2000*).

Consider the creep compliance function $J(t)$ in the Prony series form given as:

$$J(t) = \alpha_0 + \sum_{i=1}^{N} \alpha_i (1 - e^{\frac{-t}{\lambda_i}}) \tag{3.4}$$

where

N is the number of terms in the Prony series,

α_0, α_i, and λ_i are the coefficients defining the Prony series, and

t is the time.

Assume that the material is stress-free for time $t < 0$. Integration of equation (3.3) by parts leads to the following relationship:

$$\varepsilon(t) = \frac{\sigma(t)}{E_0} - \int_0^t \frac{\partial J(t-\tau)}{\partial \tau} \sigma(\tau) d\tau \tag{3.5}$$

$$E_0 = \frac{1}{J(0)} \tag{3.6}$$

where

E_0 is the instantaneous modulus of the material, and

$J(0)$ is the creep compliance at time $t = 0$.

If the Prony series coefficients α_0, α_i, and λ_i are expressed as follows:

$$\alpha_0 = \frac{1}{E_0} \qquad \alpha_i = \frac{1}{E_i} \qquad \lambda_i = \frac{\eta_i}{E_i} \tag{3.7}$$

where

E_i is the spring stiffness for term i,

η_i is the dashpot viscosity for term i, and

λ_i is the relaxation time for term i,

then, the Prony series has a simple physical interpretation in the form of a model consisting of an elastic spring connected in series with a generalized Kelvin-Voigt model as shown in Figure 3.2.

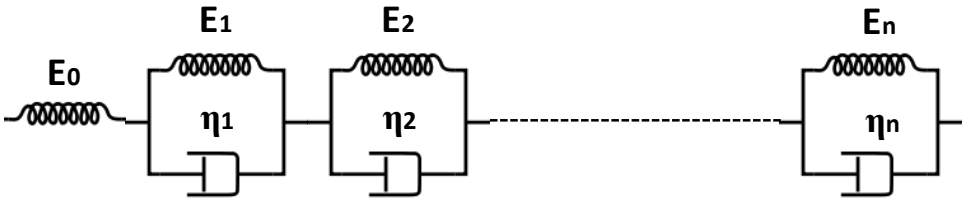

Figure 3.2 Schematic of generalized *N*-term Kelvin-Voigt model.

The creep compliance function of this model can be written based on equations (3.4) and (3.7) as follows (*Ferry 1970*):

$$J(t) = \frac{1}{E_0} + \sum_{i=1}^{N} \frac{1}{E_i}\left(1 - e^{\frac{-E_i t}{\eta_i}}\right) \tag{3.8}$$

Another advantage of defining the creep compliance function in terms of the Prony series is that it allows for replacing the integral stress-strain relationship (equation [3.5]) by a differential relationship, where the total strain at any time *t* is given as:

$$\varepsilon(t) = \varepsilon^{el}(t) + \varepsilon^{cr}(t) = \frac{\sigma(t)}{E_0} + \sum_{i=1}^{N} \varepsilon_i^{cr}(t) \tag{3.9}$$

where

ε^{el} is the elastic component of strain, and

ε^{cr} is the creep component of strain.

Substituting equation (3.8) in equation (3.5) gives the total strain at any time *t* as:

$$\varepsilon(t) = \frac{\sigma(t)}{E_0} + \sum_{i=1}^{N} \int_0^t \frac{1}{\eta_i} e^{\frac{-E_i(t-\tau)}{\eta_i}} \sigma(\tau) d\tau \tag{3.10}$$

By differentiating the creep component of the total strain given by the integral equation (3.10) for any *i*-th term of the Prony series with respect to time *t*.

$$\dot{\varepsilon}_i^{cr}(t) = \frac{1}{\eta_i}\sigma(t) - \frac{E_i}{\eta_i}\int_0^t \frac{1}{\eta_i} e^{\frac{-E_i(t-\tau)}{\eta_i}} \sigma(\tau) d\tau \tag{3.11}$$

Substituting the *i*-th creep strain term from equation (3.10) into equation (3.11):

$$\dot{\varepsilon}_i^{cr}(t) = \frac{1}{\eta_i}\sigma(t) - \frac{E_i}{\eta_i}\varepsilon_i^{cr}(t) \tag{3.12}$$

For a very small interval of time, assuming that the elastic stress σ(*t*) does not change within the time interval, the increment of creep strain during the time interval can be approximated by generalizing equation (3.12) for all terms of the Prony series as follows:

$$\Delta\varepsilon^{cr}(t) \cong \sum_{i=1}^{n}\left[\left(\sigma(t) - E_i\varepsilon_i^{cr}(t)\right)\frac{\Delta t}{\eta_i}\right] \tag{3.13}$$

where

$\Delta\varepsilon^{cr}(t)$ is the increment of creep strain, and

Δt is the increment of time.

The total strain at the end of any time interval Δt is the sum of the strain at the start of the time interval and the increment of creep strain during the time interval, given as:

$$\varepsilon(t_{j+1}) = \varepsilon(t_j) + \Delta\varepsilon^{cr}(t_j) \tag{3.14}$$

where

t_j represents the start of the time increment, and

t_{j+1} represents the end of the time increment.

At the initial time t_1 (i.e. j = 0), the creep strain $\varepsilon^{cr}(t_1) = 0$ and equation (3.9)

becomes the elastic stress-strain relationship. The increment of creep strain at any time *t* is dependent on the applied stress during that time interval, the creep strain at the start of the time interval in the individual Kelvin-Voigt elements, the spring stiffness and dashpot viscosity of the Kelvin-Voigt elements, and the time interval Δt_j. This implies that the differential formulation of the creep compliance function does not require storage of the entire strain history.

Analogous to the elastic constitutive equation (*Timoshenko 1970*), the three-dimensional viscoelastic relationship between stresses σ_{mn} and strains ε_{mn} can be written as:

$$\varepsilon_{mn} = \tilde{J}\left[(1+\mu)\sigma_{mn} - \mu\sigma_{kk}\delta_{mn}\right] \tag{3.15}$$

where

m, *n*, and k represent spatial dimensions *x*, *y*, and *z*, respectively,

μ is the Poisson's ratio, and

δ_{mn} is the Kronecker delta function given as follows:

$$\delta_{mn} = \begin{cases} 1, & m = n \\ 0, & m \neq n \end{cases} \tag{3.16}$$

$\tilde{J}$ is a creep compliance operator defined as follows:

$$\tilde{J}f(t) = \frac{f(t)}{E_0} - \int_0^t \frac{\partial J(t-\tau)}{\partial \tau} f(\tau) d\tau \tag{3.17}$$

The increment of creep strain at the end of the time interval Δt for a three-dimensional analysis can be written by combining equations (3.13) and (3.15) as follows:

$$\Delta\varepsilon_{mn}^{cr}(t) \cong \sum_{i=1}^{N}\left[\left\{\begin{array}{l}\tilde{J}\left\{(1+\mu)\sigma_{mn}(t)-\mu\sigma_{kk}\delta_{mn}(t)\right\} \\ \qquad -\tilde{J}^{-1}\left\{E_i\varepsilon_i^{cr}{}_{mn}(t)+\dfrac{\mu}{1+\mu}E_i\varepsilon_i^{cr}{}_{kk}(t)\delta_{mn}\right\}\end{array}\right\}\frac{\Delta t}{\eta_i}\right] \quad (3.18)$$

The following section describes a finite element model based on the viscoelastic constitutive equation presented herein.

3.2 Development of Finite Element Model for the Analysis of Viscoelastic Slab-on-Grade

The finite element method is an efficient tool for computing the unknown variables (such as displacements or forces) for an engineering problem (*Cook et al. 1974, Reddy 1984*). Several FE codes developed specifically for pavement analysis (such as ILLI-SLAB [*Tabatabie and Barenberg 1980*], WESLIQID [*Chou 1981*], KENSLAB [*Huang 1993*]) are based on plate theory for modeling pavement layers. The plate theory is traditionally adopted for modeling of concrete layers because the horizontal dimensions of a pavement slab are considerably greater than its thickness and the high stiffness of PCC makes bending the main mode of deformation. This justifies the use of medium-thick plates to model pavement layers.

The Kirchhoff-Love plate theory is an extension of the Euler-Bernoulli beam theory for bending of isotropic and homogenous medium-thick plates. The fundamental assumptions of the plate theory are summarized as follows (*Timoshenko and Woinowsky-Krieger 1959*):

1. The deflection of the mid-surface of the plate is small in comparison to the

thickness of the plate.

2. Straight lines initially normal to the mid-surface remain straight and normal to that surface after bending.
3. No mid-surface straining or in-plane straining, stretching, or contracting occurs due to bending.
4. The component of stress normal to the mid-surface is negligible.

In this section, the formulation of a FE model for a slab-on-grade is presented. A viscoelastic plate is placed on a Winkler foundation that could be elastic or viscoelastic. The plate is subjected to traffic loads (in form of a uniformly distributed load over the tire footprint area) and thermal loads (in form of an arbitrary temperature profile varying through the thickness of the plate). The viscoelastic problem is converted into a series of elastic problems such that fictitious loads act on the plate depending on the stress history in the viscoelastic plate. Although readily available in literature (*Zienkiewicz and Taylor* 1967, *Cook et al. 1974*, *Ugural and Fenster 2003*), part of the formulation includes a solution for elastic plates subjected to thermal loads, provided for the sake of completeness.

3.2.1 Formulation of the Finite Element Model

A four-node rectangular plate element *ijkl*, as shown in Figure 3.3, was selected to represent the elements of the pavement layer. The coordinate system adopted to develop the formulation is also marked in Figure 3.3. The element has three degrees of freedom

at each node.

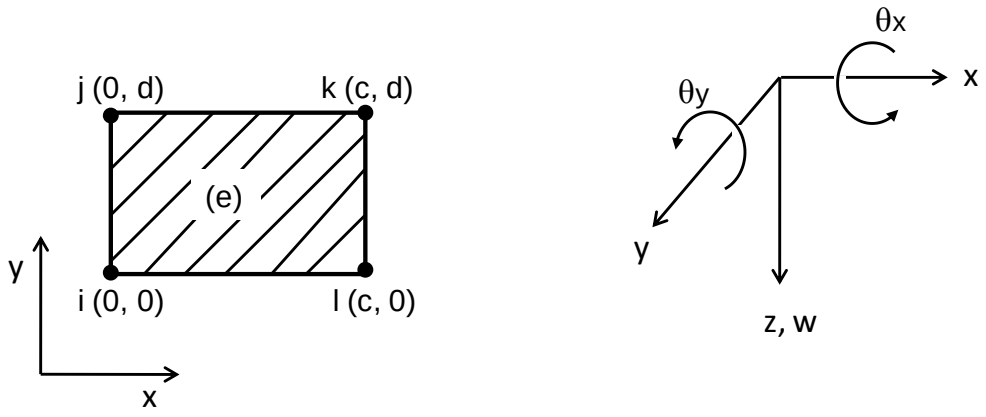

Figure 3.3 Finite element *ijkl*.

From the assumptions of medium-thick plate theory, it is deduced that the vertical shear strains γ_{xz} and γ_{yz} and the normal strain ε_z due to vertical loading may be neglected. Thus, the remaining strains at any given point in the plate can be written in terms of displacements as:

$$\varepsilon_x = \frac{\partial u}{\partial x} \qquad \varepsilon_y = \frac{\partial v}{\partial y} \qquad \gamma_{xy} = \frac{\partial u}{\partial y} + \frac{\partial v}{\partial x} \tag{3.19}$$

where

u, *v*, and *w* are the deflections in the *x*, *y*, and *z* directions respectively, and

ε and γ are the normal and shear strains, respectively.

Since only slab bending is considered, the horizontal deflections can be written in terms of the slopes at the mid-surface given as:

$$u = -z\frac{\partial w}{\partial x} \qquad v = -z\frac{\partial w}{\partial y} \tag{3.20}$$

where

z is the distance from the neutral axis of the plate.

The strains for an element in the plate can be re-written in matrix form by combining equations (3.19) and (3.20) as follows:

$$\{\varepsilon\}_e = z\{\kappa\}_e \tag{3.21}$$

$$\{\kappa\}_e = \left\{ -\frac{\partial^2 w}{\partial x^2} \quad -\frac{\partial^2 w}{\partial y^2} \quad -2\frac{\partial^2 w}{\partial x \partial y} \right\}^T \tag{3.22}$$

where

subscript *e* denotes an individual element in the plate, and

κ represents the curvatures of the element.

Further, if the plate is elastic, the stress-strain relation is given by Hooke's law as follows:

$$\sigma_x = \frac{E}{1-\mu^2}\left(\varepsilon_x + \mu\varepsilon_y\right) - \frac{E}{1-\mu^2}\left(\varepsilon_{0x} + \mu\varepsilon_{0y}\right) \tag{3.23a}$$

$$\sigma_y = \frac{E}{1-\mu^2}\left(\varepsilon_y + \mu\varepsilon_x\right) - \frac{E}{1-\mu^2}\left(\varepsilon_{0y} + \mu\varepsilon_{0x}\right) \tag{3.23b}$$

$$\tau_{xy} = \frac{E}{2(1+\mu)}\gamma_{xy} - \frac{E}{2(1+\mu)}\gamma_{0xy} \tag{3.23c}$$

where

E is the Young's modulus,

μ is the Poisson's ratio,

ε_0 and γ_0 are the normal and shear components of initial strains, respectively, and

σ and τ are the normal and shear stresses, respectively.

The stresses produce bending and twisting moments that can be represented using

the following relations:

$$M_x = \int_{-h/2}^{h/2} z\sigma_x dz \qquad M_y = \int_{-h/2}^{h/2} z\sigma_y dz \qquad M_{xy} = \int_{-h/2}^{h/2} z\tau_{xy} dz \tag{3.24}$$

Combining equations (3.22), (3.23), and (3.24) leads to the following relationship between the moments in the element and curvatures:

$$\{M\}_e = [D]\left(\{\kappa\}_e - \{\kappa_0\}_e\right) \tag{3.25}$$

$$[D] = \frac{Eh^3}{12(1-\mu^2)}\begin{bmatrix} 1 & \mu & 0 \\ \mu & 1 & 0 \\ 0 & 0 & (1-\mu)/2 \end{bmatrix} \tag{3.26}$$

where

[*D*] is the plate flexural stiffness matrix,

κ_0 represents the initial curvatures due to inelastic strains, and

h is the plate thickness.

The displacement of a node *i* can be defined using equation (3.20) as:

$$\{\delta_i\} = \{\theta_{yi} \quad \theta_{xi} \quad w_i\}^T = \left\{\left(\frac{\partial w}{\partial x}\right)_i \quad \left(\frac{\partial w}{\partial y}\right)_i \quad w_i\right\}^T \tag{3.27}$$

where

θ_y and θ_x are the slopes about the x-axis and y-axis, respectively.

Therefore, the displacement of the four-node element *ijkl* can be written as:

$$\{\delta\}_e = \{\theta_{yi} \quad \theta_{xi} \quad w_i \quad \theta_{yj} \quad \theta_{xj} \quad w_j \quad \theta_{yk} \quad \theta_{xk} \quad w_k \quad \theta_{yl} \quad \theta_{xl} \quad w_l\}^T \tag{3.28}$$

A fourth-order polynomial is commonly used to represent the displacement function in the following form (*Zienkiewicz and Taylor 1967, Khazanovich 1994, Khazanovich et al. 2000*):

$$w = a_1 + a_2 x + a_3 y + a_4 x^2 + a_5 xy + a_6 y^2 + a_7 x^3 + a_8 x^2 y + a_9 xy^2 + a_{10} y^3 + a_{11} x^3 y + a_{12} xy^3 \tag{3.29}$$

The curvatures of the plate element are related to the displacements by the following equations:

$$\{\kappa\}_e = [B]\{\delta\}_e \tag{3.30}$$

where

[*B*] is the strain-displacement matrix (*Zienkiewicz and Taylor 1967*).

The equation of equilibrium for nodal forces can be written by minimizing the total potential energy for all the elements of the system as follows:

$$\sum_{1}^{ne} \{\Delta\delta\}_e^T \left(\int_{\Omega^e} z^2 [B]^T [\overline{D}] \left([B]\{\delta\}_e - \{\kappa_0\}_e \right) dV - \int_{\Omega^e} [N]^T \{F\}_e \, dV \right) = 0 \tag{3.31a}$$

or, writing equation (3.31a) in terms of a single plate element, we have:

$$\int_{\Omega^e} z^2 [B]^T [\overline{D}][B] dV \{\delta\}_e = \int_{\Omega^e} [N]^T \{F\}_e \, dV + \int_{\Omega^e} z^2 [B]^T [\overline{D}] \{\kappa_0\}_e \, dV \tag{3.31b}$$

where

$[\overline{D}]$ is the material property matrix given as:

$$[\overline{D}] = \frac{E}{(1-\mu^2)} \begin{bmatrix} 1 & \mu & 0 \\ \mu & 1 & 0 \\ 0 & 0 & (1-\mu)/2 \end{bmatrix} \tag{3.32}$$

The left hand side of equation (3.31b) represents the product of stiffness and deflection of the plate element. The stiffness of the plate element is defined in terms of the element stiffness matrix given as:

$$[k]_e = \int_{\Omega^e} z^2 [B]^T [\overline{D}][B] dV = \int_{A^e} [B]^T [D][B] dA \tag{3.33}$$

where

$[k]_e$ is the element stiffness matrix, and

V and A are the volume and the area of the element, respectively.

The right hand side of equation (3.31b) represents the force acting on the plate element due to external loads and initial strains. The first term $\{F\}_e$ is the element force vector due to external loads and self weight of the plate, and the second term is the element force vector due to inelastic curvatures, given as:

$$\{F_0\}_e = \int_{\Omega^e} z^2 [B]^T [\overline{D}] \{\kappa_0\}_e \, dV \tag{3.34}$$

The deflections at all the nodes in the plate are computed using equation (3.31a). Further details on this process are included in Section 3.2.5. After the deflections in the plate are determined, the total strain in the element is calculated using equations (3.21) and (3.30) as shown in equation (3.35). Further, the stress in the element is computed in terms of elastic strains as shown in equation (3.36).

$$\{\varepsilon(x, y, z)\}_e = z[B]\{\delta\}_e \tag{3.35}$$

$$\{\sigma(x, y, z)\}_e = [\overline{D}](\{\varepsilon(x, y, z)\} - \{\varepsilon_o(x, y, z)\})_e \tag{3.36}$$

The stresses at any node of the plate are obtained by averaging the stresses from the adjoining nodes when two or more elements share a common node. It should be noted that the initial strains ε_0 could be equal to the thermal strains and/or viscoelastic creep strains as discussed next.

3.2.2 Thermal Loading

Consider a temperature distribution $T(z)$ throughout the plate thickness that is a linear function of depth and can be expressed as follows:

$$T(z) = \frac{\Delta T}{h} z \tag{3.37}$$

where

h is the thickness of the plate,

z is the distance from the neutral axis of the plate, and

ΔT is the difference of the temperatures between the top and bottom of the plate.

The inelastic curvatures due to the temperature variation in the plate are given as:

$$\{\kappa_{therm}\} = \{\alpha T(z) \quad \alpha T(z) \quad 0\}^T = \left\{\alpha\left(\frac{\Delta T}{h}\right) \quad \alpha\left(\frac{\Delta T}{h}\right) \quad 0\right\}^T \tag{3.38}$$

where

α is the coefficient of thermal expansion.

If the slab is free to expand or contract, then the force due to inelastic curvatures F_{therm} can be written using equation (3.34) as follows:

$$\{F_{therm}\} = \int_{\Omega^e} z^2 [B]^T [\overline{D}] \left\{\frac{\alpha\Delta T}{h} \quad \frac{\alpha\Delta T}{h} \quad 0\right\}^T dV \tag{3.39}$$

Since the temperature gradient ΔT does not vary along the horizontal direction of the slab, equation (3.39) can be simplified as:

$$\{F_{therm}\} = \left(\int_{A^e} [B]^T [D]\, dA\right) \left\{\frac{\alpha\Delta T}{h} \quad \frac{\alpha\Delta T}{h} \quad 0\right\}^T \tag{3.40}$$

3.2.3 Viscoelastic Analysis

Unlike thermal strains, which do not vary along the horizontal direction of the plate element, the creep strains are a function of the spatial coordinates of the plate element. Therefore, for a three-dimensional analysis, the increment of creep strains given by equation (3.18) is rewritten for the *i*-th Kelvin-Voigt element as follows:

$$\Delta\varepsilon_{ix}^{cr}(t_j) \cong \left[\sigma_x(t_j) - \frac{E_i}{(1-\mu^2)}\left\{\varepsilon_{ix}^{cr}(t_j) + \mu\varepsilon_{iy}^{cr}(t_j)\right\}\right] * \frac{\Delta t_j}{\eta_i} - \mu\left[\sigma_y(t_j) - \frac{E_i}{(1-\mu^2)}\left\{\varepsilon_{iy}^{cr}(t_j) + \mu\varepsilon_{ix}^{cr}(t_j)\right\}\right] * \frac{\Delta t_j}{\eta_i} \tag{3.41a}$$

$$\Delta\varepsilon_{iy}^{cr}(t_j) \cong \left[\sigma_y(t_j) - \frac{E_i}{(1-\mu^2)}\left\{\varepsilon_{iy}^{cr}(t_j) + \mu\varepsilon_{ix}^{cr}(t_j)\right\}\right] * \frac{\Delta t_j}{\eta_i} - \mu\left[\sigma_x(t_j) - \frac{E_i}{(1-\mu^2)}\left\{\varepsilon_{ix}^{cr}(t_j) + \mu\varepsilon_{iy}^{cr}(t_j)\right\}\right] * \frac{\Delta t_j}{\eta_i} \tag{3. 41b}$$

$$\Delta\gamma_{ixy}^{cr}(t_j) \cong 2(1+\mu)\left[\tau_{xy}(t_j) - \frac{E_i}{2(1+\mu)}\gamma_{ixy}^{cr}(t_j)\right] * \frac{\Delta t_j}{\eta_i} \tag{3. 41c}$$

where

$\varepsilon_{ix}^{cr}(t_j)$ and $\varepsilon_{iy}^{cr}(t_j)$ are the normal creep strains in the *x* and *y* directions, respectively, and $\gamma_{ixy}^{cr}(t_j)$ is the shear creep strain,

σ_x and σ_y are the normal stresses in the *x* and *y* directions, respectively, and τ_{xy} is the shear stress.

At any time t_{j+1}, consider a gradient of creep strain in the plate such that the creep strains at any depth *z* are a linear function of depth. Analogous to equation (3.38), the inelastic curvatures due to creep strains at any time t_{j+1} can be written as:

$$\kappa^{cr}(t_{j+1}) = \frac{\varepsilon^{cr}_{bot}(t_{j+1}) - \varepsilon^{cr}_{top}(t_{j+1})}{h} \tag{3.42}$$

where

$\kappa^{cr}(t_{j+1})$ are the inelastic curvatures due to creep strains at the end of the time interval,

$\varepsilon^{cr}_{bot}(t_{j+1})$ is the creep strain at the bottom of the plate element at the end of the time interval, and

$\varepsilon^{cr}_{top}(t_{j+1})$ is the creep strain at the top of the plate element at the end of the time interval.

Due to the presence of inelastic curvatures at any time t_{j+1}, it can be said that fictitious forces, accounting for the viscoelastic creep strains, act on the plate element at any time t_{j+1}. Using equation (3.34), the "creep" force is written as follows:

$$\left\{F_{creep}(t_{j+1})\right\} = \int_{\Omega^e} z^2 [B]^T [\overline{D}] \left\{\kappa^{cr}_x(t_{j+1}) \quad \kappa^{cr}_y(t_{j+1}) \quad \kappa^{cr}_{xy}(t_{j+1})\right\}^T dV \tag{3.43}$$

where

κ^{cr}_x, κ^{cr}_y, and κ^{cr}_{xy} are the normal and shear components of the inelastic curvatures due to creep strains in the *x*-direction, *y*-direction, and *xy* plane, respectively, at any time t_{j+1}.

Since the inelastic curvatures due to creep strains are a function of the spatial coordinates of the plate element, approximating functions are used to represent the curvatures at any point in the plate in terms of nodal inelastic curvatures. The following functions were adopted:

$$N_1 = \left(1 - \frac{x}{c}\right)\left(1 - \frac{y}{d}\right) \tag{3.44a}$$

$$N_2 = \left(1 - \frac{x}{c}\right)\left(\frac{y}{d}\right) \tag{3.44b}$$

$$N_3 = \left(\frac{x}{c}\right)\left(\frac{y}{d}\right) \tag{3.44c}$$

$$N_4 = \left(\frac{x}{c}\right)\left(1 - \frac{y}{d}\right) \tag{3.44d}$$

where

N_1, N_2, N_3, and N_4 are the approximating functions for inelastic curvatures due to creep strains at nodes *i*, *j*, *k*, and *l*, respectively of the element shown in Figure 3.3.

The fictitious creep force given in equation (3.43) can be re-written using equation (3.44) as follows:

$$\left\{F_{creep}(t_{j+1})\right\} = \int_{\Omega^e} z^2 [B]^T [\overline{D}] \left\{\kappa^{cr}(t_{j+1})\right\} \{N\}^T \, dV \tag{3.45}$$

where

κ^{cr} is a matrix containing the normal and shear components of the inelastic curvature due to creep strains at nodes *i*, *j*, *k*, and *l* of the plate element, i.e.

$$\left\{\kappa^{cr}\right\} = \begin{bmatrix} \kappa_x^{cr\,i} & \kappa_x^{cr\,j} & \kappa_x^{cr\,k} & \kappa_x^{cr\,l} \\ \kappa_y^{cr\,i} & \kappa_y^{cr\,j} & \kappa_y^{cr\,k} & \kappa_y^{cr\,l} \\ \kappa_{xy}^{cr\,i} & \kappa_{xy}^{cr\,j} & \kappa_{xy}^{cr\,k} & \kappa_{xy}^{cr\,l} \end{bmatrix} \tag{3.46}$$

and, $\{N\}$ is the vector containing approximating functions, as follows:

$$\{N\} = \{N_1 \quad N_2 \quad N_3 \quad N_4\} \tag{3.47}$$

3.2.4 FE Formulation of the Winkler Foundation

The FE model developed under this research provides a generalization of the current framework for the commercial package ISLAB2000 (*Khazanovich et al. 2000*). ISLAB2000 incorporates many subgrade models (such as Winkler [*1861*], Pasternak [*1954*], and Kerr-Vlasov [*1964*]) that provide the foundation support for the slab. Among them, the Winkler foundation is the simplest foundation model, which is defined using a proportionality constant between the applied pressure and plate deflection at any point. ISLAB2000 utilizes two idealizations for the Winkler foundation: the spring formulation and the energy-consistent Winkler formulation (*Khazanovich et al. 2000*). The energy consistent Winkler formulation permits the use of a coarser mesh and significantly less computational resources than would be required by the spring foundation to achieve the same level of accuracy. This was an important feature of the past when memory requirements and computational time were significant considerations in the slab-on-grade analysis. Recent advances in computer technology have made these factors less important. While the energy-consistent Winkler formulation is more efficient, the spring formulation permits a simpler implementation of the analysis of separation of the slab from the foundation in the case of curling or void analysis. If the mesh size is sufficiently fine, then there is no significant difference between the results from spring and energy-consistent formulations of the Winkler foundation in ISLAB2000.

Under this research, the spring formulation of the Winkler foundation is adopted to model the foundation support. This formulation of the Winkler foundation models the

foundation with concentrated springs at the nodes of the plate element as shown in Figure 3.4.

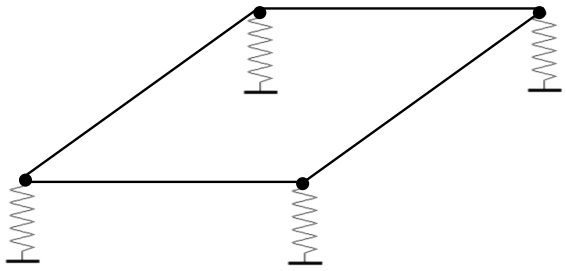

Figure 3.4 Spring idealization of Winkler foundation using concentrated springs at the nodes of the plate element.

The stiffness of the foundation is defined as a product of the coefficient of subgrade reaction and the area of the subgrade (*Khazanovich et al. 2000*). Since a four-node finite element *ijkl* is used to represent the plate element, the foundation stiffness at each node of the element corresponding to the degree of freedom representing vertical deflection can be written as follows:

$$\left[K_{dd\ foundation}\right]_e = \begin{cases} k_{subgrade} * \dfrac{A_e}{4} & \text{for } d \in (3,6,9,12) \\ 0 & \text{otherwise} \end{cases} \tag{3.48}$$

where

$\left[K_{dd\ foundation}\right]_e$ is the stiffness of the foundation supporting the plate element,

$k_{subgrade}$ is the coefficient of subgrade reaction,

A_e is the area of the element, and

d is the local degree of freedom corresponding to vertical deflection at element

nodes.

The foundation stiffness matrix $[K_{foundation}]_e$ is added to the element stiffness matrix $[k]_e$ in order to incorporate the boundary conditions for the slab-on-grade analysis when the element node is in contact with the foundation. An approach similar to that in ISLAB2000 is adopted to model the separation of the slab from the foundation for curling analysis. For an out of contact node, no contribution from the foundation is considered by setting the stiffness of the spring equal to zero (*Khazanovich et al. 2000*).

3.2.4.1 Viscoelastic Winkler Foundation

The foundation model can also incorporate a viscoelastic analysis similar to that presented for the plate in the preceding section. Analogous to equation (3.41), the increment of creep deflections in the viscoelastic Winkler foundation can be written as follows:

$$\Delta w^{cr}_{foundation}(t_j) \cong \sum_{i=1}^{n}\left[\sigma_{foundation}(t_j) - k_i w^{cr}_{foundation}(t_j)\right] * \frac{\Delta t_j}{\eta_i} \qquad (3.49)$$

where

$\Delta w^{cr}_{foundation}$ is the increment of creep deflections in the foundation at the end of time interval Δt_j,

$\sigma_{foundation}$ is the stress acting on the foundation at time t_j,

k_i and η_i are the spring stiffness and dashpot viscosity of the i-th term of the Prony series, and

μ is the Poisson's ratio.

The total creep deflections in the viscoelastic Winkler foundation at any time t_{j+1} are given by adding the creep deflections at time t_j and the increment of creep deflections during the time interval Δt_j. The fictitious forces acting on the foundation at any time t_j due to the presence of creep deflections are computed as:

$$F^{cr}_{foundation}(t_j) = k_{subgrade} * A_e * w^{cr}_{foundation}(t_j) \tag{3.50}$$

where

$w^{cr}_{foundation}(t_j)$ are the total creep deflections in the viscoelastic Winkler foundation at any time t_j.

It must be noted that the fictitious Winkler foundation creep force acts on each spring in contact with the nodes of the plate element. The foundation creep force acts only in the degree of freedom corresponding to the vertical deflection of the plate, or in other words, the foundation creep force is equal to zero for the rotational degree of freedom.

3.2.5 Assembling the Global Matrix and Computing Stresses Based on the Time-Discretized Viscoelastic Analysis

The equilibrium equation for all elements of the plate can be expressed from equation (3.31a) as follows:

$$[K]\{\delta\} = \{F\} + \{F_0\} \tag{3.51}$$

where

[K] is the global stiffness matrix,

{δ} is the global displacement vector,

$\{F\}$ is the global force vector consisting of forces due to traffic loads and self weight of the slab, and

$\{F_0\}$ is the global force vector due to inelastic strains such as thermal strain and viscoelastic creep strains from the plate and/or foundation.

The global stiffness matrix [K] is assembled by adding the terms of element stiffness matrix $[k]_e$ and the foundation stiffness matrix $[K_{dd\ foundation}]_e$ corresponding to the element *ijkl* into a global matrix at the corresponding global degrees of freedom over the total number of elements. Similarly, the global force vectors $\{F\}$ and $\{F_0\}$ are also assembled by adding the terms of the element force vectors at corresponding global degrees of freedom over all the elements. Equation (3.51) can be re-written at any time step t_j as follows:

$$\left\{\delta(t_j)\right\} = [K]^{-1}\left(\left\{F(t_j)\right\} + \left\{F_{therm}(t_j)\right\} + \left\{F_{creep}(t_j)\right\}\right) \tag{3.52}$$

Thus, the nodal displacements of the plate at time step t_j are calculated by multiplying the inverse of the global stiffness matrix [K] and the sum of the load vector $\left\{F(t_j)\right\}$, temperature load vector $\left\{F_{therm}(t_j)\right\}$, and the fictitious creep load vector $\left\{F_{creep}(t_j)\right\}$ at time step t_j. The load and the temperature load vectors depend on the magnitude of the external loads and temperature at time t_j, respectively, whereas the creep load vector depends on the stress time history. The stiffness matrix [K] from the previous time step is initially used in the next time step analysis. This permits avoiding an additional inversion of the stiffness matrix, which is the most computationally expensive step. However, if the contact conditions are changed at any node (i.e. the deflection changed its sign from the previous time step) then the foundation stiffness

matrix should be updated and the corresponding global stiffness matrix [*K*] should be computed.

Once the global displacements are calculated from equation (3.52), the element displacement can be extracted using the global degrees of freedom corresponding to each node of the element. The stresses are computed at the end of each time interval from equation (3.36) as follows:

$$\left\{\sigma(t_j)\right\}_e = \left[\overline{D}\right]\left(\left\{\varepsilon(t_j)\right\} - \left\{\varepsilon_{therm}\right\} - \left\{\varepsilon_{tot}^{cr}(t_j)\right\}\right)_e \tag{3.53}$$

The formulation of the FE model for a single layer slab-on-grade was presented in this section. The next section presents the extension of this model to multi-layered pavements.

3.3 Extension of the FE Model to Multi-Layered Composite Pavements

The FE model presented in the preceding section was developed based on the Kirchhoff-Love plate theory for a single layer plate placed on the Winkler foundation. Pavements, on the other hand, are multi-layered systems with different bonding conditions between the various layers. The interface condition between two layers in contact may vary from zero friction (fully unbonded) to full friction (fully bonded). In this study, only extreme cases (fully bonded and fully unbounded) were considered. In the case of composite pavements defined as a system of AC over PCC over base layers, two layer interfaces exist – one between the AC and PCC layers and other between the PCC and base layers. This leads to four sets of interface conditions: bonded-bonded, unbonded-unbonded, bonded-unbonded, and unbonded-bonded.

As discussed in Chapter 2, multi-layered pavements can be transformed into single layer systems using the method of equivalent thickness (MET). As long as certain conditions are fulfilled that include equality of deflection profiles and equality of modulus of subgrade reaction between the multi-layered slab-on-grade and equivalent single layer slab-on-grade, the stress solution of the multi-layered slab can be expressed in terms of the stress solution of the equivalent slab (*Ioannides et al. 1992*). Thus, the plate theory is used to calculate stresses in the equivalent single layer slab, which are further used to compute the stresses in the layers of a multi-layered slab.

In this section, the equivalency equations between the composite pavement and an equivalent single layer slab are presented for bonded-bonded interface conditions of the composite slab. The equivalency equations for other interface conditions are detailed in Appendix A.

3.3.1 Equivalent Single Layer Slab

Either the thickness or the modulus of the equivalent single layer slab can be computed by equating the flexural stiffness of the equivalent slab to the flexural stiffness of the composite pavement if the Poisson's ratio of all the layers of the composite pavement and that of the equivalent slab are equal (*Ioannides et al. 1992*). The thickness (or modulus) can be computed from the following equation if the modulus (or thickness) is known.

$$\frac{E_{eq}h_{eq}^3}{\left(1-\mu^2\right)} = \frac{1}{\left(1-\mu^2\right)}\left(\begin{array}{l} E_{AC}\,h_{AC}^3 + E_{PCC}h_{PCC}^3 + E_{Base}h_{Base}^3 + \\ 12\left[\begin{array}{l} E_{AC}\,h_{AC}\left(\frac{h_{AC}}{2}-x\right)^2 + E_{PCC}h_{PCC}\left(h_{AC}+\frac{h_{PCC}}{2}-x\right)^2 \\ + E_{Base}h_{Base}\left(h_{AC}+h_{PCC}+\frac{h_{Base}}{2}-x\right)^2 \end{array}\right] \end{array}\right) \tag{3.54}$$

where

E_{eq}, E_{AC}, E_{PCC}, E_{Base} are the Young's moduli of the equivalent, AC, PCC, and base layers, respectively,

h_{eq}, h_{AC}, h_{PCC}, h_{Base} are the thicknesses of the equivalent, AC, PCC, and base layers, respectively and

x is the distance of the neutral axis of the composite pavement from the top of the AC layer.

The unit weight of the equivalent single layer is calculated as:

$$\gamma_{eq} = \frac{h_{AC}\gamma_{AC} + h_{PCC}\gamma_{PCC} + h_{Base}\gamma_{Base}}{h_{eq}} \tag{3.55}$$

where

γ_{eq}, γ_{AC}, γ_{PCC}, γ_{Base} are the unit weights of the equivalent, AC, PCC, and base layers, respectively.

3.3.2 Equivalent Linear Temperature Gradient in the Equivalent Single Layer Slab

It has been shown by Khazanovich (*1994*) that bending of a multi-layered pavement due to an arbitrary temperature distribution throughout the pavement system can be described

by the bending of an equivalent single layer slab subjected to a linear temperature gradient. The equivalent linear temperature gradient in the equivalent single layer slab was approximated in terms of the temperature data of the multi-layered pavement as follows:

$$\Delta T_{eq} = \frac{-12}{h_{eq}^2}\left(\begin{array}{l} \dfrac{\alpha_{AC}E_{AC}}{\alpha_{eq}E_{eq}}\dfrac{h_{AC}}{24}\displaystyle\sum_{i=1}^{4}\left(\begin{array}{l}(T_i - T_{oACi})*\left((3i-2)*\dfrac{h_{AC}}{4} - 3x\right) \\ +(T_{i+1} - T_{oACi+1})*\left((3i-1)*\dfrac{h_{AC}}{4} - 3x\right)\end{array}\right) \\ +\dfrac{\alpha_{PCC}E_{PCC}}{\alpha_{eq}E_{eq}}\dfrac{h_{PCC}}{60}\displaystyle\sum_{i=1}^{10}\left(\begin{array}{l}T_i*\left((3i-2)*\dfrac{h_{PCC}}{10} - 3(x-h_{AC})\right) \\ +T_{i+1}*\left((3i-1)*\dfrac{h_{PCC}}{10} - 3(x-h_{AC})\right)\end{array}\right) \\ -\dfrac{\alpha_{PCC}E_{PCC}}{\alpha_{eq}E_{eq}}\dfrac{T_{11}}{2}h_{PCC}\left(h_{PCC}+2h_{AC}-2x\right) \end{array}\right) \tag{3.56}$$

where

ΔT_{eq} is the difference between the top and bottom surface temperatures of the equivalent single layer slab,

T_i and T_{oi} are the temperature and reference temperature at point *i*, respectively,

α_{eq}, α_{AC}, α_{PCC} and α_{Base} are coefficients of thermal expansion of the equivalent, AC, PCC and base layers, respectively.

Appendix A details the procedure for calculating the equivalent linear temperature gradient given in equation (3.56).

3.3.3 Equivalent Linear Creep Strain Gradient in the Equivalent Single Layer Slab

Analogous to an arbitrary temperature profile that can be expressed in terms of an equivalent linear temperature gradient; the arbitrary creep strain profile of the composite pavement can also be expressed as an equivalent linear creep strain gradient present in the equivalent single layer slab. Therefore, analogous to equation (3.56) for equivalent linear temperature gradient, the equivalent linear creep strain gradient can be written as:

$$\Delta T^{cr} = \frac{-12}{h_{eq}^2}\left(\frac{E_{AC}}{E_{eq}}\frac{h_{AC}}{24}\sum_{i=1}^{4}\left(\begin{array}{l}(\varepsilon_i^{cr} - \varepsilon_{oACi}^{cr})*\left((3i-2)*\frac{h_{AC}}{4} - 3x\right) \\ +(\varepsilon_{i+1}^{cr} - \varepsilon_{oACi+1}^{cr})*\left((3i-1)*\frac{h_{AC}}{4} - 3x\right)\end{array}\right)\right) \tag{3.57}$$

where

ΔT^{cr} is the difference between the top and bottom surface creep strains in the equivalent single layer slab, and

$\varepsilon^{cr}{}_i$ and $\varepsilon^{cr}{}_{oi}$ are the creep strains and the reference creep strains at point *i*, respectively.

3.3.4 Additional Stresses in the Composite Pavements Due to Non-linear-strain-causing Temperature and Non-linear-strain-causing Creep Strains Components

As discussed in Chapter 2, it was shown by Khazanovich (*1994*) that any arbitrary temperature profile can be separated into three components: constant-strain-causing temperature component, linear-strain-causing temperature component, and nonlinear-strain-causing temperature component. The constant-strain-causing temperature component does not cause stresses if the pavement is free to expand and contract. The

linear-strain-causing temperature component produces bending stresses that can be calculated from the FE solution for bending of an equivalent single layer slab subjected to an equivalent linear temperature gradient determined from equation (3.56). The nonlinear-strain-causing temperature component produces self-equilibrating stresses.

The total temperature at any point in the slab can be presented in terms of the various temperature components. Therefore, the nonlinear-strain-causing temperature component is given as:

$$T_{NL}(z) - T_o(z) = T(z) - \left[T_c(z) - T_o(z)\right] - \left[T_L(z) - T_o(z)\right] - T_o(z) \tag{3.58}$$

where

T is the temperature at the point of interest in the composite pavement,

z is the depth of the point of interest from the neutral axis,

T_0 is the reference temperature,

T_C is the constant-strain-causing temperature component,

T_L is the linear-strain-causing temperature component, and

T_{NL} is the nonlinear-strain-causing temperature component.

The stress due to the nonlinear-strain-causing temperature component, σ_{NL} is equal to:

$$\sigma_{NL}(z) = -\frac{E(z)\alpha(z)}{(1-\mu)}\left(T_{NL}(z) - T_o(z)\right) \tag{3.59}$$

where

E, α, and μ are the Young's modulus, coefficient of thermal expansion, and Poisson's ratio, respectively, at the point of interest.

For the case of a single layer viscoelastic slab creep strains are linear through the slab thickness. However, for a multi-layer slab, this is not necessarily the case. Similarly to the nonlinear-strain-causing temperature component, the nonlinear-strain-causing creep strain component is defined as:

$$\left\{\varepsilon_{NL}^{cr}(z)\right\}-\left\{\varepsilon_{0}^{cr}(z)\right\}=\left\{\varepsilon^{cr}(z)\right\}-\left[\left\{\varepsilon_{c}^{cr}(z)\right\}-\left\{\varepsilon_{0}^{cr}(z)\right\}\right]-\left[\left\{\varepsilon_{L}^{cr}(z)\right\}-\left\{\varepsilon_{0}^{cr}(z)\right\}\right]-\left\{\varepsilon_{0}^{cr}(z)\right\} \quad (3.60)$$

where

ε^{cr} is the creep strain at the point of interest in the composite pavement,

z is the depth of the point of interest from the neutral axis,

ε_{0}^{cr} is the reference creep strain,

ε_{c}^{cr} is the constant-strain-causing creep strain component,

ε_{L}^{cr} is the linear-strain-causing creep strain component, and

ε_{NL}^{cr} is the nonlinear-strain-causing creep strain component.

The stress due to the nonlinear-strain-causing creep strain component, σ_{NL}^{cr} is given as:

$$\left\{\sigma_{NL}^{cr}(z)\right\}=-[\overline{D}]\left(\left\{\varepsilon_{NL}^{cr}(z)\right\}-\left\{\varepsilon_{0}^{cr}(z)\right\}\right) \quad (3.61)$$

where $[\overline{D}]$ is the material property matrix defined in equation (3.32).

3.3.5 Total Stress in the Composite Pavements

Finally, the total stress at any point in the multi-layered composite pavement at any time *t* can be written as:

$$\sigma(x,y,z,t) = \beta(z) * \sigma_{eq}(x,y,t) + \sigma_{NL}(z) + \sigma_{NL}^{cr}(x,y,z,t) \tag{3.62}$$

$$\beta(z) = \frac{2z}{h_{eq}} \frac{E(z)}{E_{eq}} \tag{3.63}$$

where

β is the factor that converts the linear bending stresses at the bottom of the equivalent single layer slab to the linear bending stresses in the multi-layered slab at the depth of interest *z*,

σ_{eq} is the stress at the bottom surface of the equivalent single layer slab,

σ_{NL} is the stress due to the nonlinear-strain-causing temperature component at the depth of interest, and

σ_{NL}^{cr} is the stress due to the nonlinear-strain-causing creep stain component at the depth of interest.

3.4 Step-by-Step Procedure for Computing the Stresses in the Composite Pavement

In this section, the step-by-step procedure used to develop the FE code based on the FE formulation is presented. The FE code was programmed using the programming language FORTRAN 90 (*Visual Numerics, Inc. 1997*) and the commercial package MATHEMATICA (*Wolfram Research, Inc. 1988*).

Step 1: Read inputs – The input file format mirrors an ISLAB2000 input file. The inputs required for the analysis of composite pavements include slab size, mesh configuration, layer properties, interface conditions, properties of the Winkler foundation, temperature

profile, and traffic loading. Additional inputs such as number and size of time increments and coefficients of the Prony series for representing the viscoelastic AC layer (or viscoelastic Winkler foundation, if present) were also included in the input file.

Step 2: Determine the equivalent single layer slab parameters – The thickness and unit weight for an equivalent single layer slab with a Young's modulus of 4.0E+6 psi and coefficient of thermal expansion of 5.5E-6 1/°F are computed depending on the interface conditions of the composite pavement. Also, the equivalent linear temperature gradient in the equivalent single layer slab and the corresponding non-linear-strain-causing temperature stresses in the composite pavement are computed. Appendix A details the procedure adopted in this step for different interface conditions in the composite pavement.

Step 3: Generate a finite element mesh – A finite element mesh consisting of regular four-node rectangular plate elements with three degrees of freedom per node is generated over the dimensions of the equivalent single layer slab.

Step 4: Compute the stiffness matrix – The element stiffness matrix $[k]_e$ is computed using equation (3.33). The boundary conditions present due to contact of the equivalent single layer slab with the spring formulation of the Winkler foundation are enforced on the element stiffness matrix. Finally, the global stiffness matrix $[K]$ is generated by assembling the element stiffness matrix for each element at the appropriate global degree

of freedom. The global stiffness matrix is generated in sparse format.

Step 5: Compute the global force vector – The forces due to traffic loading, self-weight of the slab, thermal strains, and creep strains are computed at time t_j. At the initial time t_1, the fictitious forces due to creep strains are equal to zero. The global forces acting on the equivalent single layer slab are calculated by adding all the forces at the appropriate degree of freedom for each element.

Step 6: Compute displacements – Using Cholesky's factorization, the system of equations (3.52) is solved to find the global displacements.

Step 7: Check contact condition – The contact between the equivalent single layer slab and the Winkler foundation is checked using the vertical displacement of the nodes. If the vertical displacement at a plate node is positive, it indicates that the node is in contact with the foundation. If the vertical displacement at a node is negative, it indicates that the node is not in contact with the foundation. The change in sign of a nodal displacement between one time step and the next implies that the contact condition at the node has changed. The foundation stiffness matrix $[K_{dd\ foundation}]_e$ is then revised for those nodes and the global stiffness matrix $[K]$ is updated to reflect the change. Steps 4 and 6 are repeated if the contact condition changes between any two time steps.

Step 8: Compute stresses in the equivalent single layer slab – The total strain and elastic

stress in the equivalent single layer slab are computed using equations (3.35) and (3.53), respectively, at time t_j.

Step 9: Compute creep strains – The increment of creep strains corresponding to the *i*-th term of the Kelvin-Voigt element are computed using equation (3.41) at time t_j. The resulting creep strain for each Kelvin-Voigt element and the total creep strain in the equivalent single layer slab at time t_j are updated.

Step 10: Calculate nodal stresses – The average stress at each node at the top and bottom of the equivalent single layer slab is computed at time t_j. Further, the stresses for each layer of the composite pavement system are computed. For example, the total stresses at the top and bottom of the PCC layer of the composite pavement are calculated as follows:

$$\sigma_{PCC,Top} = \frac{2*(-x+h_{AC})}{h_{eq}}\sigma_{eq} + \sigma_{NL,top} + \sigma_{NL,top}^{cr} \tag{3.64}$$

$$\sigma_{PCC,Bot} = \frac{2*(h_{PCC}+h_{AC}-x)}{h_{eq}}\sigma_{eq} + \sigma_{NL,bot} + \sigma_{NL,bot}^{cr} \tag{3.65}$$

Repeat steps 5 to 10 for the next time t_{j+1}.

Step 11: Output results – The displacement and stresses in the composite pavement at each node are printed in ISLAB2000 output format.

3.5 Validation of the Finite Element Model

The FE model presented in the preceding sections has the capability of analyzing a multi-layered pavement incorporating elastic and/or viscoelastic layers placed over an elastic or a viscoelastic Winkler foundation. This section presents simple examples validating the finite element implementation. The following cases are considered:

1. A viscoelastic plate placed on a viscoelastic Winkler foundation,
2. A viscoelastic plate with simply supported corners,
3. Verification of formulation for multi-layered slabs, and
4. Sensitivity of the viscoelastic FE model to internal parameters.

3.5.1 Viscoelastic Plate on Viscoelastic Winkler Foundation

To verify the FE code, a semi-analytical solution is obtained for a viscoelastic plate placed on the viscoelastic Winkler foundation when the creep compliance functions of the viscoelastic plate and the viscoelastic Winkler foundation are proportional. The semi-analytical solution is compared with the finite element solution.

The governing equation for an elastic plate resting on an elastic Winkler foundation has the following form (*Timoshenko and Woinowsky-Krieger 1959*):

$$D_0 \nabla^4 w(x) + k_0 w(x) = p(x) \tag{3.66}$$

where

w is the deflection of the plate,

k_0 is the coefficient of subgrade reaction of the Winkler foundation,

p is the load per unit area acting on the plate,

x represents the spatial coordinates x, y, and z, and

D_0 is the stiffness of the plate given as follows:

$$D_0 = \frac{E_0 h^3}{12(1-\mu^2)} \tag{3.67}$$

where

E_0 is the Young's modulus of the plate,

h is the thickness of the plate, and

μ is the Poisson's ratio.

Consider a viscoelastic plate resting on a viscoelastic Winkler foundation. The governing equation for the plate can be written as (*Li et al. 2009*):

$$\tilde{D}\nabla^4 w(x,t) + \tilde{k} w(x,t) = p(x,t) \tag{3.68}$$

where

$w(x,t)$ is the deflection of the viscoelastic plate at time t,

$p(x,t)$ is the load per unit area acting on the viscoelastic plate at time t,

$\tilde{D}$, the "stiffness" of the viscoelastic plate, is an operator defined as:

$$\tilde{D} f(t) = \frac{E_0 h^3}{12\ (1-\mu^2)} \tilde{J}^{*-1} f(t) = D_0 \tilde{J}^{*-1} f(t) \tag{3.69}$$

and, $\tilde{k}$ the "operator of subgrade reaction" of the viscoelastic foundation relating the deflection of the subgrade with the history of the applied pressure at the same point. Assume that the operator of subgrade reaction has the following form:

$$\tilde{k} f(t) = k_0 \tilde{J}^{*-1} f(t) \tag{3.70}$$

The operator $\tilde{J}^*$ is the normalized creep compliance operator defined using

equations (3.6) and (3.17) in Section 3.1 as follows:

$$\tilde{J}^{*} f(t) = \frac{\tilde{J} f(t)}{J(0)} \tag{3.71}$$

The creep compliance of operators $\tilde{D}$ and $\tilde{k}$ is proportional. By substituting equations (3.69) and (3.70) in (3.68), we get:

$$D_0 \tilde{J}^{*-1} \nabla^4 w(x,t) + k_0 \tilde{J}^{*-1} w(x,t) = p(x,t) \tag{3.72a}$$

or,

$$D_0 \nabla^4 \left(\tilde{J}^{*-1} w(x,t) \right) + k_0 \left(\tilde{J}^{*-1} w(x,t) \right) = p(x,t) \tag{3.72b}$$

Now, a fictitious deflection w_1 is introduced such that:

$$w_1(x,t) = \tilde{J}^{*-1} w(x,t) \tag{3.73}$$

Substituting equation (3.73) into equation (3.72) results in:

$$D_0 \nabla^4 w_1(x,t) + k_0 w_1(x,t) = p(x,t) \tag{3.74}$$

For any time *t*, equation (3.74) is identical to the governing equation for an elastic plate placed on the elastic Winkler foundation. If the plate is loaded so that:

$$\begin{aligned} p(x,t) &= p_0(x) H(t) \\ H(t) &= \begin{cases} 1 & if \ \mathrm{t} \geq 0 \\ 0 & if \ \mathrm{t} < 0 \end{cases} \end{aligned} \tag{3.75}$$

where, $H(t)$ is the Heaviside step function, then the deflection of the plate has the following form:

$$w_1(x,t) = w_1(x) H(t) \tag{3.76}$$

If a solution of the elastic problem is obtained analytically or numerically, then the solution of the corresponding viscoelastic problem can be obtained as follows:

$$w(x,t) = \tilde{J}^{*}\left(w_1(x)H(t)\right) \tag{3.77}$$

It can be also easily shown that for this boundary value problem the stresses in the viscoelastic plate are proportional to the applied loading. Since the applied load does not change in time for $t \geq 0$, the stresses in the viscoelastic slab do not vary with time for $t \geq 0$.

To verify the finite element program, a semi-analytical solution was obtained and compared with the finite element solution in which a 15 ft long, 12 ft wide, and 9 in-thick viscoelastic plate was placed on a viscoelastic Winkler foundation. The plate was loaded with a constant 100 psi pressure acting at the center of the slab over a footprint of 60 in x 48 in. A uniform mesh of element size equal to 6 in was generated on the plate surface. The load and mesh configuration are shown in Figure 3.5.

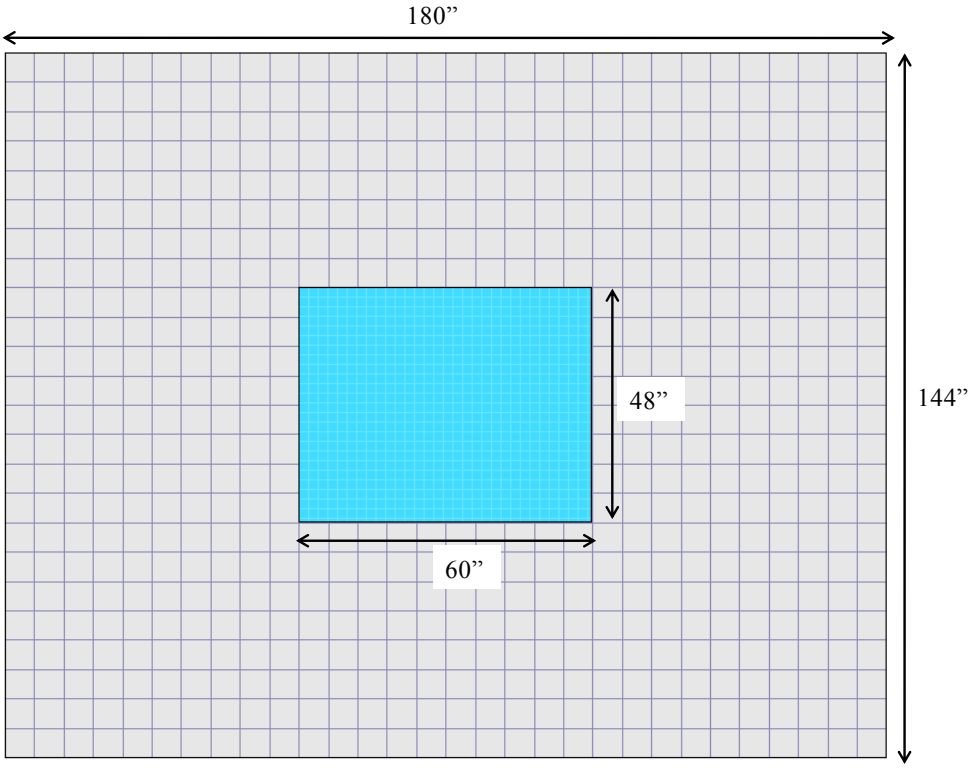

Figure 3.5 Mesh and load configuration for the composite pavement subjected to a wheel load.

The creep compliance of the viscoelastic material is represented by a Prony series in the form of a two-term generalized Kelvin-Voigt model presented in Figure 3.2. Table 3.1 lists the parameters of the Kelvin-Voigt model used to define the creep compliance function for the viscoelastic plate and the viscoelastic Winkler foundation.

Table 3.1 Parameters of the Kelvin-Voigt model for the plate and Winkler foundation.

Instantaneous modulus		**Normalized creep compliance parameters**			
Plate	Winkler foundation	Spring stiffness		Dashpot viscosity	
E_0, psi	k_0, psi/in	E_1*	E_2*	η_1*	η_2*
4.0e6	100	0.0238	0.0254	2.8269	0.2494

The FE solution is obtained by executing the FE code for a viscoelastic plate placed on a viscoelastic Winkler foundation. The semi-analytical solution for deflections at any time t is derived by multiplying the elastic deflections at the initial time $t = 0$ obtained from the FE solution with the operator $\tilde{J}^*$, as given in equation (3.77). Figure 3.6 presents the deflections computed using the FE model and the semi-analytical solution for a total time of 400 seconds.

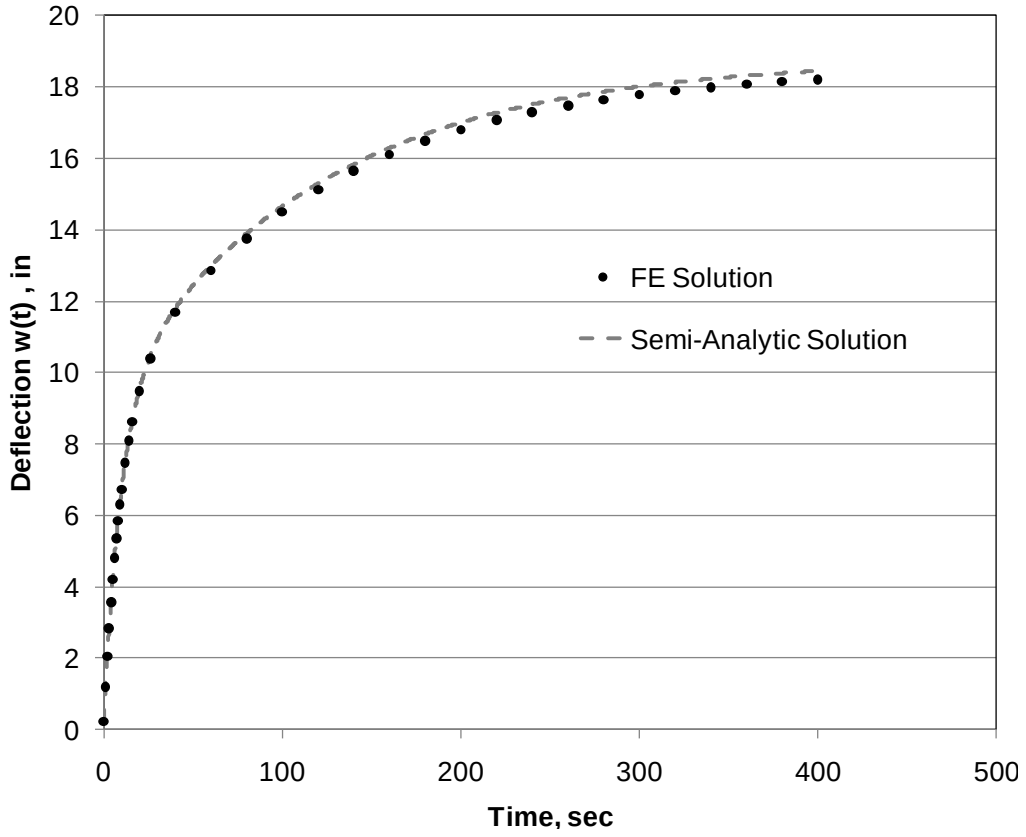

Figure 3.6 Comparison of deflections for a viscoelastic plate placed on a viscoelastic Winkler foundation.

A good agreement is found between the deflections obtained from the semi-analytical solution and the FE solution. Figure 3.7 presents the bottom surface stress at the center of the plate computed using the FE model for a total time of 400 seconds.

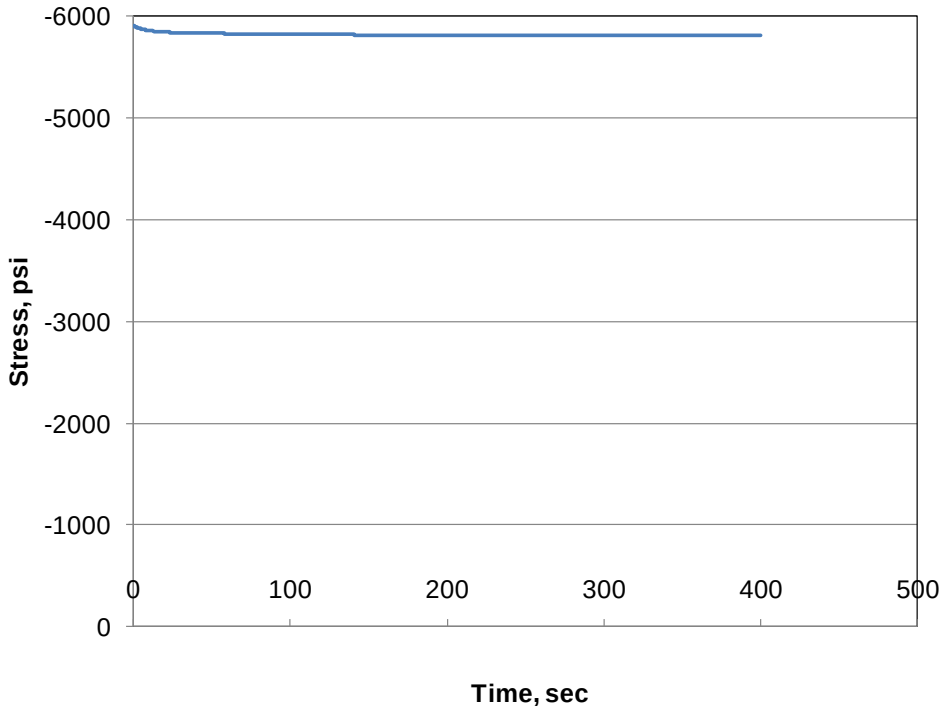

Figure 3.7 Stress at the bottom of the viscoelastic plate placed on viscoelastic Winkler foundation.

A small variation is observed in the stresses at the bottom of the viscoelastic plate during the initial increments of time. Since the time is discretized into small intervals, the observed error is attributed to the size of the time interval selected.

3.5.2 Viscoelastic Plate with Simply Supported Corners

Consider a viscoelastic plate supported at the corners so that the vertical deflections of the corners are equal to zero. The solution of the plate can be derived if appropriate

boundary conditions are satisfied. The governing equation and the boundary conditions are given as follows:

$$\tilde{D}\nabla^4 w(x,t) = p(x,t) \tag{3.78}$$

and,

$$w(x,t) = 0 \quad \text{for } x \in S \tag{3.79}$$

where

$\tilde{D}$ is the stiffness operator for the viscoelastic plate is defined by equation (3.69),

$w(x,t)$ is the deflection of the plate at time t,

$p(x,t)$ is the applied load at time t and is defined by equation (3.75), and

S is the set of spatial coordinates at which the boundary conditions are imposed.

Applying equations (3.69) and (3.73) to equation (3.78), yields the following equation:

$$D_0\nabla^4\left(\tilde{J}^{*-1} w(x,t)\right) = p(x,t) \tag{3.80a}$$

or,

$$D_0\nabla^4\left(w_1(x,t)\right) = p(x,t) \tag{3.80b}$$

Multiplying both sides of equation (3.79) by the operator $\tilde{J}^*$ from the left and applying equation (3.73) leads to the following:

$$\tilde{J}^{*-1} w(x,t) = \tilde{J}^{*-1} 0 \quad \text{for } x \in S \tag{3.81a}$$

or,

$$w_1(x,t) = 0 \quad \text{for } x \in S \tag{3.81b}$$

Equations (3.80b) and (3.81b) are identical to the governing equation and boundary condition, respectively, for an elastic plate with simply supported corners. This implies that equation (3.77), which relates the viscoelastic deflections to the elastic deflections as a function of the operator $\tilde{J}^*$ at any time *t*, is also a solution for a viscoelastic plate with simply supported corners. The solution given by equation (3.77) is used to verify the FE solution for a viscoelastic plate with simply supported corners.

A 15 ft long, 12 ft wide, and 9 in thick viscoelastic plate with simply supported corners is analyzed using the FE model. The plate is loaded with a 100 psi pressure over a footprint of 60 in x 48 in at all times as shown in Figure 3.5. The creep compliance function for the viscoelastic plate is defined using the parameters of the Kelvin-Voigt model presented in Table 3.1.

The FE solution for the deflections of the viscoelastic plate with simply supported corners is obtained by executing the FE code. The semi-analytical solution for deflections at any time *t* is derived by multiplying the elastic deflections at the initial time $t = 0$ obtained from the FE solution with the operator $\tilde{J}^*$. Figure 3.8 presents the comparison of deflections computed using the FE model and the semi-analytical solution for a total time of 400 seconds.

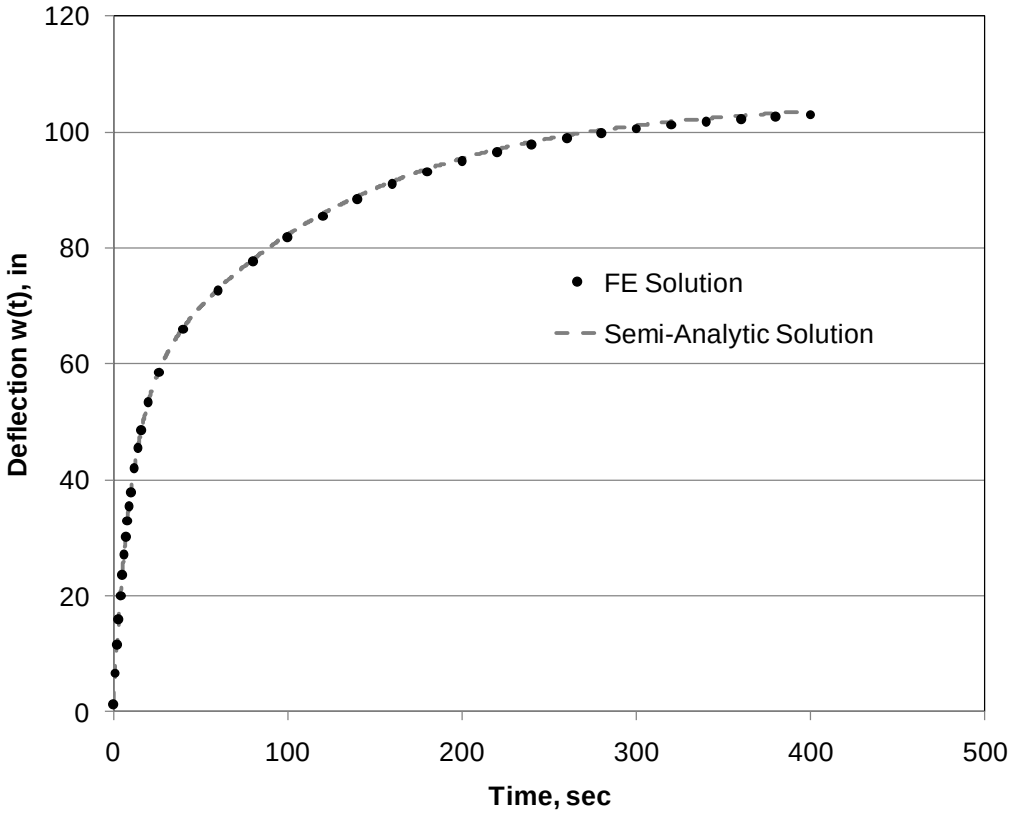

Figure 3.8 Comparison of deflections for a viscoelastic plate with simply supported corners.

The deflections obtained from the semi-analytical solution and the FE solution for a viscoelastic plate with simply supported corners match well.

3.5.3 Verification of the Formulation for Multi-Layered Slabs

The FE code has built-in functionality to analyze single-layer, two-layered and three-layered pavements. To verify the ability of the FE code to analyze a multi-layered slab-on-grade, several verification examples were considered. A multi-layered composite slab resting on an elastic Winkler foundation was loaded with 100 psi of pressure acting in the

form of a single axle dual wheel configuration. The size of the slab was 180 in x 144 in. The coefficient of subgrade reaction for the elastic Winkler foundation was equal to 100 psi/in. A uniform mesh of element size 6 in x 6 in was generated as shown in Figure 3.9.

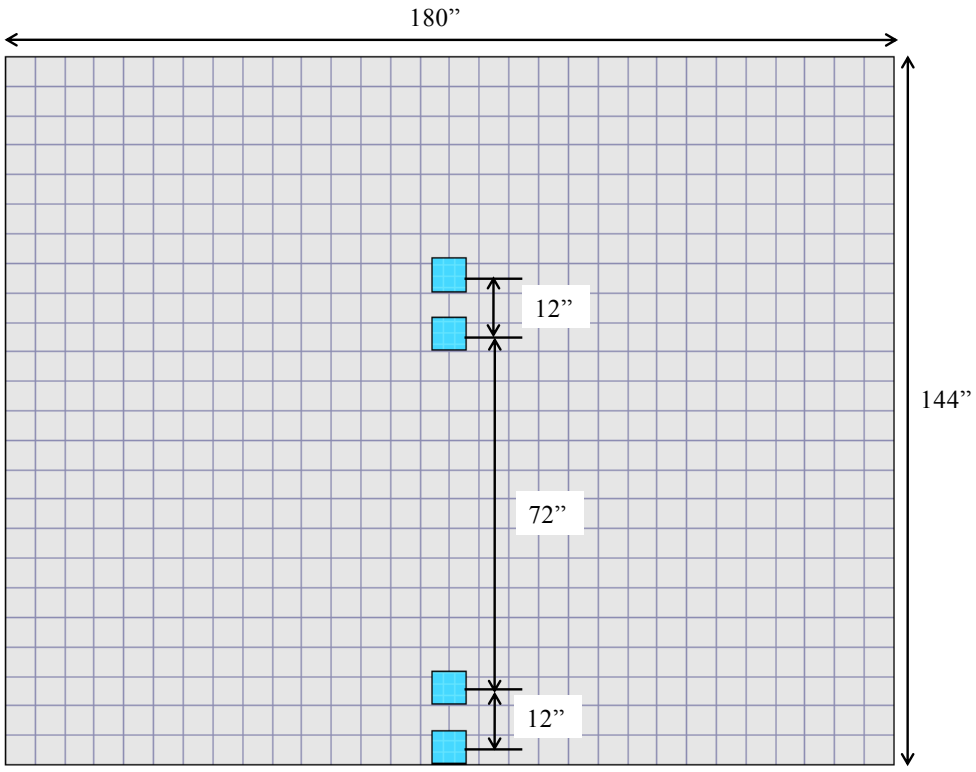

Figure 3.9 Mesh and loading configuration for the composite pavement subjected to a single-axle dual-wheel load.

Elastic and viscoelastic analyses were conducted to verify the ability of the FE code to analyze a multi-layered slab-on-grade. If the FE code is robust, the stresses at a particular point obtained from the analysis of a three-layered pavement system and a corresponding single-layer (or two-layered) system must be equal. It must be noted that all the layers of the three-layered slab and the layer(s) of the corresponding single or two-layered slab should have the same Poisson’s ratio μ.

The elastic analysis was conducted at the initial time (t = 0). Table 3.2 presents the layer properties for the following cases considered for the elastic analysis:

- Case 1 – To verify the ability of the FE code to analyze single-layer systems, a three-layer slab-on-grade is compared with a corresponding single-layer slab-on-grade when all layers have the same material properties. In this case, the thickness of the corresponding single-layer slab is equal to the sum of the thicknesses of all the layers of the three-layer slab.
- Case 2 – To verify the ability of the FE code to analyze two-layer systems, a three-layer slab-on-grade was compared with a corresponding two-layer slab-on-grade. The first and second layers of the three-layer slab had the same material properties, and the thickness of the first layer of the corresponding two-layer slab was equal to the sum of the thicknesses of the first and second layers of the three-layer slab.
- Case 3 – The ability of the FE code to analyze a three-layer system is verified when one of the layers is eliminated by setting its thickness equal to zero. In this case, a corresponding two-layer slab-on-grade is analyzed with the same layer thicknesses and material properties as those for the second and third layers of the three-layer slab.

Table 3.2 Layer properties for the elastic analysis.

	Three-layered pavement		**Single- / two-layered pavement**	
Case 1	h1 = 9 in	E = 4.0E+06 psi	h = 20 in	E = 4.0E+06 psi
	h2 = 5 in	E = 4.0E+06 psi		
	h3 = 6 in	E = 4.0E+06 psi		

	Three-layered pavement		Single- / two-layered pavement	
Case 2	h1 = 9 in	E = 4.0E+06 psi	h1 = 14 in	E = 4.0E+06 psi
	h2 = 5 in	E = 4.0E+06 psi		
	h3 = 6 in	E3 = 4.0E+04 psi	h2 = 6 in	E2 = 4.0E+04 psi
Case 3	h1 = 0 in	E1 = 2.0E+05 psi	h1 = 5 in	E1 = 4.0E+06 psi
	h2 = 5 in	E2 = 4.0E+06 psi	h2 = 6 in	E2 = 4.0E+04 psi
	h3 = 6 in	E3 = 4.0E+04 psi		

Figure 3.10 presents the comparison of stresses at the bottom of the second layer of a three-layer system at the center of the slab.

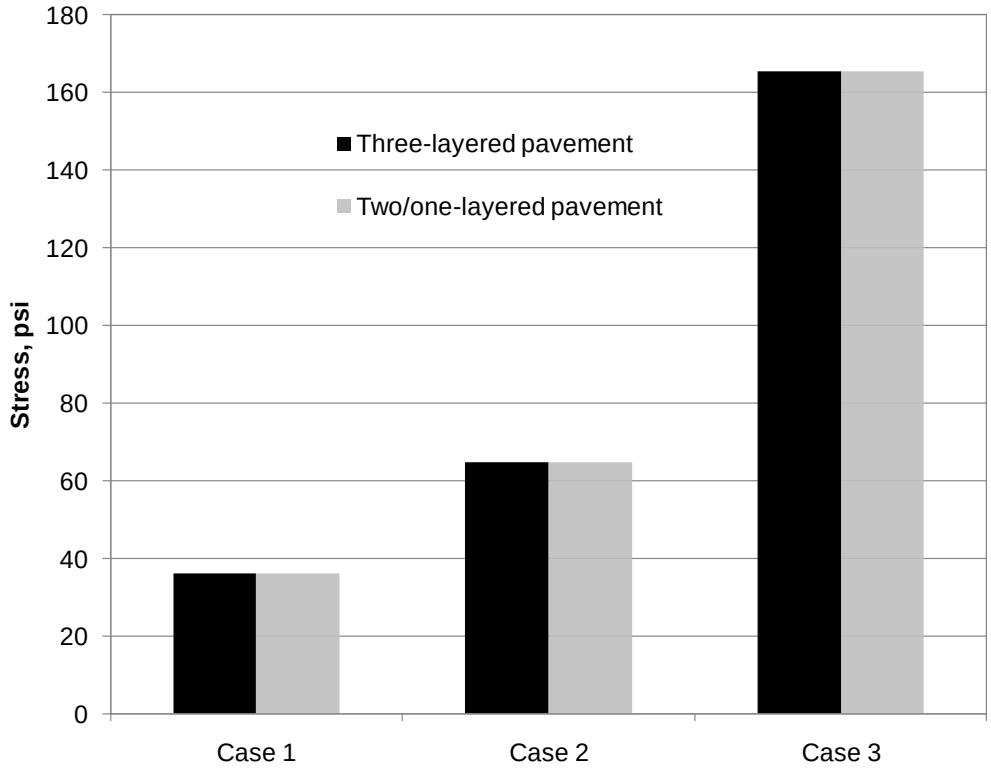

Figure 3.10 Stress from three-layered analysis versus single- or two-layered analyses.

Next, a viscoelastic analysis is conducted with a 9 in thick viscoelastic surface layer (layer 1) for the multi-layered slab. The creep compliance function for the first

layer is represented using the generalized two-term Kelvin-Voigt model. The parameters of the Kelvin-Voigt model are presented in Table 3.3.

Table 3.3 Kelvin-Voigt parameters for the viscoelastic surface layer.

Element #	Spring stiffness, psi	Dashpot viscosity, psi-sec
0	200000	--
1	95265	11307535
2	101500	997600

For all the cases in the viscoelastic analysis, the stresses from a three-layered pavement system are compared with the stresses from a corresponding two-layered system.

- Case 4 – The ability of the FE code to perform a viscoelastic analysis for multi-layered systems was verified. The second and third layers of a three-layer slab had the same material properties. The thickness of the second layer of a corresponding two-layer slab was equal to the sum of thicknesses of the second and third layers of the three-layer slab.
- Case 5 – The ability of the FE code to perform a viscoelastic analysis was verified when the second layer of a three-layer slab was eliminated by setting its thickness equal to zero. In this case, a corresponding two-layer slab-on-grade was analyzed with layer thicknesses and material properties the same as those for the first and third layers of the three-layer slab.
- Case 6 – This case is similar to case 5 but the third layer of the three-layer slab was eliminated by setting its thickness equal to zero.

Table 3.4 presents the properties of the underlying layers of the multi-layered pavements considered for the viscoelastic analysis.

Table 3.4 Layer properties for multi-layered composite pavement.

	Three-layered pavement (3LS)		**Two-layered pavement (2LS)**	
Case 4	h2 = 5 in	E2 = 4.0E+06 psi	h2 = 11 in	E2 = 4.0E+06 psi
	h3 = 6 in	E3 = 4.0E+06 psi		
Case 5	h2 = 0 in	E2 = 4.0E+06 psi	h2 = 6 in	E2 = 4.0E+04 psi
	h3 = 6 in	E3 = 4.0E+04 psi		
Case 6	h2 = 5 in	E2 = 4.0E+06 psi	h2 = 5 in	E2 = 4.0E+06 psi
	h3 = 0 in	E3 = 4.0E+04 psi		

Figures 3.11 and 3.12 present the comparison of stresses at the bottom of the viscoelastic surface layer (layer 1) at the center of the slab.

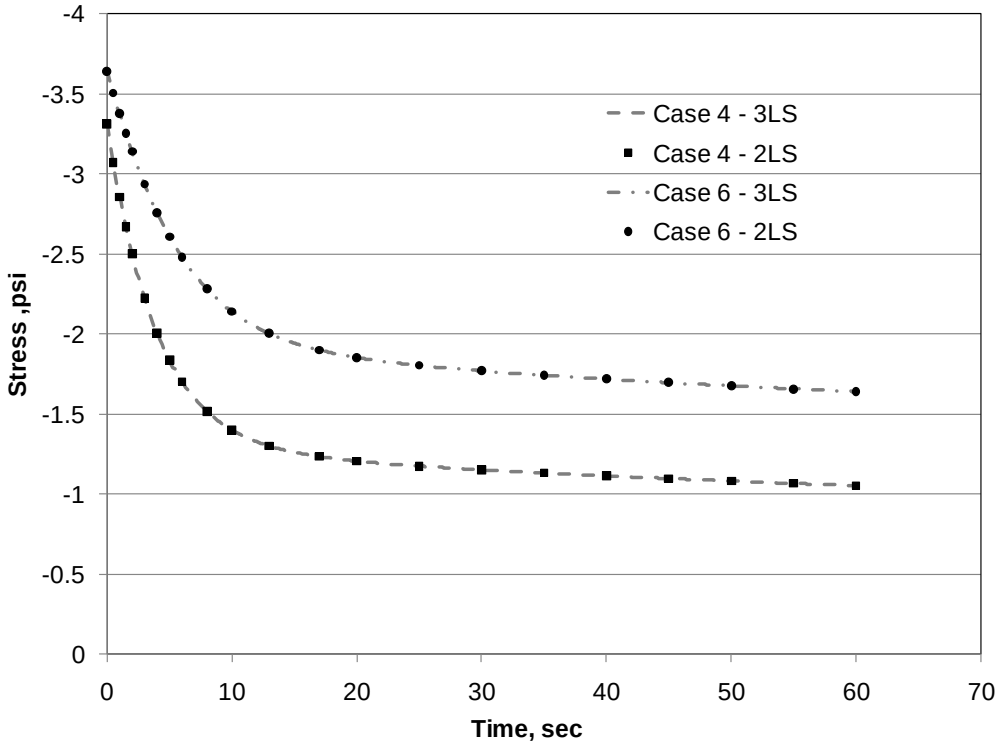

Figure 3.11 Stress versus time for cases 4 and 6 using the viscoelastic FE model.

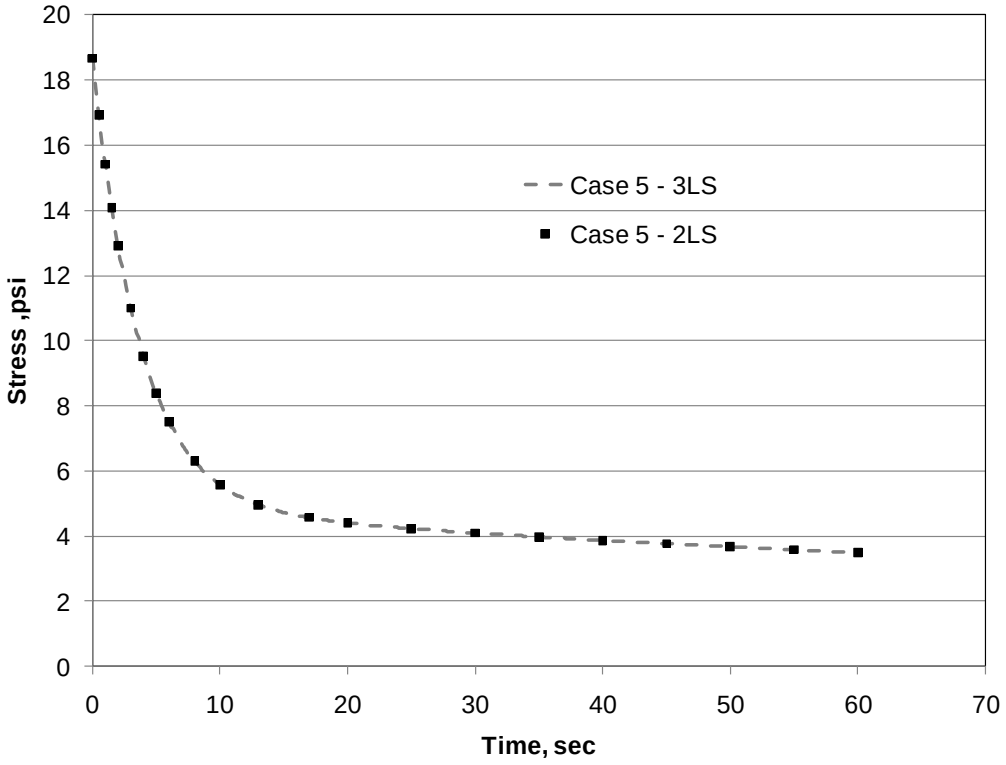

Figure 3.12 Stress versus time for case 5 using the viscoelastic FE model.

Excellent agreement is obtained between the stress from the three-layered analyses and that from the single or two-layered analyses for all cases.

3.5.4 Sensitivity of the Viscoelastic FE Model to Internal Parameters

The sensitivity of the FE model to the following internal parameters was verified:

1. Implementation of creep compliance function using the Prony series
    a. Parameters of the Kelvin-Voigt element
    b. Number of Kelvin-Voigt elements
2. Presence of the viscoelastic layer

3.5.4.1 Sensitivity of the FE Model to Parameters of Kelvin-Voigt Element

As established in Section 3.1, the creep compliance function is commonly expressed in the form of an *N*-term Prony series. For each term of the Prony series there are two coefficients defining the stress-strain relationship of a viscoelastic material. These coefficients can be interpreted as the spring stiffness and dashpot viscosity of commonly adopted physical models such as the Kelvin-Voigt model. In this example, sensitivity of the FE model to the parameters of the Kelvin-Voigt model is verified.

Consider the single layer viscoelastic plate presented in Section 3.5.1. The plate geometry, mesh, and loading geometry are as shown in Figure 3.5. The plate rests on an elastic Winkler foundation with a coefficient of subgrade reaction equal to 100 psi/in. The viscoelastic material characterization of the plate is defined using the spring and dashpot properties of a one-term Kelvin-Voigt element connected to an elastic spring, presented in Table 3.5.

Table 3.5 Parameters of the Kelvin-Voigt element for the viscoelastic plate.

Element #	**Spring stiffness, psi**	**Dashpot viscosity, psi-sec**
0	98988.175	--
1	95265	1.0E+04 to 1.0E+07

The dashpot viscosity of the Kelvin-Voigt element is varied between 1.0E+04 psi-sec and 1.0E+07 psi-sec (1.0E+04, 1.0E+05, 2.0E+05, 4.0E+05, 1.0E+06, 1.0E+07). Deflections and stresses in the plate under the applied load are computed using the FE model. Figures 3.13 and 3.14 show the deflections and top surface stresses at the plate

center versus time, respectively, for the factorial of dashpot viscosities of the Kelvin-Voigt element.

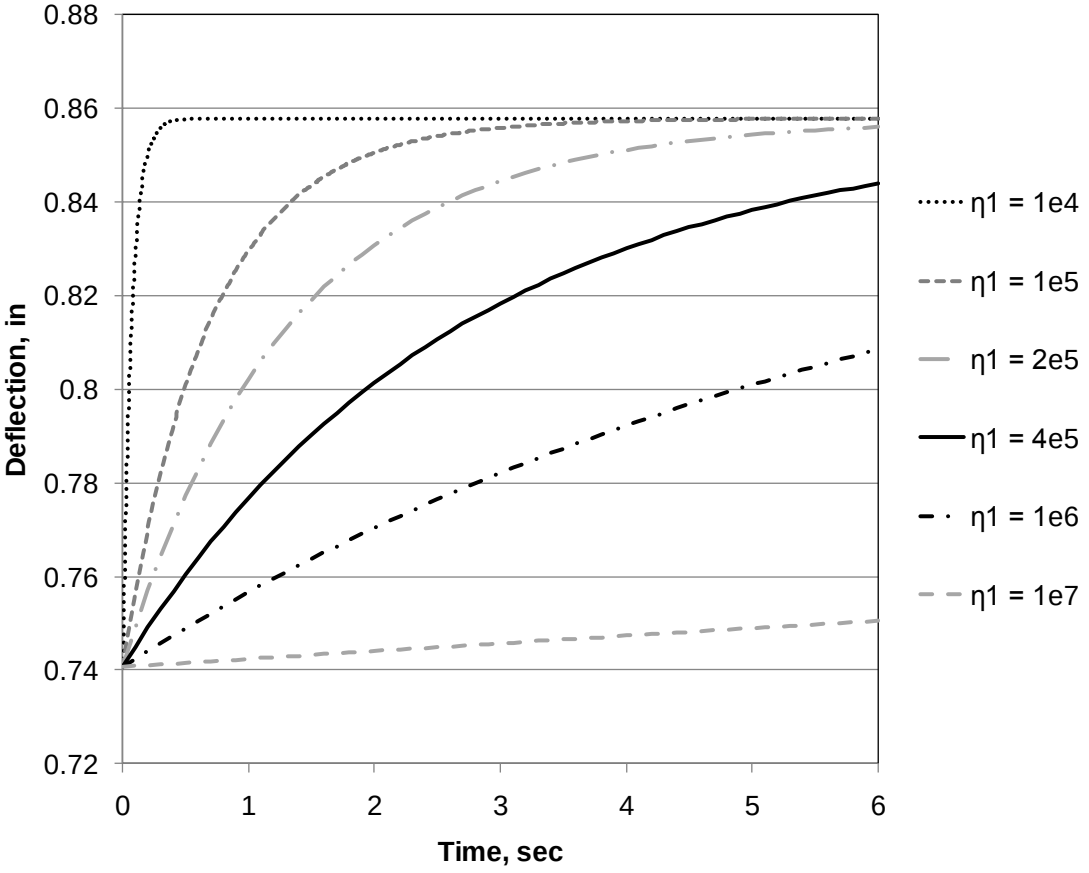

Figure 3.13 Deflection versus time for a factorial of dashpot viscosities of the Kelvin-Voigt element.

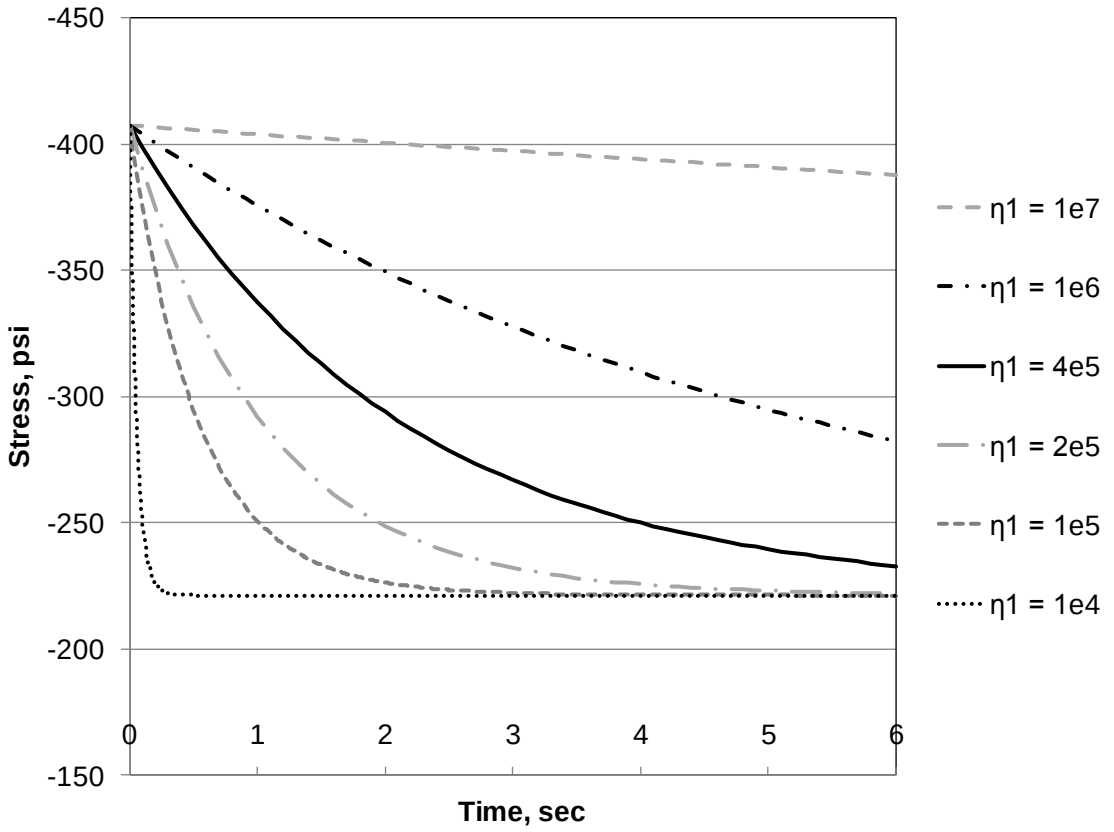

Figure 3.14 Stress versus time for a factorial of dashpot viscosities of the Kelvin-Voigt element.

The deflection and stress for the factorial of dashpot viscosities vary between the deflection and stress for the extreme values of the viscosity considered. Therefore, it can be said that the viscoelastic FE model is not sensitive to the parameters of the Kelvin-Voigt element.

3.5.4.2 Sensitivity of the FE Model to the Number of Kelvin-Voigt Elements

Consider the single layer viscoelastic plate presented in Section 3.5.1. The plate geometry, mesh, and loading geometry are as shown in Figure 3.5. The plate rests on an

elastic Winkler foundation with the coefficient of subgrade reaction equal to 100 psi/in. To verify the sensitivity of the viscoelastic FE model on the number of Kelvin-Voigt elements adopted to represent the creep compliance function, the viscoelastic behavior of the plate is defined using two material models considered as follows:

1. Material model 1 – a single Kelvin-Voigt model attached to an elastic spring in series as shown in Figure 3.6(a), and
2. Material model 2 – a two-element generalized Kelvin-Voigt model attached to an elastic spring in series as shown in Figure 3.6(b).

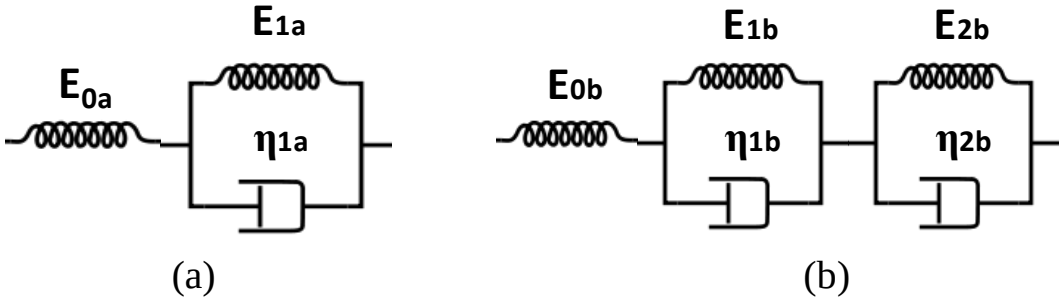

Figure 3.15 Schematic for (a) material model 1 and (b) material model 2.

The parameters of material models 1 and 2 are presented in Table 3.6. Material model 2 is an extension of material model 1. Under certain conditions described below, the creep compliance functions defined by material models 1 and 2 can be exactly equal. In such cases, the deflections and stresses at any node between slabs incorporating material models 1 and 2 should also be exactly equal.

Table 3.6 Prony series coefficients for material models 1 and 2.

	Material Model 1		**Material Model 2**	
Element #	**Spring stiffness, psi**	**Dashpot viscosity, psi-sec**	**Spring stiffness, psi**	**Dashpot viscosity, psi-sec**
0	E_{0a}	--	200000	--
1	95265	2.0E+05	95265	2.0E+05
2			101500	η_{2b}

The instantaneous modulus E_{0a} for material model 1 can be expressed using the parameters of material model 2 when the following conditions are present:

$$\frac{1}{E_{0a}} = \frac{1}{E_{0b}} \qquad \text{when } \eta_{2b} \text{ is a large value} \qquad (3.82)$$

$$\frac{1}{E_{0a}} = \frac{1}{E_{0b}} + \frac{1}{E_{2b}} \qquad \text{when } \eta_{2b} \text{ is a small value} \qquad (3.83)$$

where

E_{0a} is the instantaneous modulus of material model 1,

E_{0b} is the instantaneous modulus of material model 2, and

E_{2b} and η_{2b} are the spring stiffness and dashpot viscosity of the second Kelvin-Voigt element of material model 2, respectively.

Two values for the dashpot viscosity of the second Kelvin-Voigt element of material model 2 are considered (a) η_{2b} = 1.0E+13 and (b) η_{2b} = 1.0E+03. The creep compliance function (equation [3.8]) is plotted for material models 1 and 2 in Figure 3.16, when the instantaneous modulus E_{0a} varies with the dashpot viscosity η_{2b}.

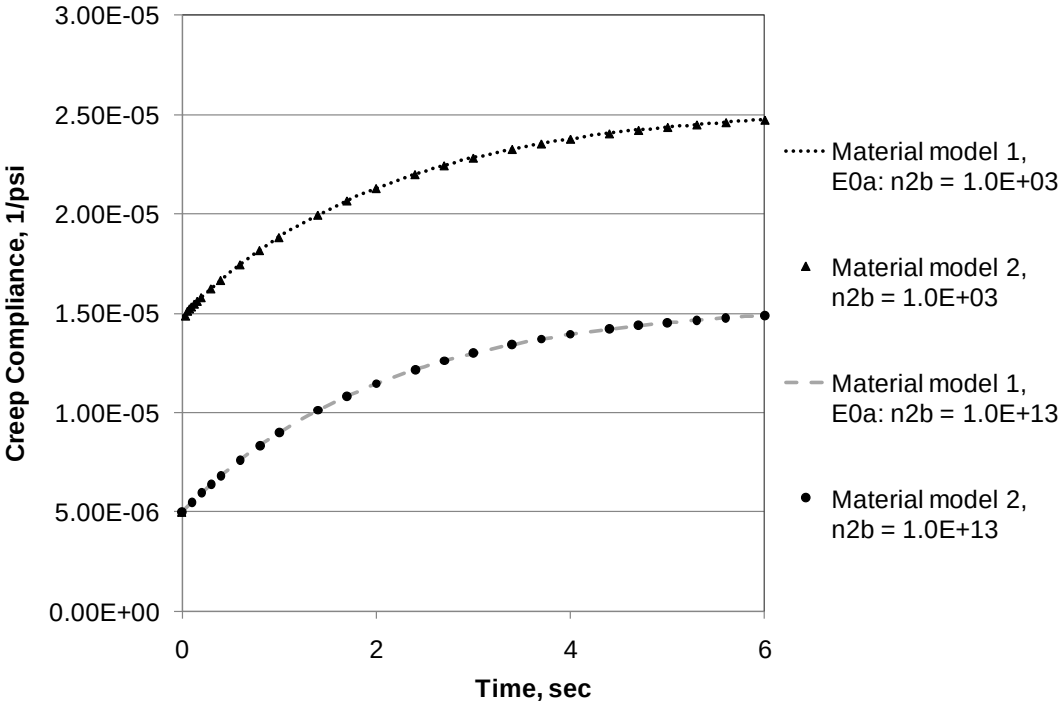

Figure 3.16 Creep compliance for material models 1 and 2.

Further, deflections and stresses in the plate under the applied load are calculated using the FE model. Figures 3.17 and 3.18 plot the deflections and bottom surface stresses at the slab center versus time, respectively, for material models 1 and 2.

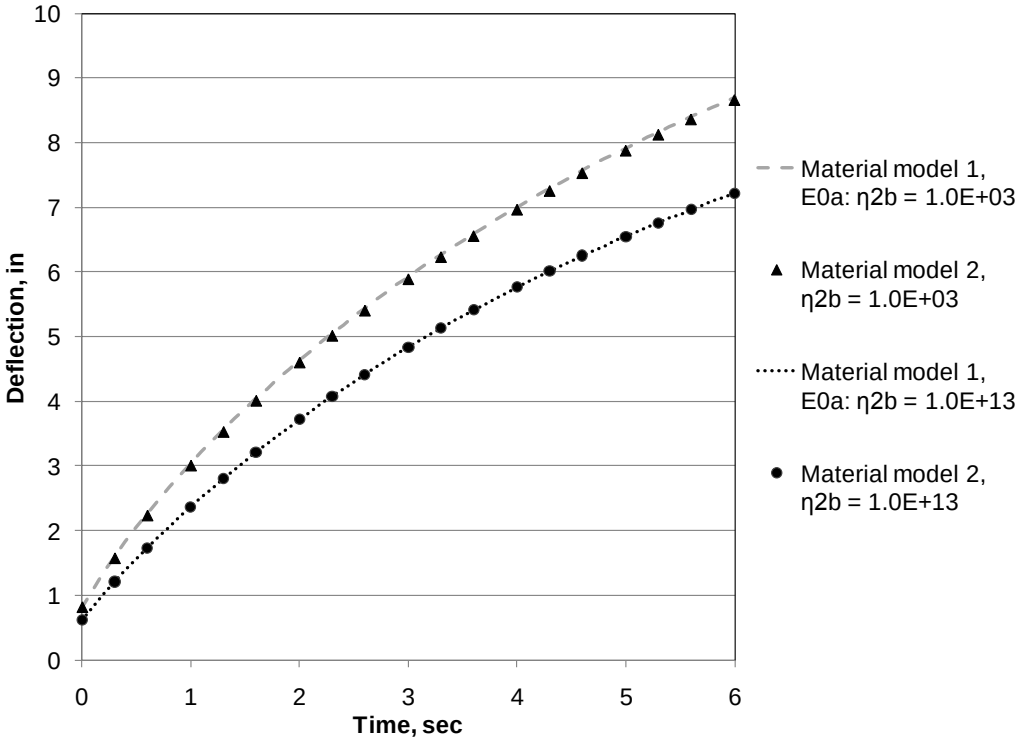

Figure 3.17 Deflection of the plate incorporating material models 1 and 2.

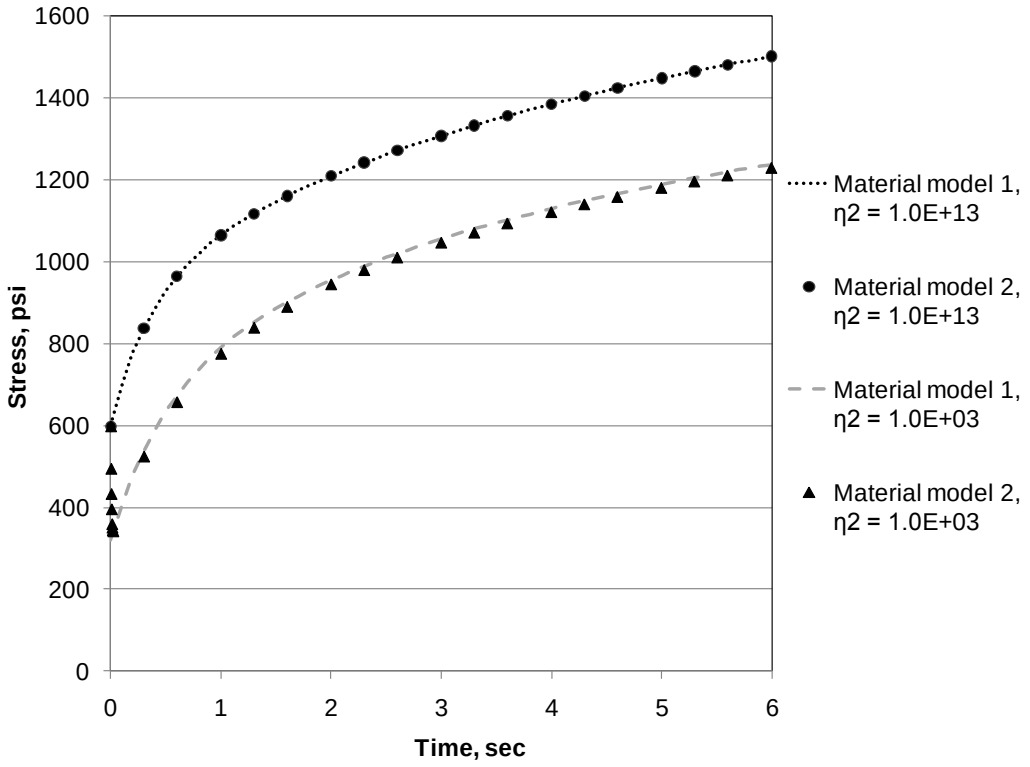

Figure 3.18 Stress at the bottom of the plate incorporating material models 1 and 2.

Excellent agreement is obtained for the creep compliance, deflection, and stress between material models 1 and 2. Therefore, it can be established that the viscoelastic FE model is not sensitive to the number of Kelvin-Voigt elements used in the representation of the creep compliance function.

3.5.4.3 Sensitivity of the FE Model to the Presence of Viscoelastic Layer

The sensitivity of the FE model to the presence of the viscoelastic AC layer is verified by varying the thickness of the AC layer of the composite pavement. A composite pavement with slab geometry, foundation support, mesh configuration, and wheel loading the same as those presented in Section 3.5.3 is used for this example. A factorial of thicknesses for

the AC layer is considered varying between 0 and 9 in (0, 1, 2, 3, 4, 5, 6, 7, 8, and 9). The layer properties for the baseline case are given in Table 3.7. All the layer interfaces are fully bonded. Additionally, an elastic two-layer system consisting of fully bonded PCC and base layers is also considered. The thicknesses and material properties for the PCC and base layers are same as those of the composite pavement.

Table 3.7 Layer properties for the baseline composite pavement.

	Material definition	**Thickness, h (in)**	**Layer modulus, E (psi)**	**Poisson's ratio, μ**	**Unit weight, γ (lb/in3)**
AC	Viscoelastic	9	Reference Table 3.3	0.15	0.087
PCC	Elastic	5	4.0E+06	0.15	0.087
Base	Elastic	6	4.0E+04	0.15	0.087

Figure 3.19 presents the FE results for PCC bottom stresses at the center of the slab at different times of the viscoelastic analysis. The elastic PCC bottom stresses at the center of the slab from the two-layer system are also shown in the figure.

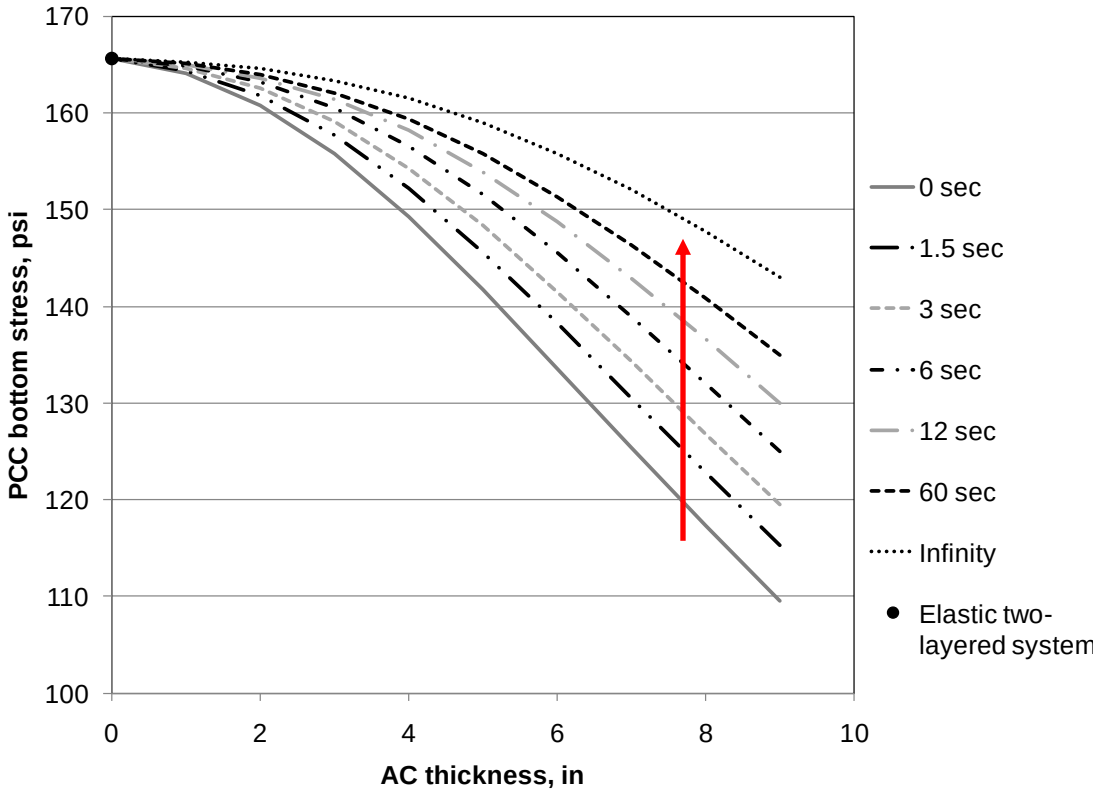

Figure 3.19 PCC bottom stresses versus AC thickness.

As expected, lower values of stress at the bottom of PCC layer are obtained for thicker AC layers at any time *t*. The stress in the PCC layer converges to the PCC stresses from the elastic two-layer system when the thickness of the AC layer tends to zero at any time *t*. Also, for any thickness of the AC layer, the stress solution converges as time increases to the stress at infinite time. The difference between the stress at time *t* = 0 and time *t* at infinity is most prominent for thicker AC layers, and the difference reduces as the thickness of the viscoelastic AC layer reduces.

Thus, the FE model developed under this research is capable of analyzing pavements that incorporate elastic or viscoelastic layers and is not sensitive to the internal parameters used to develop the FE model.

3.6 Summary

In this chapter, a finite element model of a composite pavement incorporating viscoelastic layers placed on a subgrade was presented. The FE model has the capability of analyzing the pavement under traffic loading and temperature gradients. The time-dependent stress-strain behavior due to the presence of a viscoelastic AC layer was incorporated into the FE model using the differential form of the creep compliance function represented by the Prony series. The FE model was validated against semi-analytical solutions using simple examples. Finally, the sensitivity of the FE model to internal parameters was analyzed and it was found that the model is internally consistent as well as robust for computing the elastic or viscoelastic stress solutions for up to three-layer pavement systems.

CHAPTER 4. STRESS SOLUTIONS USING THE 2-MODULI APPROACH

The Mechanistic Empirical Pavement Design Guide (MEPDG) uses a load duration dependent dynamic modulus to characterize the constitutive relationship for asphalt concrete (AC). The loading duration for traffic loads depends on the vehicle speed. For a typical interstate pavement with vehicle speeds of roughly 60 mph, the loading duration ranges between 0.01 sec and 0.05 seconds. The analysis of fatigue cracking (i.e. cracking due to repeated traffic loads) in the AC layer for flexible pavements does not involve temperature-induced stresses, which develop much more slowly. The cracking due to temperature gradients is computed separately using a thermal cracking model developed for flexible pavements.

In the case of composite pavements, there is an interaction between curling and deformations due to traffic loading. Temperature gradients and traffic loads both cause bending stresses that cannot be simply added when composite pavements are subjected to a combination of temperature gradients and instantaneous traffic loads. This is so because temperature curling causes a separation of the slab from the subgrade making the system to behave non-linearly. Moreover, the loading durations of the temperature gradients and fast moving traffic loads are significantly different. Therefore, for the case of composite pavements in the MEPDG framework, the material representation of the AC layer using a single dynamic modulus seems to be an over-simplification.

A finite element (FE)-based model incorporating the viscoelastic behavior of the AC layer in composite pavements was presented in Chapter 3. Although that FE model provides a robust framework for analyzing the viscoelastic slab-on-grade problems, it requires providing the creep compliance of the pavement layer(s), which is not a direct input or output of the MEPDG. In order to maintain compatibility with the MEPDG framework, a procedure is developed such that two different moduli are used to represent the AC layer for different loading durations determined using the MEPDG process. The *2-moduli approach* shall substitute for the time-discretized viscoelastic analysis presented in Chapter 3 by a combination of three elastic solutions such that the total stresses in the pavement are computed as a combination of the stresses from these three solutions.

This chapter discusses the difference in the MEPDG prediction for AC moduli under traffic loads and temperature gradients, the *2-moduli approach* developed to replace the time-discretized viscoelastic analysis, a stress computation procedure for combined stresses under traffic loads and temperature gradients using the *2-moduli approach*, and verification of the stresses using simple examples.

4.1 AC Moduli under Traffic Loads and Temperature Gradients

One of the limitations identified in the adoption of the jointed plain concrete pavement (JPCP) fatigue cracking model for composite pavements was the use of a single load duration dependent dynamic modulus to characterize the stress-strain relationship in the viscoelastic AC layer. A preliminary investigation, presented in Section 2.4, suggested that the AC modulus may be significantly different under fast moving traffic loads and

temperature loading. The MEPDG assumes the temperature gradient to be a step function of time with duration of one hour. Therefore, to maintain consistency with the MEPDG, the duration of temperature loads is selected to be one hour. An analysis of the AC dynamic modulus, based on the MEPDG guidelines, was conducted and the results are presented herein.

In the following example, the modulus for the AC layer of a composite pavement located in Minneapolis, MN was analyzed. The pavement structure and layer thicknesses are given in Table 4.1. All other inputs were taken as the MEPDG defaults.

Table 4.1 Structural details of the composite pavement analyzed in the MEPDG.

Layer No.	**Type**	**Material**	**Thickness, (in)**
1	Wearing	AC	4
2	Structural	PCC	6
3	Base	A-1-a	8
4	Subgrade	A-6	Semi-infinite

The AC dynamic modulus was calculated for the 3rd quintile monthly AC temperatures at the mid-depth of the AC layer obtained from Enhanced Integrated Climatic Model (EICM) outputs in the MEPDG. The AC dynamic modulus was calculated using equations (2.26) and (2.27) presented in Section 2.4.1 for the loading time *t* corresponding to (a) the MEPDG default traffic speed of 60 mph, and (b) 3600 seconds (i.e., one hour of temperature loading). Figure 4.1 illustrates the MEPDG-generated dynamic modulus of the AC layer versus pavement age corresponding to the traffic duration and temperature duration for the first two years of the design life of the composite pavement.

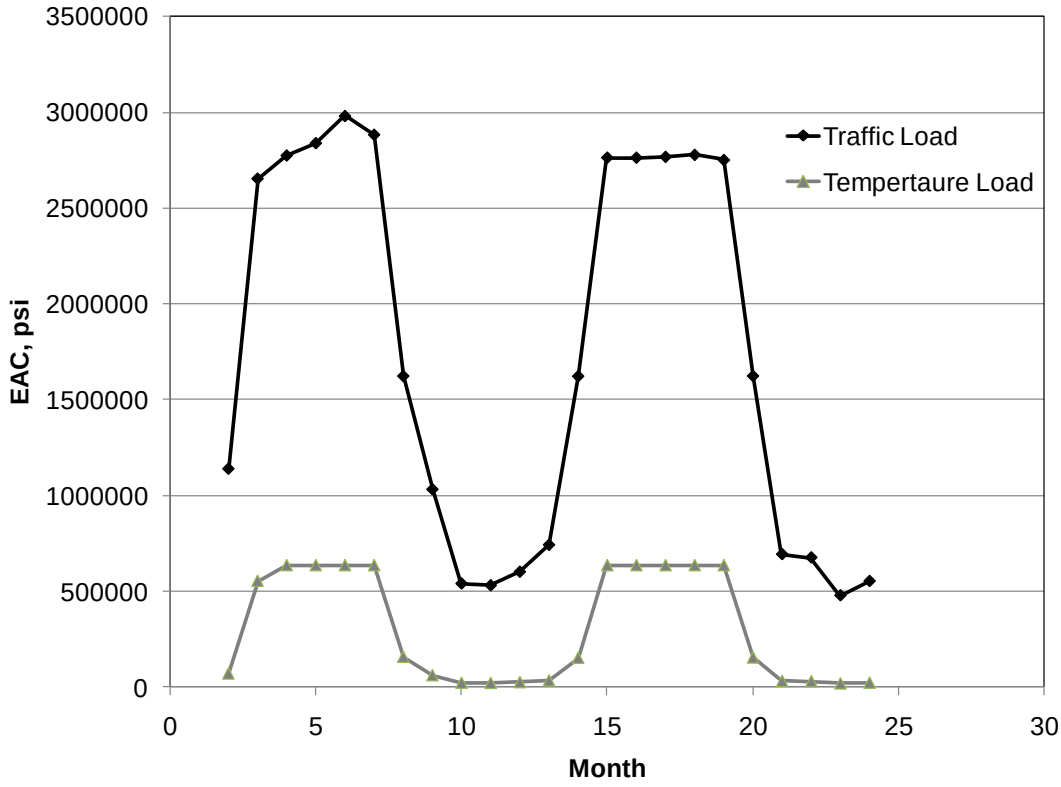

Figure 4.1 Asphalt dynamic modulus using the MEPDG versus pavement age.

It can be established from Figure (4.1) that the AC dynamic modulus is significantly different under typical traffic load durations and one hour of temperature loading. Therefore, for composite pavements under combined traffic and temperature loading, the use of a single dynamic modulus to characterize the stress-strain relationship in the viscoelastic AC layer may be insufficient.

4.2 The 2-Moduli Approach

Consider a composite pavement subjected to an arbitrary temperature distribution throughout the slab thickness acting on the time interval $0 < t < t_T$ and axle loading at the

end of the time interval. As was demonstrated above, the AC dynamic modulus is significantly different under typical traffic loads and temperature gradients. It is proposed that two separate AC dynamic modulus should be considered as follows:

1. The traffic-duration-dependent dynamic modulus, *EACL* that characterizes the pavement response under typical traffic loads
2. The temperature-duration-dependent dynamic modulus, *EACT* that characterizes the pavement response for the duration of temperature loads, t_T.

The stresses obtained by executing separately the curling analysis and the traffic load analysis cannot be simply added to obtain the stress under a combination of traffic loads and temperature curling (*AASHTO 2008*). This is due to the fact that the slab-foundation interaction is non-linear. Under compression, the deformation of the foundation increases linearly with an increase in surface pressure, but the foundation cannot resist vertical upward movement. The curling of the slab due to the daytime temperature gradient causes a void under the center of slab as a result of separation from the foundation. The night-time temperature gradient causes a void under the edges of the slab. Hence, due to non-linear interaction of slab with the foundation, two different loading cases (and resulting stresses) cannot be linearly superimposed to mimic the combined loading.

To account for the effect of load duration dependency of the AC layer and non-linear slab foundation interaction, a procedure that involves a combination of solutions of

three elastic boundary value problems (BVP) is developed. This procedure is presented next.

4.3 Stress Computation Procedure using the 2-Moduli Approach

The *2-moduli approach* is an alternative to the more involved viscoelastic analysis presented in Chapter 3. This method is a combination of three elastic BVPs. The first elastic BVP considers slab curling only and uses the temperature-duration-dependent AC modulus, *EACT* to characterize the AC stiffness. The second elastic BVP involves determination of the stress field in the composite pavement subjected to curling with the AC layer characterized by the traffic-duration-dependent AC modulus, *EACL*, and having the same deflection profile as that determined by the first elastic solution. In the third elastic BVP, the traffic-duration-dependent AC modulus, *EACL*, is used to determine the stress field from the combined effect of curling and axle loading. The total stresses in the pavement are computed as a combination of the stresses from these three solutions.

4.3.1 The First Elastic Problem

Problem 1 models a three-layer system of AC, PCC, and base layers as shown in Figure 4.2. The system rests on the spring idealization of an elastic Winkler foundation. The AC layer is modeled as an elastic material with an elastic modulus corresponding to the temperature-duration-dependent modulus, *EACT*. The PCC and base layers are elastic with the modulus of elasticity equal to E_{PCC} and E_{Base}, respectively. The thicknesses of the AC, PCC, and base layers are h_{AC}, h_{PCC}, and h_{Base}, respectively. The unit weights of

the AC, PCC, and base layers are γ_{AC}, γ_{PCC}, and γ_{Base}, respectively. All of the layers have Possion's ratio equal to μ. The coefficient of thermal expansion for the AC layer is α_{AC} while that for the PCC and base layers is selected as α_{PCC}. The interface conditions between the layers could be either fully bonded or unbonded.

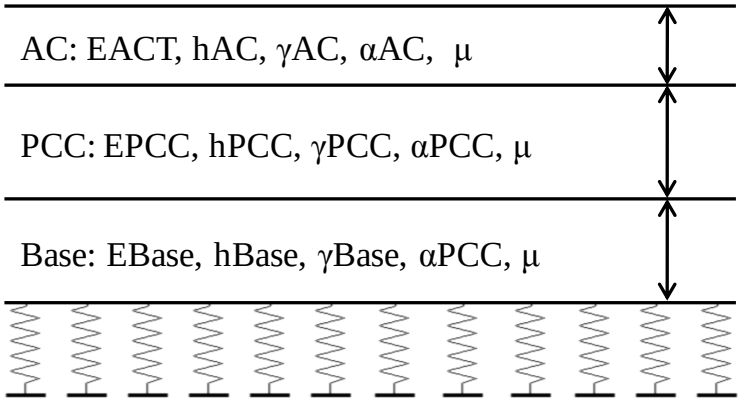

Figure 4.2 System 1.

The pavement system of problem 1 is subjected to a positive temperature gradient $T(z)$ as shown in Figure 4.3. The deflection profile of the slab under the temperature gradient $T(z)$ is recorded. The stress at the bottom of the PCC layer at the mid-slab location under temperature gradient $T(z)$ is denoted as σ_1. Solutions detailing the computation of this stress are discussed later in the chapter.

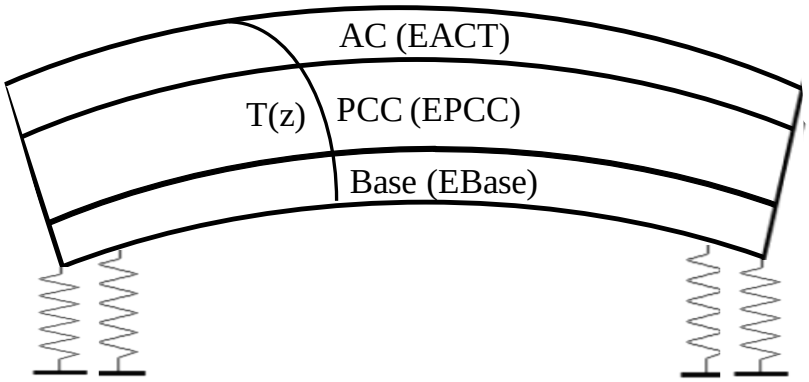

Figure 4.3 System 1 under positive temperature gradient $T(z)$ only.

4.3.2 The Second Elastic Problem

Problem 2 has the same three-layer structure and material properties as problem 1 except that the AC layer is modeled as an elastic material with elastic modulus corresponding to the traffic-duration-dependent modulus, *EACL*. The pavement system of problem 2 is presented in Figure 4.4. The layer interface conditions are the same as those chosen in problem 1.

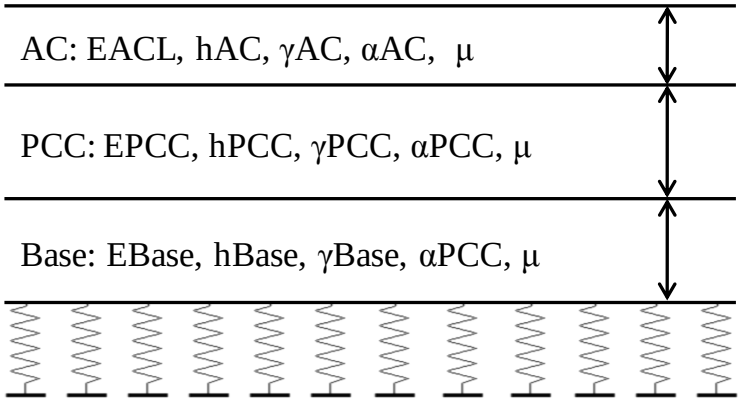

Figure 4.4 System 2.

Assume that a fictitious force F_{fict} acts on the pavement system such that its deflection profile is exactly the same as that from problem 1, i.e. the deflection at each node of system 2 is exactly equal to the deflection at the corresponding node in system 1. Since the deflection profile does not change between problems 1 and 2, it ensures that the subgrade below system 2 is under the same stress distribution as the subgrade below system 1, and that the contact area between the slab and foundation did not change. This ensures that the non-linear behavior of the slab-foundation interaction is properly accounted for. Figure 4.5 presents system 2 under a fictitious force F_{fict}. The stress resulting from the fictitious force F_{fict} at the bottom of the PCC layer at the mid-slab location is denoted as σ_2. Solutions detailing the computation of this stress are discussed later in the chapter.

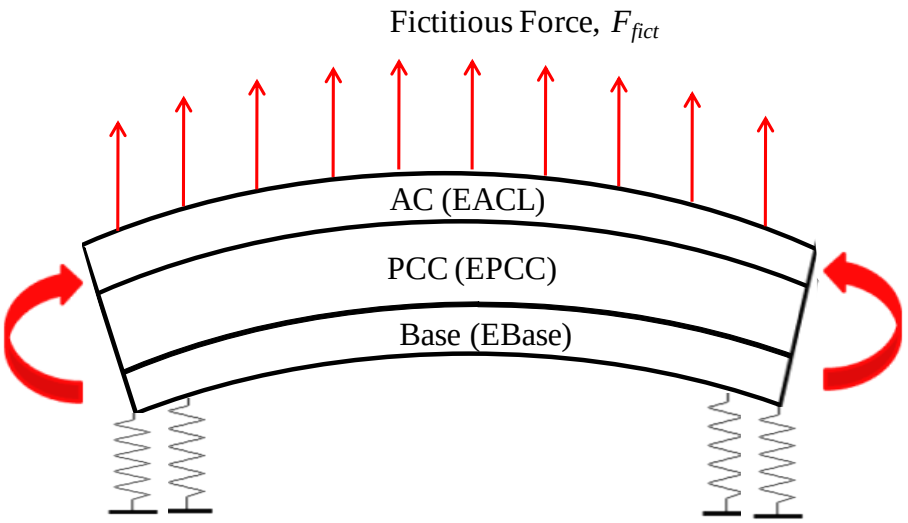

Figure 4.5 System 2 under fictitious force F_{fict}.

4.3.3 The Third Elastic Problem

Since system 2 characterizes the AC layer with an elastic modulus corresponding to the traffic-duration-dependent modulus, *EACL*, the traffic load *F* can be superimposed on top of the fictitious loading F_{fict}. Therefore, in the third elastic problem (problem 3), system 2 is loaded by a total load consisting of traffic load *F* and fictitious load F_{fict} as shown in Figure 4.6. The stress at the bottom of the PCC layer at the mid-slab location due to the total load is denoted as σ_3. Solutions detailing the computation of this stress are discussed later in the chapter.

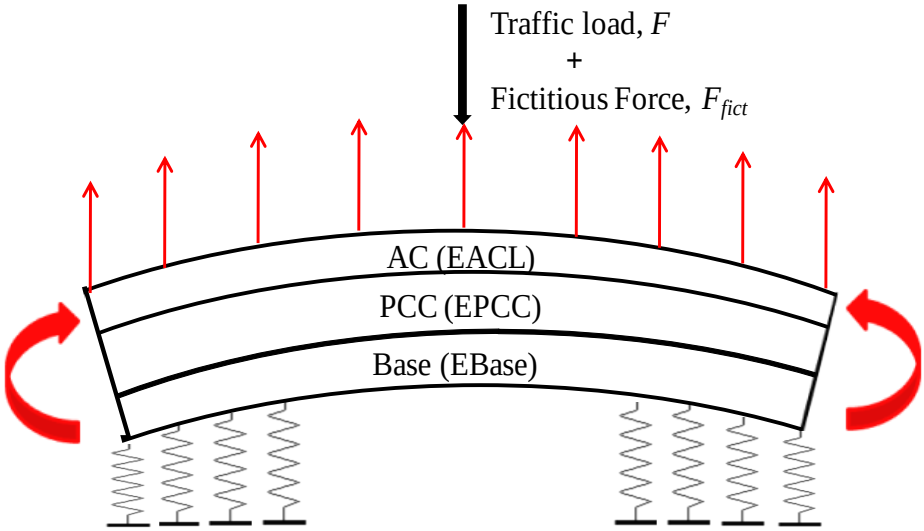

Figure 4.6 System 2 under mid-slab traffic load *F* and fictitious force F_{fict}.

4.3.4 Combined Stress

Finally, to obtain the stress distribution in the pavement due to the combined effect of temperature and axle loading, solutions of the three elastic problems are combined as follows:

$$\sigma_{2M} = \sigma_1 + (\sigma_3 - \sigma_2) \tag{4.1}$$

where

σ_{2M} is the combined stress at a given location,

σ_1 is the stress at the given location from the first elastic solution,

σ_2 is the stress at the given location from the second elastic solution, and

σ_3 is the stress at the given location from the third elastic solution.

It should be noted that the combined stress (equation [4.1]) is an approximation of the viscoelastic boundary value problem if the viscoelastic properties of the AC layer are as follows (Figure 4.7):

$$\begin{aligned} J(t) &= \frac{1}{E_0} + \frac{1}{E_1}\left(1 - e^{\frac{-E_1 t}{\eta_1}}\right) \\ \frac{1}{E_0} &= \frac{1}{EACL} \\ \frac{1}{E_1} &= \frac{1}{EACT} - \frac{1}{EACL} \\ \frac{\eta_1}{E_1} &<< t_T \end{aligned} \tag{4.2}$$

where

t_T is the duration of the temperature loading prior to application of the axle load.

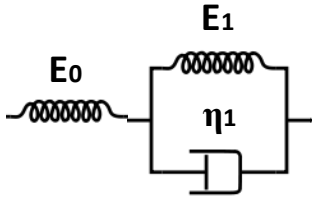

Figure 4.7 Kelvin-Voigt model connected to an elastic spring in series.

Several examples verifying this statement are presented later in the chapter. The next section presents the FE formulation to obtain the elastic solutions of the BVPs discussed above.

4.4 Brief Formulation for the FE Model Based on the 2-Moduli Approach

The *2-moduli approach* outlined in Section 4.3 has been incorporated into a FE code, and it is similar to the viscoelastic FE model presented in Chapter 3. In this section, the main differences of the formulation are highlighted. The variables of these equations follow the definitions and notations used in Chapter 3.

Recall system 1 considered in the first elastic problem in Section 4.3.1, which considers curling of the composite pavement and where the temperature-duration-dependent AC modulus *EACT* is used to characterize the AC layer. The equilibrium equation for system 1 can be expressed as follows:

$$[K_1]\{\delta\} = \{F_{therm}\} \tag{4.3}$$

where

$[K_1]$ is the global stiffness matrix for system 1 with temperature-duration-dependent AC modulus *EACT*,

$\{F_{therm}\}$ is the global force vector due to temperature distribution $T(z)$, and

$\{\delta\}$ is the global displacement vector of system 1.

The global stiffness matrix $[K_1]$ and the global thermal force vector $\{F_{therm}\}$ are assembled using the procedure described in Section 3.2. The displacements of the slab, δ_1 can be written as:

$$\{\delta_1\} = [K_1]^{-1}\{F_{therm}\} \tag{4.4}$$

Since system 1 is subjected to the temperature distribution $T(z)$, elastic stress in an element of system 1 can be calculated as:

$$\{\sigma_1\}_e = [\overline{D}_T](\{\varepsilon_1\} - \{\varepsilon_{therm}\})_e \tag{4.5}$$

where

subscript e denotes an individual element in the plate,

$\{\sigma_1\}$ is the elastic stress from the first elastic solution,

$[\overline{D}_T]$ is the material property matrix corresponding to modulus EACT and is given by equation (3.32),

$\{\varepsilon_1\}$ is the total strain corresponding to the global displacements δ_1 and is given by equation (3.35), and

$\{\varepsilon_{therm}\}$ is the thermal strain given by equations (3.21) and (3.38).

System 2, considered in the second elastic problem, characterizes the viscoelastic AC layer using the traffic-duration-dependent modulus *EACL*. The deflection profile of system 2 due to the application of a fictitious force F_{fict} must be exactly the same as that of system 1. Therefore, the fictitious force F_{fict} can be computed as follows:

$$\{F_{fict}\} = [K_2]\{\delta_1\} \tag{4.6}$$

where

K_2 is the global stiffness matrix for system 2 with the traffic-duration-dependent AC modulus *EACL*.

Since no initial strains act on system 2 and the global displacements of system 2 are exactly the same as those of system 1, the elastic stress in an element of system 2 can be calculated as follows:

$$\{\sigma_2\}_e = [\overline{D}_L]\{\varepsilon_1\}_e \tag{4.7}$$

where

$\{\sigma_2\}$ is the elastic stress from the second elastic solution, and

$[\overline{D}_L]$ is the material property matrix corresponding to the modulus *EACL* computed using equation (3.32).

In the third elastic problem, system 2 is subjected to traffic loads F along with the fictitious force F_{fict}. The global displacements δ under a combination of loads can be computed as follows:

$$\{\delta\} = [K_2]^{-1}\left(\{F\} + \{F_{fict}\}\right) \tag{4.8}$$

where

$\{F\}$ is the global force vector due to traffic loads, and

$\{F_{fict}\}$ is the global fictitious force vector from the second elastic solution.

The elastic stress from the third elastic problem can be calculated as follows:

$$\{\sigma_3\}_e = [\overline{D}_L]\{\varepsilon_T\}_e \tag{4.9}$$

where

$\{\sigma_3\}$ is the elastic stress from the third elastic solution, and

$\{\varepsilon_T\}$ is the total strain corresponding to the global displacements δ.

Finally, using equation (4.1) the combined stresses are calculated in the pavement.

4.5 Step-by-Step Procedure for Computing the Combined Stresses

A step-by-step procedure used to develop the second FE code for computing the combined stresses using the three elastic solutions is presented.

Steps 1 through 8 given in Section 3.4 are repeated for an equivalent single layer slab 1 corresponding to system 1 and an equivalent single layer slab 2 corresponding to system 2. The modifications applied to these steps are noted below.

Step 1: Read inputs – In place of the creep compliance parameters for the viscsoelastic FE inputs, the traffic-duration-dependent AC modulus *EACL* and temperature-duration-dependent AC modulus *EACT* are given in the input file.

Step 2: Determine parameters of equivalent single layer slab 1 corresponding to system 1 – The thickness and unit weight for an equivalent single layer slab 1 are computed depending on the temperature-duration-dependent AC modulus *EACT* and the interface conditions of system 1.

Step 5: Compute the global force vector for the equivalent single layer slab 1 – The global force vector due to the thermal strains and self-weight of the slab is computed at the appropriate degree of freedom for each element.

Step 9: Calculate nodal stresses for the first elastic solution – Stresses for each layer of the composite pavement system are computed. For example, the total stress at the bottom of the PCC layer of the composite pavement for the first elastic solution is calculated as follows:

$$\sigma_{PCC,Bot\_1} = \frac{2*(h_{PCC} + h_{AC} - x_1)}{h_{eq\_1}} \sigma_{eq\_1} + \sigma_{NL,bot} \tag{4.10}$$

where

σ_{PCC,Bot_1} and σ_{eq_1} are the elastic stresses at the bottom of the PCC layer of system 1 and at the bottom of equivalent single layer slab 1, respectively,

h_{eq_1}, h_{AC}, and h_{PCC} are the thicknesses of the equivalent single layer slab 1, AC, and PCC layers, respectively,

x_1 is the distance of the neutral axis of system 1 from the top of the AC layer, and

$\sigma_{NL,bot}$ is the stress due to the nonlinear-strain-causing temperature component.

Step 10: Determine parameters of equivalent single layer slab 2 corresponding to system 2 – The thickness and unit weight for an equivalent single layer slab 2 are computed depending on the traffic-duration-dependent AC modulus *EACL* and the interface conditions of system 2 (which are the same as those chosen for system 1).

Step 11: Compute the stiffness matrix – Repeat step 4 to generate the global stiffness matrix [K_2] corresponding to system 2.

Step 12: Compute the fictitious force vector in the equivalent single layer slab 2 – The global fictitious force vector acting on equivalent single layer slab 2 is computed using the global displacements from the first elastic solution according to equation (4.6).

Step 13: Compute stresses in the equivalent single layer slab 2 – Repeat step 8 to obtain the stresses in the equivalent single layer slab 2 corresponding to the second elastic problem.

Step 14: Calculate nodal stresses for the second elastic solution – Stress for each layer of the composite pavement system is computed. For example, the total stress at the bottom of the PCC layer of the composite pavement for the second elastic solution is calculated as follows:

$$\sigma_{PCC,Bot\_2} = \frac{2*(h_{PCC} + h_{AC} - x_2)}{h_{eq\_2}} \sigma_{eq\_2} \tag{4.11}$$

where

σ_{PCC,Bot_2} and σ_{eq_2} are the elastic stresses at the bottom of the PCC layer of system 2 and at the bottom of equivalent single layer slab 2, respectively,

h_{eq_2} is the thickness of the equivalent single layer slab 2, and

x_2 is the distance of the neutral axis of system 2 from the top of the AC layer.

Step 15: Compute the global force vector for the third elastic solution – The global force vector is computed by adding the traffic loading to the fictitious force acting on system 2

at the appropriate degree of freedom for each element.

Step 16: Compute displacements for the third elastic solution – Same as step 6.

Step 17: Check contact condition – Same as step 7.

Step 18: Compute stresses in the equivalent single layer slab 2 – Repeat step 8 to obtain the stresses in the equivalent single layer slab 2 corresponding to the third elastic problem.

Step 19: Calculate nodal stresses for the third elastic solution – The stress for each layer of the composite pavement system is computed. For example, the total stress at the bottom of the PCC layer of the composite pavement for the third elastic solution is calculated as follows:

$$\sigma_{PCC,Bot\_3} = \frac{2*(h_{PCC} + h_{AC} - x_2)}{h_{eq\_2}} \sigma_{eq\_3} \tag{4.12}$$

where

σ_{PCC,Bot_3} and σ_{eq_3} are the elastic stresses at the bottom of the PCC layer of system 2 and at the bottom of equivalent single layer slab 2, respectively for the third elastic solution.

Step 20: Compute combined stress – The combined stress from the three elastic solutions

is calculated using equation (4.1).

Step 21: Output results – The displacements and combined stresses in the composite pavement at each node are printed in ISLAB2000 output format.

4.6 Verification of the Combined Stress Obtained Using the 2-Moduli Approach

The stress computation procedure presented in Section 4.3 is verified using simple examples for the following cases:

1. Comparison with the viscoelastic FE model (presented in Chapter 3) for a fictitious tire footprint.
2. Comparison with the viscoelastic FE model for a typical tire footprint.
3. Comparison of the combined stress obtained using the *2-moduli approach* with a simple addition of stresses obtained by executing separately the curling analysis and the traffic load analysis, to confirm the presence of non-linear slab-foundation interaction.

4.6.1 Comparison with the Viscoelastic FE Model – Example 1

A three-layered composite pavement placed on an elastic Winkler foundation is loaded with a single wheel load that has a tire footprint of 60 in x 48 in and tire pressure of 100 psi. The wheel load is applied at the center of the slab. A uniform mesh consisting of 6 in x 6 in elements is generated in the horizontal plane. Both interfaces (AC-PCC and

PCC-base) are fully bonded. Figure 3.5 shows the mesh and loading configuration for the composite pavement under this wheel load.

The composite pavement is also subjected to a non-linear temperature distribution given in Table 4.2. The temperature profile is adopted from a typical MEPDG hourly thermal distribution for the AC and PCC layers. To maintain consistency with the MEPDG, the temperature in the base layer is assumed to be constant and equal to the temperature at the bottom of layer 2. The depth of the temperature data point in a layer is given from the top of the corresponding layer.

Table 4.2 Temperature profile for the composite pavement.

Layer		**No. of temperature data points**										
		1	**2**	**3**	**4**	**5**	**6**	**7**	**8**	**9**	**10**	**11**
AC	Reference temperature = 55.90 °F											
	Depth, in	0.0	1.0	2.0	3.0	4.0						
	Temp., °F	90.9	86.0	81.0	76.4	71.8						
PCC	Reference temperature = 55.90 °F											
	Depth, in	0.0	0.8	1.6	2.4	3.2	4.0	4.8	5.6	6.4	7.2	8.0
	Temp., °F	71.8	69.0	66.9	64.8	63.0	61.4	60.0	58.7	57.6	57.0	55.9

The material properties for the constituent layers of the composite pavement are presented in Table 4.3.

Table 4.3 Layer properties for the composite pavement.

Layer	Thickness, h (in)	Layer modulus, E (psi)	Poisson's ratio, M	Unit weight, γ (lb/in3)	Coefficient of thermal expansion, α (1/°F)
AC	4	*EACT* = 39448.9 *EACL* = 2.0E+05	0.15	0.087	1.65E-05
PCC	8	4.0E+06	0.15	0.087	5.50E-06
Base	0	4.0E+04	0.15	0.087	5.50E-06

The AC layer of the composite pavement is represented by (a) the creep compliance function using a two-term generalized Kelvin-Voigt model when the stresses are computed using the viscoelastic FE model presented in Chapter 3 and (b) the moduli *EACL* and *EACT* when stresses are computed using the *2-moduli approach*. The traffic-duration-dependent AC modulus *EACL* is equal to the instantaneous modulus of the generalized Kelvin-Voigt model. The temperature-duration-dependent AC modulus *EACT* is equal to the inverse of creep compliance computed using the generalized Kelvin-Voigt model at the end of one hour of loading. Table 4.4 presents the material properties of the AC layer for the viscoelastic FE model and the *2-moduli approach*.

Table 4.4 Material properties for the AC layer.

	Element #	Spring stiffness, psi	Dashpot viscosity, psi-in
Viscoelastic FE Model	0	200000	
	1	95265	11307535
	2	101500	997600
2-Moduli Approach		**AC Modulus, psi**	
	EACL	200000	
	EACT	39448.9	

The viscoelastic FE solution is obtained by executing the FE code presented in Chapter 3 for the composite pavement configuration detailed herein. The temperature distribution is applied for 3600 seconds (1 hour) during which the creep strains and corresponding fictitious creep forces develop in the AC layer. At the end of one hour, the wheel load is applied to the pavement.

The combined stress using the *2-moduli approach* was obtained by executing the stress computation procedure detailed in Section 4.3 above. Tables 4.5 and 4.6 present the deflections and longitudinal stresses from the viscoelastic FE model at the end of the load application and the three elastic solutions for select nodes at the bottom of the PCC layer.

Table 4.5 Deflections and stress at the bottom of the PCC layer at slab center.

	Location, in		**Deflection, in**	**Rotation**		**Longitudinal Stress, psi**
	X	**Y**		**θy**	**θx**	
Three elastic solution						
# 1	90	72	-0.0054	0.00	0.00	78.65
# 2	90	72	-0.0054	0.00	0.00	-96.61
# 3	90	72	0.2401	0.00	0.00	1947.8
Combined stress						2123.06
Viscoelastic FE solution	90	72	0.2401	0.00	0.00	2122.84
% Error						-0.01%

Table 4.6 Deflections and stress at the bottom of the PCC layer at an edge node.

	Location, in		Deflection, in	Rotation		Longitudinal Stress, psi
	X	Y		θy	θx	
Three elastic solution						
# 1	90	0	0.0188	-0.0007	0.00	74.35
# 2	90	0	0.0188	-0.0007	0.00	-101.04
# 3	90	0	0.1220	0.0015	0.00	716.08
Combined stress						891.462
Viscoelastic FE solution	90	0	0.1220	0.0015	0.00	891.461
% Error						-0.00015%

The stress from the viscoelastic FE solution and the combined stress from three elastic solutions match very well at the both the center of the slab and the edge node as shown by the 0.01% and 0.00015% errors, respectively.

4.6.2 Comparison with the Viscoelastic FE Model – Example 2

Consider the three-layered composite pavement presented in Section 4.6.1 above. The pavement is loaded with a single-axle dual-wheel (SADW) load that has a tire footprint of 7 in x 7 in and tire pressure of 100 psi. The SADW load is applied at the mid-slab location such that one of the wheels is at the edge of the slab. The pavement is also subjected to the temperature distribution given in Table 4.2. Figure 3.8 shows the mesh and loading configuration for the composite pavement under the SADW load. The layer properties of the composite pavement are given in Tables 4.3 and 4.4 above. The AC layer is represented in the manner similar to example 1 (Section 4.6.1) using (a) the creep

compliance function for the viscoelastic FE model and (b) moduli *EACL* and *EACT* for the *2-moduli approach*. Tables 4.7 and 4.8 present the deflections and longitudinal stresses obtained using the viscoelastic FE model and the three elastic solutions for select nodes at the bottom of the PCC layer.

Table 4.7 Deflections and stress at the bottom of the PCC layer at slab edge.

	Location, in		**Deflection, in**	**Rotation**		**Longitudinal Stress, psi**
	X	**Y**		**θy**	**Θx**	
Three elastic solution						
# 1	90	0	0.0188	-0.0007	0.00	74.35
# 2	90	0	0.0188	-0.0007	0.00	-101.04
# 3	90	0	0.0466	-0.0011	0.00	268.11
Combined stress						443.5
Viscoelastic FE solution	90	0	0.0466	-0.0011	0.00	443.3
% Error						-0.046%

Table 4.8 Deflections and stress at the bottom of the PCC layer at an interior node.

	Location, in		**Deflection, in**	**Rotation**		**Longitudinal Stress, psi**
	X	**Y**		**θy**	**Θx**	
Three elastic solution						
# 1	72	54	-0.0034	-0.00015	0.00008	69.44
# 2	72	54	-0.0034	-0.00015	0.00008	-106.09
# 3	72	54	0.0106	-0.00026	-0.00004	-21.51
Combined stress						154.02
Viscoelastic FE solution	72	54	0.0106	-0.00026	-0.00004	153.76
% Error						-0.169%

The stress from the viscoelastic FE solution and the combined stress from the three elastic solutions match fairly well at both the center of the slab and the interior node as shown by the .046% and .169% errors, respectively. The slight difference noted in both the examples is attributed to the accumulation of error due to the length of time interval considered in the viscoelastic FE solution.

4.6.3 Comparison with Simple Addition of the Stresses

To confirm that the stress in a pavement is not a direct addition of stresses due to traffic load and temperature gradient, a typical composite pavement slab placed on an elastic Winkler foundation is considered. A 15 ft long by 12 ft wide pavement slab is loaded with single-axle dual-wheel (SADW) loads at the edge of the slab as shown in Figure 4.8. The SADW loads have a tire footprint of 7 in x 7 in and tire pressure of 100 psi. A uniform mesh consisting of 6 in x 6 in elements is generated. The modulus of subgrade reaction for the Winkler foundation is equal to 100 psi/in. The interface between the AC and PCC layers of the composite pavement is fully bonded while that between the PCC and base layers is fully unbonded.

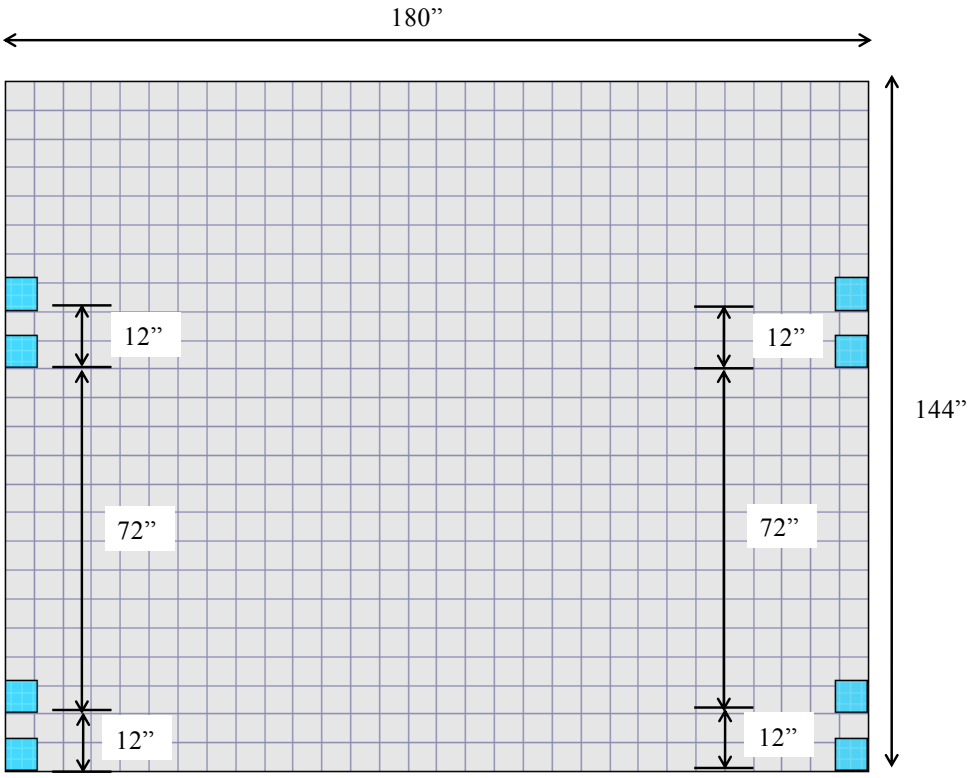

Figure 4.8 Mesh and load configuration for the composite pavement subjected to SADW edge loading.

The composite pavement is also subjected to a non-linear night-time temperature distribution given in Table 4.9.

Table 4.9 Temperature profile for the composite pavement.

Layer		**No. of temperature data points**										
		1	**2**	**3**	**4**	**5**	**6**	**7**	**8**	**9**	**10**	**11**
AC	Reference temperature = 55.90 °F											
	Depth, in	0.0	0.5	1.0	1.5	2.0						
	Temp., °F	40.9	46.0	49.0	52.9	57.8						

Layer		No. of temperature data points										
		1	**2**	**3**	**4**	**5**	**6**	**7**	**8**	**9**	**10**	**11**
PCC	Reference temperature = 55.90 °F											
	Depth, in	0.0	0.7	1.4	2.1	2.8	3.5	4.2	4.9	5.6	6.3	7.0
	Temp., °F	57.8	60.2	62.5	64.7	66.9	68.0	70.9	72.8	74.5	76.2	78.8

The material properties for the constituent layers of the composite pavement are presented in Table 4.10.

Table 4.10 Layer properties for the composite pavement.

Layer	**Thickness, h (in)**	**Layer modulus, E (psi)**	**Poisson's ratio, μ**	**Unit weight, γ (lb/in3)**	**Coefficient of thermal expansion, α (1/°F)**
AC	2	*EACT* = 39448.9 *EACL* = 2.0E+05	0.15	0.087	1.65E-05
PCC	7	4.0E+06	0.15	0.087	5.50E-06
Base	6	4.0E+04	0.15	0.000	5.50E-06

The stress in the pavement is computed using the *2-moduli approach* presented in Section 4.3 above. Further, the stress is computed when the composite pavement is subjected to (a) the temperature load only and the AC layer has temperature-duration-dependent modulus *EACT* and (b) the traffic load only and the AC layer has traffic-duration-dependent modulus *EACL*. The combined PCC top stress at the edge of the slab using the *2-moduli approach* is compared against the sum of stresses from case (a) and case (b). The results are presented in Table 4.11 below.

Table 4.11 Deflections and stresses at the top of the PCC layer at slab edge.

	Location, in		**Deflection, in**	**Rotation**		**Longitudinal Stress, psi**
	X	**Y**		**θy**	**θx**	
Three elastic solution						
# 1	90	0	-0.0077	0.00	0.00	108.74
# 2	90	0	-0.0077	0.00	0.00	-138.36
# 3	90	0	0.0038	0.00	0.00	204.06
Combined stress						451.17
Viscoelastic FE solution	90	0	0.0038	0.00	0.00	451.12
EACT, temperature load only	90	0	-0.0077	0.00	0.00	108.74
EACL, traffic load only	90	0	0.0033	0.00	0.00	284.05
						392.79
% Difference						14.86%

The difference between the stresses from the two approaches, which was 14.86%, clearly demonstrate that the stress from individual traffic and temperature loads cannot simply be added to obtain the combined stress. This phenomenon is due to the non-linear behavior of the slab-foundation interaction.

4.7 Comparison of the Stress Solution using the 2-Moduli Approach with the Stress Solution using the MEPDG Process

The stresses obtained using the *2-moduli approach* are compared with the stresses obtained using the MEPDG procedure in order to assess the difference between the two

procedures. The MEPDG considers the temperature distribution present in the layers of the pavement to be a step function of time with duration of one hour. In this example, the temperature distribution with the maximum temperature difference between the top of the AC layer and the bottom of the PCC layer was selected for each month over two years of data. The stress in the pavement was then computed using the selected temperature distribution for each month in combination with the traffic loading. The MEPDG employs neural networks (NNs) to compute the stresses in rigid and composite pavement. These NNs are trained using a factorial of ISLAB2000 cases. Therefore, to maintain consistency with the MEPDG, ISLAB2000 cases were executed such that the composite pavement was subjected to a combination of the temperature distribution corresponding to each month of the analysis and traffic loading.

Consider the three-layered composite pavement presented in Section 4.6.2. Twenty-four cases corresponding to twenty-four months are analyzed such that the pavement is subjected to the SADW load given in Section 4.6.2 and the selected temperature distribution with maximum gradient for each month. The properties of the constituent layers of the composite pavement are given in Table 4.12. The AC layer is represented using the *2-moduli approach* such that (a) the traffic-duration-dependent modulus *EACL* is dependent on the vehicle loading rate and (b) the temperature-duration-dependent modulus *EACT* is dependent on one hour of temperature loading. Also, both *EACL* and *EACT* for each month are calculated using the 3rd quintile AC temperatures at the mid-depth of the AC layer for the corresponding month.

Table 4.12 Layer properties for the composite pavement.

Layer	**Thickness, h (in)**	**Layer modulus, E (psi)**	**Poisson's ratio, M**	**Unit weight, γ (lb/in3)**	**Coefficient of thermal expansion, α (1/°F)**
AC	2	*EACT* *EACL*	0.15	0.087	1.00E-13
PCC	7	4.0E+06	0.15	0.087	5.50E-06
Base	0	4.0E+04	0.15	0.087	5.50E-06

ISLAB2000 cannot currently analyze a three-layered system if both the layer interfaces are fully bonded. While this is rarely a limitation for the analysis of rigid pavements, it introduces some limitation when fully bonded composite pavements are analyzed. Therefore, to maintain compatibility with ISLAB2000, the thickness of the base layer of the composite pavement is set to zero. The stresses obtained using the *2-moduli approach* and by executing the ISLAB2000 case for replicating the MEPDG procedure are presented in Figure 4.9. The stress is computed at the bottom of the PCC layer at the edge of the slab.

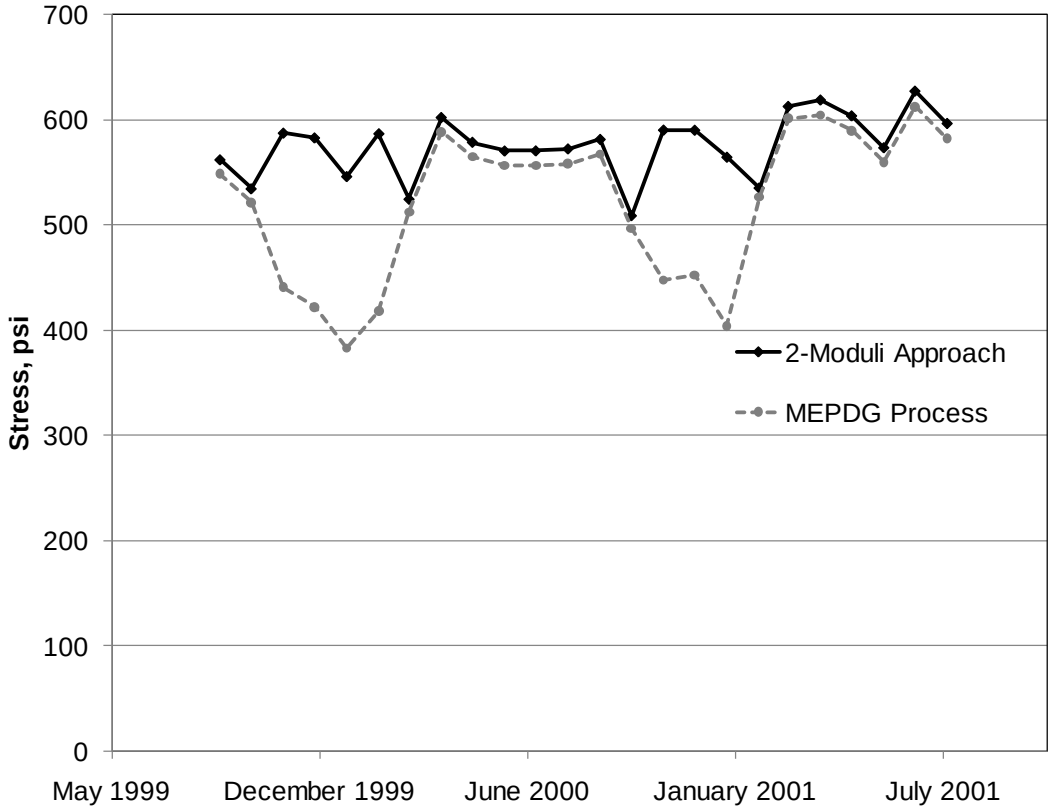

Figure 4.9 Comparison of stress using the 2-moduli approach and the MEPDG procedure.

A difference between the stresses from the *2-moduli approach* and the MEPDG procedure is observed. There could be several factors that contribute to this difference. The MEPDG uses a single traffic loading based AC dynamic modulus (*EACL*) whereas the 2-moduli approach employs moduli *EACT* and *EACL*. This may cause a difference between the self-equilibrating stresses present in a layer due to the non-linear-strain-causing temperature component, which directly affects the total stress at any point in the pavement.

4.8 Summary

The MEPDG employs a single load duration based AC dynamic modulus. It was identified that when a composite pavement is subjected to a combination of traffic load and temperature distribution, for which the loading durations are significantly different, the use of a single AC dynamic modulus seems insufficient. Therefore, a procedure to analyze the load duration dependent behavior of the layer using two separate AC dynamic moduli, or the *2-moduli approach*, was introduced. The combined stress from the *2-moduli approach* was compared with the stress at the end of the viscoelastic analysis conducted using the viscoelastic FE model presented in Chapter 3 and a good agreement was observed. It was found that the combined stress procedure using the *2-moduli approach* is efficient in predicting the stress solution and can be used as a substitute for the viscoelastic analysis. Finally, the stress procedure using the *2-moduli approach* was compared to the existing MEPDG stress procedure and a significant difference was observed between the stresses during certain periods of time.

CHAPTER 5. DEVELOPMENT OF A FRAMEWORK FOR IMPLEMENTATION OF THE 2-MODULI APPROACH INTO MEPDG

The objective of this research is to develop a framework for the structural analysis of composite pavements, which can be implemented into the existing or future versions of the Mechanistic Empirical Pavement Design Guide (MEPDG). The *2-moduli approach* presented in Chapter 4 is an attractive alternative to the elastic analysis currently implemented by the MEPDG and the more rigorous viscoelastic finite element (FE) model presented in Chapter 3. As was discussed in Chapter 2, a direct implementation of a FE solution into the MEPDG is not feasible due to the computational time constraint.

The current structural analysis of composite pavements implemented into the MEPDG utilizes rapid solutions that are developed based on the results of a factorial of ISLAB2000 runs. In order to accommodate a large number of design parameters in the MEPDG, the following techniques were adopted (*AASHTO 2008*):

1. Replacement of the structural system by a combination of two simpler systems.
2. Equivalency techniques to reduce the number of independent input parameters.

Sections 2.3 provides the details of the techniques employed by the MEPDG for the simplification of stress analysis in the existing fatigue cracking distress models for rigid and composite pavements. In this chapter, similar methods are introduced for the

simplification of the stress analysis using the *2-moduli approach* presented in Chapter 4. Further, examples are presented to verify the simplification and its compatibility with the MEPDG framework.

5.1 Simplification of the Structural System

The MEPDG employs a framework of artificial neural networks (NNs) to predict the stress solutions for rigid and composite pavements under traffic loading, temperature distribution, or their combinations (*AASHTO 2008*). The NNs are based on a combination of two simpler systems presented in Section 2.3.2 to compute stresses in the original multi-slab system. A similar approach is adopted for the development of a MEPDG compatible framework that shall incorporate the stress solutions obtained using the *2-moduli approach*.

The original multi-slab composite pavement system consists of one or more connected pavement slabs and a shoulder that provides edge support to the slab to the slab through load transfer between the pavement slab and the shoulder (refer to Figure 2.4a). The original system is subjected to an axle load acting over a tire footprint area and a temperature distribution which varies throughout the depth of the pavement. The asphalt concrete (AC) layer of the composite pavement is characterized using the traffic-duration-dependent AC modulus *EACL* when the pavement is subjected to the axle load and the temperature-duration-dependent AC modulus *EACT* when the pavement is subjected to temperature distribution.

A single slab system – system A (refer to Figure 2.4b) – is the first system used to

simplify the representation of the original multi-slab pavement. The details of the geometry of system A are provided in Section 2.3.2 and therefore, are not repeated herein. System A is subjected to three separate loading regimes as follows:

- Temperature curling only,
- Combined axle loading and temperature curling, and
- Axle loading only.

For computing the stresses corresponding to the combined axle loading and temperature curling load regime, the boundary value problem (BVP) detailed in Section 4.3 is used. The AC layer of the composite pavement system A is represented using the traffic-duration-dependent modulus *EACL* when the pavement is subjected to the axle load and the temperature-duration-dependent modulus *EACT* when the pavement is subjected to the temperature distribution. For computing the stresses due to temperature curling only and axle loading only, either the FE code presented in Chapter 3 or ISLAB2000 may be used. The footprint of the axle load for system A is considered to be 7 in by 7 in.

A two-slab system – system B (refer to Figure 2.4c) – is the other system used to simplify the representation of the original multi-slab pavement. Similar to system A, the details of system B are not repeated here. System B is used to account for the effect of tire footprint geometry and shoulder support. Since a curling analysis of system B is not required, the AC layer of the composite pavement of system B is represented using the traffic-duration-dependent modulus *EACL* only. Again, either the FE code or

ISLAB2000 may be used for computing the stress due to axle loading only.

Similar to the total stress obtained using the MEPDG procedure (equation [2.23]), the stress in the original multi-slab composite system is related to the stress in systems A and B as follows:

$$\sigma_{Tot} = \sigma_1^A(0,T) + LTE \ * \left[\left(\sigma_3^A(P,T^*) - \sigma_2^A(0,T^*)\right) - \sigma^A(P,0) + \sigma^B(0)\right] \qquad (5.1)$$

where

σ_{Tot} is the stress in the original multi-slab composite pavement,

$\sigma_1^A(0,T)$ is the stress in system A due to temperature curling only and is equal to the stress from the first elastic BVP of the *2-moduli approach*,

$\sigma_2^A(0,T^*)$ and $\sigma_3^A(P,T^*)$ are stresses in system A due to the combined axle loading and temperature curling and are equal to the stresses from the second and third elastic BVPs of the *2-moduli approach*, respectively,

$\sigma^A(P,0)$ is the stress in system A due to axle loading only,

$\sigma^B(0)$ is the stress in system B when the shoulder provides no edge support, and

LTE is the load transfer efficiency between the pavement slab and the shoulder.

Equation (5.1) is verified using a 15 ft long by 12 ft wide composite pavement placed on an elastic Winkler foundation. The modulus of subgrade reaction for the Winkler foundation is equal to 100 psi/in. The material properties of the constituent layers are presented in Table 5.1. Both of the layer interfaces are fully bonded. The stresses $\sigma^A(P,0)$ and $\sigma^B(0)$ are computed using projects designed in ISLAB2000.

Table 5.1 Layer properties for the composite pavement.

Layer	Thickness, h (in)	Layer modulus, E (psi)	Poisson's ratio, μ	Unit weight, γ (lb/in3)	Coefficient of thermal expansion, α (1/°F)
AC	4	*EACT* = 39448.9 *EACL* = 2.0E+05	0.15	0.087	1.65E-05
PCC	8	4.0E+06	0.15	0.087	5.50E-06
Base	0	4.0E+04	0.15	0.087	5.50E-06

In this example, the thickness of the base layer is purposely selected to be zero inches. This is done to maintain compatibility with ISLAB2000 since ISLAB2000 is not capable of analyzing fully bonded three-layered systems. However, it must be noted that other options such as combining the thickness of layers 2 and 3 (while maintaining the exact same properties for the two layers) can also be used to maintain compatibility with ISLAB2000.

The composite pavement is subjected to a non-linear temperature distribution given in Table 5.2 below.

Table 5.2 Temperature profile for the composite pavement.

Layer		No. of temperature data points										
		1	2	3	4	5	6	7	8	9	10	11
AC	Reference temperature = 55.90 °F											
	Depth, in	0.0	1.0	2.0	3.0	4.0						
	Temp., °F	90.9	86.0	81.0	76.4	71.8						
PCC	Reference temperature = 55.90 °F											
	Depth, in	0.0	0.8	1.6	2.4	3.2	4.0	4.8	5.6	6.4	7.2	8.0

Layer		No. of temperature data points										
		1	2	3	4	5	6	7	8	9	10	11
	Temp., °F	71.8	69.0	66.9	64.8	63.0	61.4	60.0	58.7	57.6	57.0	55.9

The axle load present on the slab is in the form of single axle dual wheel (SADW) load with a total load of 18000 lbs. The tire footprint is 9 in by 5 in and the load is applied at an offset, *s* from the longitudinal edge of the slab. A uniform mesh of 6 in by 6 in elements is generated on the slab. Figure 5.1 presents the mesh and the loading configuration of the composite pavement.

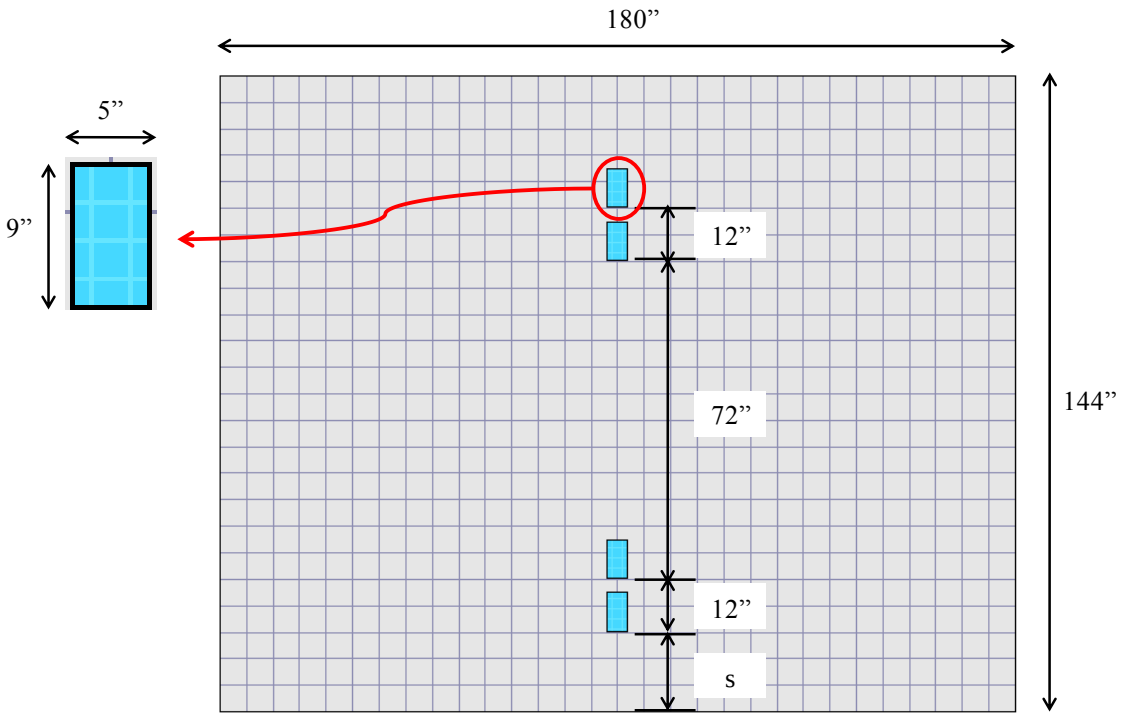

Figure 5.1 The original composite pavement system.

System A is the first simplified structural system with slab dimensions, layer

properties, axle type, total axle load, wheel offset, and non-linear temperature distribution exactly the same as that of the original composite pavement. However, the tire footprint for system A is selected as a square with 7 in sides. The schematic of system A is shown in Figure 5.2.

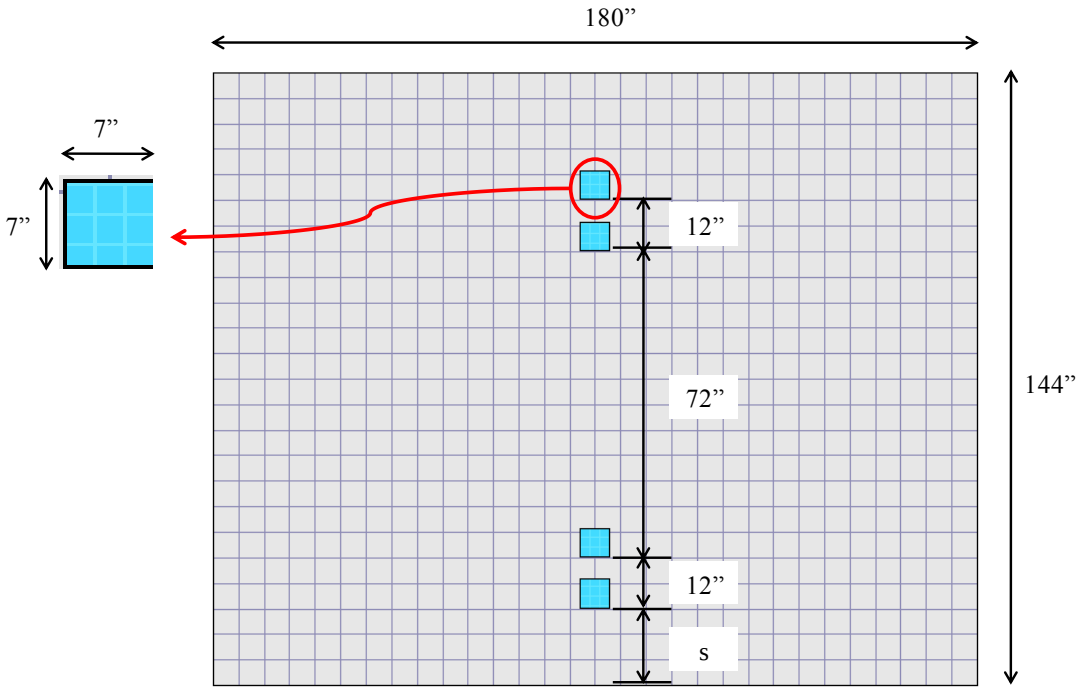

Figure 5.2 System A.

System B, the other simplified structural system, is considered as a single slab with layer properties, axle type, total axle load, wheel offset, and load footprint geometry exactly the same as that of the composite pavement. However, the dimensions for the slab in system B are selected as 30 ft long by 12 ft wide to ignore slab size effects. The schematic of system B is shown in Figure 5.3.

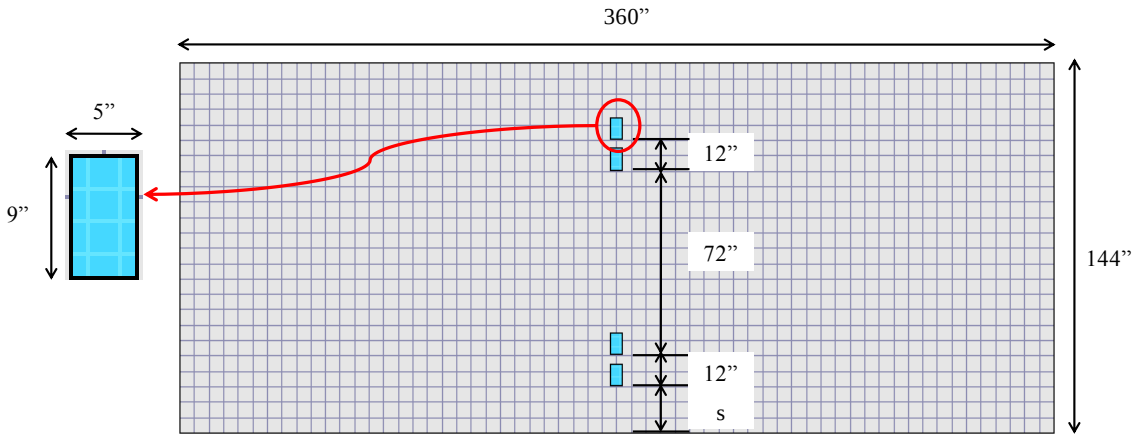

Figure 5.3 System B.

A factorial of 98 cases was considered by varying the offset *s* (i.e., distance of the axle load from the slab edge) and the thickness of the PCC layer. The offset is varied from 0 to 24 in (0, 2, 4, 6, 12, 18, and 24). The thickness of the PCC layer is varied from 2 to 15 in (2, 3, 4, 5, 6, 7, 8, 9, 10, 11, 12, 13, 14, and 15). The stress at the bottom of the PCC layer in the original composite pavement was calculated using the combined stress procedure detailed in Section 4.3 (equations [4.1]) and it was verified against the stress obtained from systems A and B using equation (5.1). The comparison of the stresses is presented in Figure 5.4.

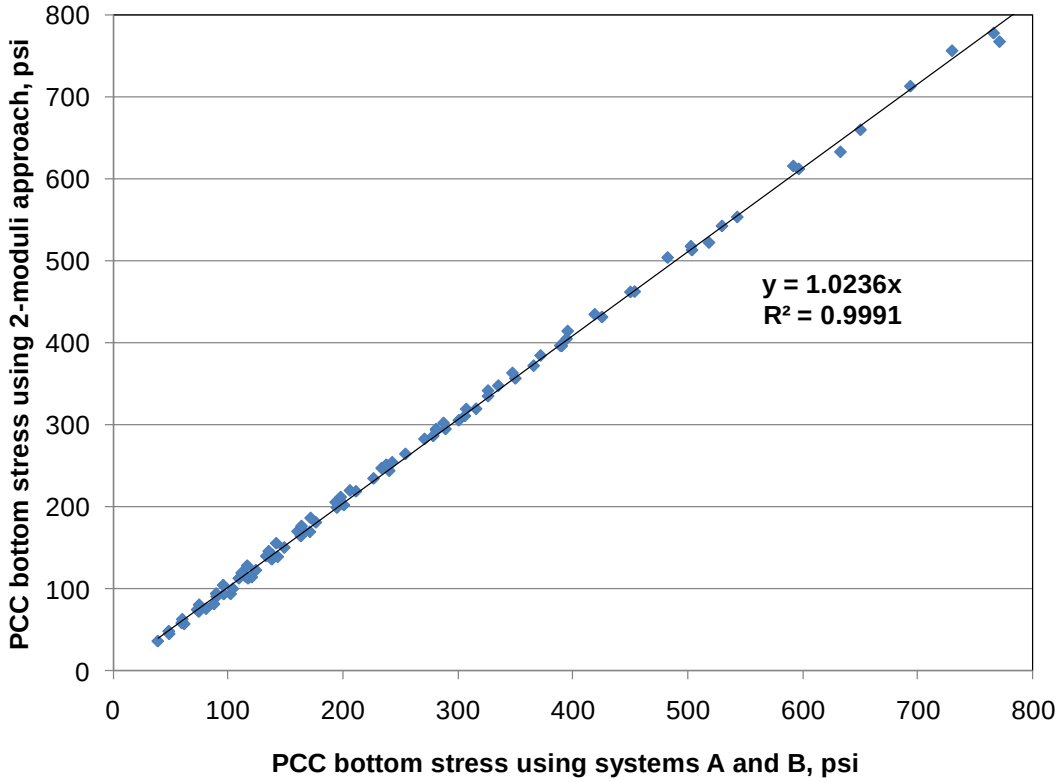

Figure 5.4 Comparison of PCC bottom stresses in the original composite pavement system using the *2-moduli approach* and simplified systems A and B.

A very good match is observed between the stresses obtained using the two methods mentioned above. This implies that similar to the MEPDG, simplified structural systems can be used to represent a composite pavement system for computing stresses using the *2-moduli approach* developed in this research.

Another technique employed by the MEPDG to simplify stress analysis is the use of equivalency conditions to analyze single layer systems in place of multi-layered pavement systems. Using this technique, the number of independent input parameters required for the analysis of multi-layered pavement can be substantially reduced. This was a significant contribution towards the development and training of the MEPDG

neural networks. The following section presents the application of this technique for computation of stresses using the *2-moduli approach*.

5.2 Equivalency Techniques for Multi-Layered Pavements

The stresses in a multi-layered pavement subjected to a combination of traffic loads and temperature distribution are dependent on several factors (*AASHTO 2008*). The MEPDG identifies up to 30 input parameters for the distress model of fatigue cracking in jointed plain concrete pavements (JPCP). These parameters include but are not limited to slab geometry, material properties of the constituent layers, foundation properties, temperature distribution, load geometry and properties, joint spacing, and load transfer efficiency. In the case of composite pavements, there are additional input parameters due to the presence of a viscoelastic asphalt concrete (AC) layer that influence the distress model of fatigue cracking for composite pavements.

In order to reduce the number of input parameters required for the analysis, the solution of a multi-layered pavement is expressed in terms of the solution of a simpler equivalent system. The equivalent system is generally selected as a single layer slab-on-grade. Finally, using equivalency conditions discussed below, the deflection and stress in the multi-layered pavement can be computed in terms of the deflection and stress in the equivalent single layer system, respectively. This technique has been adopted in the MEPDG for the analysis of rigid and composite pavements.

The equivalency between any two pavement systems is established based on the following criteria (*Korenev and Chernigovskaya 1962*; *Ioannides et al. 1992*; and

Khazanovich 1994):

1. Equivalency of slab stiffness, $D = \frac{E\ h^3}{12(1-\mu^2)}$
2. Equivalency of Korenev's non-dimensional temperature gradient, $\phi = \frac{2\alpha(1+\mu)l^2}{h^2}\frac{k}{\gamma}\Delta T$
3. Equivalency of radius of relative stiffness, $l = \sqrt[4]{\frac{D}{k}}$, and
4. Equivalency of normalized load ratio, $q^* = \frac{P}{LW\gamma h}$

where

D is the stiffness of the slab,

h and γ are the thickness and unit weight of the layer, respectively,

E and μ are the Young's modulus and Poisson's ratio of the layer,

α is the coefficient of thermal expansion of the layer,

k is the modulus of subgrade reaction,

ΔT is the equivalent linear temperature gradient given by equation (3.56),

P is the applied axle load, and

L and W are the length and width of the slab, respectively.

If the above mentioned equivalency conditions are satisfied, then the deflections and stresses in the two pavements are related as follows:

$$w_1 = \frac{\gamma_1 h_1 k_2}{\gamma_2 h_2 k_1} w_2 \tag{5.2}$$

$$\sigma_1 = \frac{h_2 \gamma_1}{h_1 \gamma_2} \sigma_2 \tag{5.3}$$

where

w is the deflection of the pavement,

σ is the stress in the pavement, and

subscripts 1 and 2 denote pavement systems 1 and 2, respectively.

A simple example to verify the applicability of equivalency conditions for the stress analysis using the *2-moduli approach* is presented next. The original three-layered composite pavement system presented in Section 5.1, placed on an elastic Winkler foundation, is loaded under a SADW wheel load at an offset of 2 in from the slab edge (Figure 5.1). The modulus of subgrade reaction for the Winkler foundation is equal to 100 psi/in. The properties of the constituent layers are given in Table 5.1. Both of the layer interfaces are fully bonded. The pavement is also subjected to the non-linear temperature distribution given in Table 5.2.

Corresponding to the multi-layered systems 1 and 2 of the BVPs described in Chapter 4, two equivalent single layer slabs (SL1 and SL2) are obtained. Slab SL1 corresponds to the temperature-duration-dependent AC modulus *EACT* and slab SL2 corresponds to the traffic-duration-dependent AC modulus *EACL*. Both the slabs are placed on an elastic Winkler foundation with a coefficient of subgrade reaction equal to 100 psi/in.

Using the equivalency of slab stiffness, either the thickness or the Young's modulus of the equivalent single layer slab can be computed. For this example, the

Young's modulus of the equivalent single layer slab E_{eq} is assumed to be known and the corresponding thickness h_{eq} is calculated as follows:

$$h_{eq} = \sqrt[3]{\frac{1}{E_{eq}}\left(\begin{array}{l} E_{AC}\, h_{AC}^3 + E_{PCC}h_{PCC}^3 + E_{Base}h_{Base}^3 + \\ 12\left[\begin{array}{l} E_{AC}h_{AC}\left(\frac{h_{AC}}{2} - x\right)^2 + E_{PCC}h_{PCC}\left(h_{AC} + \frac{h_{PCC}}{2} - x\right)^2 \\ + E_{Base}h_{Base}\left(h_{AC} + h_{PCC} + \frac{h_{Base}}{2} - x\right)^2 \end{array}\right] \end{array}\right)} \quad (5.4)$$

where

x is the distance of the neutral axis from the top of the AC layer.

And, the unit weight of the equivalent single layer slab γ_{eq} is calculated as:

$$\gamma_{eq} = \frac{\left(\gamma_{AC}h_{AC} + \gamma_{PCC}h_{PCC} + \gamma_{Base}h_{Base}\right)}{h_{eq}} \quad (5.5)$$

The properties of the slabs SL1 and SL2 are presented in Table 5.3 where the thickness and the unit weight are computed using equations (5.4) and (5.5), respectively.

Table 5.3 Layer properties for slabs SL1 and SL2.

	Young's modulus, (psi)	**Poisson's ratio**	**Coefficient of thermal expansion, (1/°F)**	**Thickness, (in)**	**Unit weight, (lb/in3)**
SL1	4.0E+06	0.15	5.50E-06	8.09	0.1290
SL2	4.0E+06	0.15	5.50E-06	8.43	0.1238

Slab SL1 is subjected to an equivalent linear temperature gradient calculated using the non-linear temperature distribution present in the three-layered composite pavement system (Table 5.2) and equation (3.56). Since SL1 corresponds to the temperature-duration-dependent AC modulus *EACT* and is subjected to the temperature

gradient only, stresses in slab SL1 are computed using the first BVP presented in Section 4.3 for temperature curling only.

On the other hand, slab SL2 corresponds to the traffic-duration-dependent AC modulus *EACL* and is subjected to the fictitious force corresponding to the temperature gradient in slab SL1, which is computed using the second BVP presented in Section 4.3. Slab SL2 is also subjected to the SADW load acting on the three-layered composite pavement system. The axle type, axle load, and wheel offset of the SADW load acting on slab SL2 are exactly the same as that on the three-layered composite pavement system. The stress in slab SL2 under the sum of the fictitious force and the SADW load is computed using the third BVP presented in Section 4.3.

The bending stresses obtained at the bottom of slabs SL1 and SL2 are transformed to the bending stress at the bottom of PCC layer in the three-layered composite pavement using equations (3.62) and (3.63) as follows:

$$\sigma_{3LS} = \beta * \sigma_{SL} \tag{5.6}$$

$$\beta_1 = \frac{2*(h_{AC} + h_{PCC} - x_1)}{h_{eq1}} \frac{E_{PCC}}{E_{eq1}} \tag{5.7}$$

$$\beta_2 = \frac{2*(h_{AC} + h_{PCC} - x_2)}{h_{eq2}} \frac{E_{PCC}}{E_{eq2}} \tag{5.8}$$

where

σ_{3LS} is the stress in the three-layered system,

σ_{SL} is the stress in the equivalent single layer slab, and

β is the factor that converts the linear bending stresses at the bottom of the equivalent single layer slab to the linear bending stresses in the multi-layered slab at the depth of interest z.

The deflections and stresses obtained using the stress computation procedure presented in Chapter 4 for the three-layered composite pavement system are compared to the deflections and stresses obtained for the equivalent single layer slabs SL1 and SL2. Table 5.4 presents the deflections and stress at the bottom of the PCC layer at slab edge.

Table 5.4 Deflections and stress at the bottom of the PCC layer at slab edge.

	Location, in		**Deflection, in**	**Longitudinal stress, psi**		
	X	**Y**		σ_{SL}	**β**	σ_{3LS}
Three elastic solution – Three-layered composite pavement						
# 1	90	0	0.0188			136.19
# 2	90	0	0.0188			-101.04
# 3	90	0	0.0424			180.99
Combined stress						418.22
Three elastic solution – Equivalent single layer slabs SL1 and SL2						
SL1: # 1	90	0	0.0188	136.73	0.996	136.191
SL2: # 2	90	0	0.0188	-102.73	0.983	-101.038
SL2: # 3	90	0	0.0424	184.03	0.983	180.993
Combined stress						418.221
% Difference						0.000%

The combined stress in the three-layered composite pavement exactly matches the combined stress obtained from the equivalent single layer slabs SL1 and SL2. This implies that the stress computation procedure, presented in Chapter 4, is capable of

analyzing the multi-layered system through a combination of equivalent single layer systems.

5.3 Summary

The approach presented in this chapter permits an efficient development of rapid solutions for the stress analysis of composite pavements using the *2-moduli approach*. This approach is compatible with the MEPDG stress analysis for the MEPDG PCC fatigue cracking model, but accounts for the load duration dependent behavior of the AC layer. The use of the equivalency concept presented above would permit development of a rapid solution for an equivalent single layer system, thus significantly reducing the number of independent parameters in the statistical model.

CHAPTER 6. CONCLUSIONS

Composite pavements are complex structures incorporating both asphalt and portland cement concrete (PCC) layers. Composite pavement behavior exhibits features of both rigid and flexible pavements. Because of this, a structural analysis of composite pavements is a challenging program. This research concentrated on improving the structural modeling of stress analysis for prediction of PCC fatigue cracking compatible with the MEPDG PCC fatigue cracking modeling. A summary of the research findings is presented below.

6.1 Research Findings

The main findings of this research work can be summarized as follows:

- The use of a single load duration dependent AC dynamic modulus to characterize the behavior of the AC layer seems insufficient for composite pavements subjected to a combination of traffic loads and temperature curling because a significant difference was found in the AC dynamic modulus when a composite pavement is subjected to typical traffic loads and to one hour of temperature loads.
- A finite element (FE) model was developed to analyze a composite pavement placed on a Winkler foundation that incorporates elastic and viscoelastic layers. The FE model has the capability to analyze pavements subjected to traffic loads and temperature curling. The FE model was validated against semi-analytical

solutions.

- A stress computation procedure was developed to calculate stresses in the composite pavement subjected to a combination of traffic loads and temperature curling using two load duration dependent AC moduli. The AC moduli were computed using the existing MEPDG procedure for calculating the dynamic modulus of the AC layer.
- The stress computation procedure based on the *2-moduli approach* demonstrated that the MEPDG may significantly underestimate the stress in composite pavements subjected to a combination of traffic loading and temperature curling. Further investigation of this issue is required.
- A framework for the implementation of the proposed stress procedure into the MEPDG was developed such that minimum modifications to the existing MEPDG framework are required. The proposed stress computation procedure can be directly implemented into the MEPDG for predicting fatigue cracking in composite pavements.

6.2 Recommendations for the Future Research

Based on the findings of this research, the following recommendations for the future research are made:

- The procedure for computing the AC dynamic modulus was originally developed for flexible pavements (AC layer placed directly on top of the base layer). Modifications to this procedure are required for the analysis of composite

pavement due to the presence of a stiff portland cement concrete (PCC) layer between the AC layer and the base.

- In the case of temperature curling analysis, both the MEPDG and the proposed FE model assume the reference temperature of the AC layer as equal to the temperature at the bottom surface of the PCC layer. This assumption needs to be investigated and modified, if required.
- The FE model developed in this research is an extension of the state-of-the-art pavement computational package ISLAB2000 in terms of viscoelastic material modeling. However, not all features of ISLAB2000 are currently implemented in the FE model. Future versions of the FE code require complete merger with ISLAB2000.
- For merging the results of this research with the MEPDG fatigue cracking model for composite pavements, rapid solutions based on the stress computation procedure using the *2-moduli approach* should be generated.
- It has been observed by many researchers that the subgrade behavior of the Winkler foundation is load rate-dependent. The apparent subgrade stiffness is much higher under the fast moving axle loads than during the slow developing temperature curling and moisture warping. Therefore, it may be possible to extend a similar *2-moduli approach* to the subgrade modulus in order to overcome this limitation.

REFERENCES

1. *ABAQUS/Standard*. Hibbitt, Karlsson & Sorensen Inc. User's Manual, Vol. 1, 10.6.1, 1997.

2. *American Association of State Highway and Transportation Officials*. Guide for Design of Pavement Structures, Washington, D.C. 1993.

3. *American Association of State Highway and Transportation Officials*. Mechanistic-Empirical Pavement Design Guide, Interim Edition: A Manual of Practice. Washington, D.C. 2008.

4. *ANSYS*, Inc. Theory Reference. ANSYS Release 9.0. 4-60, 2004.

5. *Bahia H. U., Anderson D. A., and Christensen D. W.* The Bending Beam Rheometer; A Simple Device for Measuring Low-Temperature Rheology of Asphalt Binders. Journal of Association of Asphalt Paving Technologists, Vol. 61, pp. 117-153, 1992.

6. *Banan M. and Hjelmstad.* Data-Based Mathematical Modeling: Development and Application. SRS No. 590, Civil Engineering Studies, University of Illinois, Urbana, IL 1994.

7. *Ceylan H., Tutumluer E., and Barenberg E. J.* Artificial Neural Networks As Design Tools In Concrete Airfield Pavement Design. Proceedings of the 25th International Air Transportation Conference, Austin, Texas, June 14-17, pp. 447-465, 1998.

8. *Ceylan H., Tutumluer E., and Barenberg E. J.* Artificial Neural Network Analyses of Concrete Airfield Pavements Serving the Boeing B-777 Aircraft.

Transportation Research Record 1684, National Research Council, Washington, D.C., pp. 110-117, 1999.

9. *Ceylan H., Tutumluer E., and Barenberg E. J.* Effects of Combined Temperature and Gear Loading on the Response of Concrete Airfield Pavements Serving the Boeing B-777Aircraft. Proceedings of the International Air Transport Conference (IATC), 2020 Vision of Air Transportation, San Francisco, California, June 18-21, 2000.

10. *Chen T.* Determining a Prony Series for a Viscoelastic Material from Time Strain Data. NASA/TM-2000-210123, ARL-TR-2206, Langley Research Center, Hampton, Virginia, 2000.

11. *Chou Y. T.* Structural Analysis Computer Programs for Rigid Multicomponent Pavement Structures with Discontinuities - WESLIQID and WESLAYER, Technical Report GL-81-6, U.S. Army Engineer Waterways Experiment Station, May 1981.

12. *Cook R. D., Malkus D. S., and Plesha M. E.* Concepts and Applications of Finite Element Analysis. John Wiley & Sons, Inc., 1974.

13. *Daniel J. S., Kim Y. R., and Lee H.* Effects of Aging on Viscoelastic Properties of Asphalt-Aggregate Mixtures. Transportation Research Record, Vol. 1630, pp. 21-27, 1998.

14. *Darter M. I. et al.* Composite Pavement Systems. Draft Interim Report, Project SHRP2 R21, Transportation Research Board, Washington D.C. 2008.

15. *Davids W. G., Turkiyyah G. M., and Mahoney J.* EVERFE -- a New Rigid Pavement Finite Element Analysis Tool, Transportation Research Record No. 1629, pp. 69-78, Washington D. C. 1998.

16. *Di Bendetto H., Olard F., Sauzeat C., and Delaporte B.* Linear Viscoelastic Behavior of Bituminous Materials: From Binders to Mixes. International Journal of Road Materials and Pavement Design, Vol. 5, Special Issue, pp. 163-202, 2004.

17. *Di Bendetto H., Delaporte B., and Sauzeat C.* Viscoelastic Modeling and Field Validation of Flexible Pavements. International Journal of Geomechanics, March/April, pp. 149-157, 2007.

18. *Elseifi M. A., Al-Qadi I. L., and Yoo P. J.* Three-dimensional Linear Behavior of Bituminous Materials; Experiments and Modeling. Journal of Engineering Mechanics, Vol. 132, Issue 2, pp. 172 – 178, 2006.

19. *Ferry J.D.* Viscoelastic Properties of Polymers. 2nd edition, Wiley Publication, New York 1970.

20. *FORTRAN.* Visual Numerics, Inc., 1997 http://www.vni.com

21. *Gordon G. V. and Shaw M. T.* Computer Programs for Rheologists. Hanser / Gardner Publication, Munich 1994.

22. *Haussmann L. D., Tutumluer E., and Barenberg E. J.* Neural Network Algorithms for the Correction of Concrete Slab Stresses from Linear Elastic Layered Programs. Transportation Research Record 1568, National Research Council, Washington D.C., pp. 44-51, 1997.

23. *Hill S. A.* The Analytical Representation of Viscoelastic Material Properties using Optimization Techniques. NASA TM-108394, February 1993.

24. *Huang Y. H.* Pavement Analysis and Design. Prentice Hall, Englewood Cliffs, NJ 1993.

25. *Ioannides A. M., Khazanovich L., and Becque J. L.* Structural Evaluation of Base Layers in Concrete Pavement Systems. Transportation Research Record 1370, Washington D. C. 1992.

26. *Ioannides A. M. and Khazanovich L.* Nonlinear Temperature Effects in Multi-Layered Concrete Pavements. ASCE Journal of Transportation Engineering, Vol. 124, No. 2, pp. 128–136, 1998.

27. *Johnson A. R. and Quigley C. J.* A Viscohyperelastic Maxwell Model for Rubber Viscoelasticity. Rubber Chemistry and Technology, Vol. 65, No. 1, pp. 137-153, 1992.

28. *Johnson A. R., Tessler A., and Dambach M.* Dynamics of Thick Viscoelastic Beams. ASME Journal of Engineering Materials and Technology, Vol. 119, pp. 273-278, 1997.

29. *Johnson A. R.* Modeling Viscoelastic Materials Using Internal Variables. The Shock and Vibration Digest, Vol. 31, No. 2, pp. 91-100, 1999.

30. *Kerr A. D.* Elastic and Viscoelastic Foundation Models. ASME Journal of Applied Mechanics, Vol. 31, No. 3, pp. 491-498, 1964.

31. *Khazanovich L.* Structural Analysis of Multi-Layered Concrete Pavement Systems. Ph.D. Dissertation, University of Illinois, Urbana, IL 1994.

32. *Khazanovich L. and Roessler J.* DIPLOBACK: a Neural Networks-Based Backcalculation Program for Composite Pavements. Transportation Research Record 1570, Washington D. C. 1997.

33. *Khazanovich L., Yu H. T., Rao S., Galasova K., Shats E., and Jones R.* ISLAB2000—Finite Element Analysis Program for Rigid and Composite

Pavements: User's Guide. ARA Inc., ERES Consultants Division, Champaign IL, 2000.

34. *Khazanovich L., Selezneva O. I., Yu H. T., and Darter M. I.* Development of Rapid Solutions for Prediction of Critical Continuously Reinforced Concrete Pavement Stresses. Transportation Research Record 1778, pp. 64-72, Washington D.C., 2001.

35. *Korenev B. G. and Chernigovskaya E. I.* Analysis of Plates on Elastic Foundation, Gosstroiizdat, Moscow (in Russian), 1962.

36. *Lesieutre G. A. and Govindswamy K.* Finite Elements Modeling of Frequency Dependent and Temperature Dependent Dynamic Behavior of Viscoelastic Materials in Simple Shear. International Journal of Solids and Structures, Vol. 33, No. 3, pp. 419-432, 1996.

37. *Li Z. D., Yang T. Q., and Luo W. B.* An Improved Model for Bending of Thin Viscoelastic Plate on Elastic Foundation. Natural Science, Vol. 1, No. 2, pp. 120-123, 2009.

38. *Maker B. N., Ferencz R. M., and Hallquist J. O.* NIKE3D, A Nonlinear, Implicit, Three-dimensional Finite Element Code for Solid and Structural Mechanics. User's Manual 4-40, 1995.

39. *Marasteanu M. O. and Anderson D. A.* Improved Model for Bitumen Rheological Characterization. Eurobitume Workshop on Performance Related Properties for Bituminous Binders, Luxembourg, paper no. 133, 1999.

40. *Marasteanu M. O. and Anderson D. A.* Comparison of Moduli for Asphalt Binders Obtained from Different Test Devices. Journal of the Association of Asphalt Paving Technologists, Vol. 69, pp. 574-606, 2000.

41. *Marasteanu M., Velasquez R., Falchetto A. C., and Zofka A.* Development of a Simple Test to Determine the Low Temperature Creep Compliance of Asphalt Mixtures. IDEA Program Transportation Research Board, National Research Council, 2009.

42. *Mase G. E.* Continuum Mechanics. The McGraw-Hill Companies, 1970.

43. *MATHEMATICA*. Wolfram Research, Inc. 1988 http://www.wolfram.com/mathematica/

44. *Monismith C. L. and Secor K. E.* Viscoelastic Behavior of Asphalt Concrete Pavement. First International Conference on the Structural Design of Asphalt Pavements, pp. 476-498, 1962.

45. *Monismith C. L.* Analytically Based Asphalt Pavement Design and Rehabilitation: Theory to Practice, 1962-1992. Transportation Research Record No. 1354, pp. 5-26, 1992.

46. *Nesnas K. and Nunn M. E.* A Model for Top-down Cracking in Composite Pavements. RILEM 4th International Conference on Cracking in Pavements, Limoges, France, 2004.

47. *Osswald, T. A. and Menges G.* Material Science of Polymers for Engineers. 2nd edition, Hanser Gardner Publication, Inc., OH 2003.

48. *Park S. W. and Schapery R. A.* Methods of Interconversion Between Linear Viscoelastic Material Functions. Part I – A Numerical Method Based on Prony Series, International Journal of Solids and Structures, Vol. 36, pp. 1653-1675, 1999.

49. *Park S. W. and Kim Y. R.* Fitting Prony-Series Viscoelastic Models with Power-Law Presmoothing. Journal of Materials in Civil Engineering, Vol. 13, Issue 1, pp. 26-32, 2001.

50. *Pasternak P. L.* Fundamentals of a New Method of Analysis of Structures on Elastic Foundation by Means of Two Subgrade Coefficients. Gosudarstvennoe Izdatel'stvo Literatury po Stroitel'stvu i Arkhitekture, Moscow (in Russian) 1954.

51. *Pellinen T. K. and Witczak M. W.* Stress Dependent Master Curve Construction for Dynamic (Complex) Modulus. Journal of the Association of Asphalt Paving Technologists, 2002.

52. *Ping W. V. and Xiao Y.* Evaluation of the Dynamic Complex Modulus Test and Indirect Diametral Test for Implementing the AASHTO 2002 Design Guide for Pavement Structures in Florida. Florida Department of Transportation, Report No. FL/DOT/RMC/BC-352-12, January 2007.

53. *Reddy J N.* An Introduction to the Finite Element Method. McGraw-Hill, Inc., 1984.

54. *Rowe G. M., Sharrock M. J., Bouldin M.G., and Dongre R. N.* Advanced Techniques to Develop Asphalt Master Curves from the Bending Beam Rheometer. Petroleum and Coal, Vol. 43, No. 1, pp. 54-59, 2001.

55. *Saal R. N. J.* Physical Properties of Asphaltic Bitumen: Rheological Properties. J. P. Pfeiffer, ed., Elsevier, Amsterdam, The Netherlands, pp. 49-76, 1950.

56. *Saal R. N. J. and Labout J. W. A.* Rheologic Properties of Asphalts. Rheology: Theory and Applications, Ed. F. R. Eirich, Vol. II, Academic Press, New York, 1958.

57. *Sayegh G.* Viscoelastic Properties of Bituminous Mixtures. Second International Conference on the Structural Design of Asphalt Pavements, 1967.

58. *Schapery R. A.* Mechanics of Composite Materials. Vol. 2, Ed. Sendeckyj G. P., Academic Press, New York, pp. 85-169, 1974.

59. *Soussou J. E., Moavenzadeh F., Gradowczyk M. H.* Application of Prony Series to Linear Viscoelasticity. Journal of Rheology, Vol. 14, Issue 4, pp. 573-584, 1970.

60. *Tabatabie A. M. and Barenberg E. J.* Structural Analysis of Concrete Pavement Systems. ASCE Transportation Engineering Journal, Vol. 106, No. 5, pp. 493-506, 1980.

61. *Tayabji S. D. and Colley B. E.* Improved Pavement Joints. Transportation Research Record No. 930, Transportation Research Board, National Research Council, Washington D.C., pp. 69- 78, 1983.

62. *Thomlinson J.* Temperature Variations and Consequent Stresses Produced by Daily and Seasonal Temperature Cycles in Concrete Slabs. Concrete Constructional Engineering, Vol. 36, No. 6, pp. 298-307; No. 7, pp. 352-360, 1940.

63. *Timoshenko S. P.* Theory of Elasticity. McGraw-Hill Companies, 3rd Edition, 1970.

64. *Timoshenko S. P. and Woinowsky-Krieger S.* Theory of Plates and Shells. 2nd edition, McGraw-Hill, NY, 1959.

65. *Ugural A. C. and Fenster S. K.* Advanced Strength and Applied Elasticity. Pearson Education, Inc., 2003

66. *UMN Online Lecture 2011*
http://www.me.umn.edu/labs/composites/Projects/Polymer%20Heat%20Exchanger/Creep%20description.pdf

67. *Van der Poel* C. A General System Describing the Viscoelastic Properties of Bitumens and its Relation to Routine Test Data. Journal of Applied Chemistry, Vol. 4, Issue 5, pp. 221-236, May 1954.

68. *Wang Q.* Improvement of Structural Modeling of Flexible Pavements for Mechanistic-Empirical Design, Ph.D. Dissertation, University of Minnesota, December 2007.

69. *Zienkiewicz O. C. and Taylor R. L.* Finite Element Method for Solid and Structural Mechanics, 1st Edition, Elsevier, 1967.

70. *Zofka A.* Investigation of Asphalt Concrete Creep Behavior using 3-point Bending Test. Ph.D. Dissertation, University of Minnesota, 2007.

71. *Zofka A., Marasteanu M. O., and Turos M.* Determination of Asphalt Mixture Creep Compliance at Low Temperatures by Using Thin Beam Specimens. Transportation Research Record No. 2057, Transportation Research Board, pp. 134-139, Washington D. C. 2008.

APPENDIX A

This appendix details the procedure for calculation of stresses due to the non-linear-strain-causing temperature component in a composite pavement. According to Thomlinson (*1940*) any arbitrary temperature distribution, $T(z)$ can be divided into three components given as follows:

1. The constant strain-causing temperature component given as:

$$T_c(z) = T_o + \frac{\sum_{i=1}^{l} \int_h \alpha(z) E(z) [T(z) - T_o] dz}{\alpha(z) \sum_{i=1}^{l} \int_h E(z) dz} \quad \text{(A.1)}$$

where

z is the depth of the point of interest from the neutral axis,

T_0 is the reference temperature of the layer at which there are no temperature-related stresses or strains in the layer,

l is the total number of layers in the multi-layered system,

E is the Young's modulus,

α is the coefficient of thermal expansion, and

$T(z)$ is the arbitrary temperature distribution.

2. The linear strain-causing temperature component given as:

$$T_L(z) = T_o + \frac{z}{\alpha(z)} \frac{\sum_{i=1}^{l} \int_h \alpha(z)E(z)[T(z) - T_o]zdz}{\sum_{i=1}^{l} \int_h E(z)z^2 dz} \quad \text{(A.2)}$$

3. The nonlinear strain-causing temperature component.

By definition, the difference between the total temperature distribution and the reference temperature is equal to the sum of the differences of the individual temperature components and the reference temperature defined as follows:

$$T(z) - T_o = [T_c(z) - T_o] + [T_L(z) - T_o] + [T_{NL}(z) - T_o] \quad \text{(A.3)}$$

Therefore, the nonlinear-strain-causing temperature component, T_{NL}, could be written as:

$$T_{NL}(z) - T_o = T(z) - [T_c(z) - T_o] - [T_L(z) - T_o] - T_o \quad \text{(A.4)}$$

The nonlinear-strain-causing temperature component and corresponding stress at the bottom of the PCC layer are given as:

$$(T_{NL,PCC,bot} - T_o) = T_{11} - (T_{c,PCC} - T_o) - (T_{L,PCC,bot} - T_o) - T_o \quad \text{(A.5)}$$

$$\sigma_{NL,PCC,bot} = -\frac{E_{PCC}\alpha_{PCC}}{(1-\mu)}\left(T_{NL,PCC,bot} - T_o\right) \quad \text{(A.6)}$$

and, at the top of the PCC layer as:

$$(T_{NL,PCC,top} - T_o) = T_1 - (T_{c,PCC} - T_o) - (T_{L,PCC,top} - T_o) - T_o \quad \text{(A.7)}$$

$$\sigma_{NL,PCC,top} = -\frac{E_{PCC}\alpha_{PCC}}{(1-\mu)}\left(T_{NL,PCC,top} - T_o\right) \quad \text{(A.8)}$$

where

μ is Poisson's ratio of the layer.

The following sections detail the process of calculating the constant strain-causing temperature component and linear strain-causing temperature component using the temperature distribution present in the three-layered composite pavement. The procedure is detailed for all combinations of interface conditions in the composite pavement.

1. Unbonded AC-PCC and Unbonded PCC-Base Interfaces

If a pavement slab is not constrained horizontally then the constant strain-causing temperature component causes free expansion of the layer. The free expansion does not cause stresses (and strains) in any of the layers as the layers are not bonded. Therefore, the layers can be treated independently of one another to compute the constant strain-causing temperature component. For this particular interface condition, the neutral axes (NA) of the AC and the base layers are as follows:

$$\zeta_{AC} = z + \left(\frac{h_{AC} + h_{PCC}}{2} \right) \tag{A.9}$$

$$\zeta_{Base} = z - \left(\frac{h_{PCC} + h_{Base}}{2} \right) \tag{A.10}$$

The constant strain-causing temperature component for each layer is given as:

$$T_{c,AC} = T_o + \frac{\int_{-\frac{h_{AC}}{2}}^{\frac{h_{AC}}{2}} \alpha_{AC} E_{AC} \left[T(\zeta_{AC}) - T_{oAC} \right] d\zeta_{AC}}{\alpha_{AC} \int_{-\frac{h_{AC}}{2}}^{\frac{h_{AC}}{2}} E_{AC} d\zeta_{AC}} = \frac{1}{h_{AC}} \int_{-\frac{h_{AC}}{2}}^{\frac{h_{AC}}{2}} T(\zeta_{AC}) d\zeta_{AC} \tag{A.11}$$

$$T_{c,PCC} = T_o + \frac{\int_{-\frac{h_{PCC}}{2}}^{\frac{h_{PCC}}{2}} \alpha_{PCC} E_{PCC}\left[T(z) - T_o\right]dz}{\alpha_{PCC}\int_{-\frac{h_{PCC}}{2}}^{\frac{h_{PCC}}{2}} E_{PCC}dz} = \frac{1}{h_{PCC}}\int_{-\frac{h_{PCC}}{2}}^{\frac{h_{PCC}}{2}} T(z)dz \quad \text{(A.12)}$$

$$T_{c,Base} = T_o + \frac{\int_{\frac{-h_{Base}}{2}}^{\frac{h_{Base}}{2}} \alpha_{Base} E_{Base}\left[T(\zeta_{Base}) - T_{oBase}\right]d\zeta_{Base}}{\alpha_{Base}\int_{\frac{-h_{Base}}{2}}^{\frac{h_{Base}}{2}} E_{Base}d\zeta_{Base}} = \frac{1}{h_{Base}}\int_{\frac{-h_{Base}}{2}}^{\frac{h_{Base}}{2}} T(\zeta_{Base})d\zeta_{Base} \quad \text{(A.13)}$$

The MEPDG considers the temperature distribution in the AC and PCC layers at 4 and 11 points through the thickness of these layers, respectively. Therefore, the integrals of equations (A.11) to (A.13) can be approximated numerically as:

$$T_{c,AC} - T_o = \frac{1}{8}\left((T_{1AC} - T_{oAC1}) + 2*\sum_{i=2}^{4}(T_i - T_{oACi}) + (T_{5AC} - T_{oAC5})\right)$$

$$\text{(A.14)}\; T_{c,PCC} - T_o = \frac{1}{h_{PCC}}\frac{h_{PCC}}{20}\left(T_1 + 2*\sum_{i=2}^{10}T_i + T_{11}\right) - T_o \quad \text{(A.15)}$$

$$T_{c,Base} - T_o = \frac{1}{2}\left(T_{1Base} + T_{2Base}\right) - T_o \quad \text{(A.16)}$$

Using equation (A.2), the linear strain-causing temperature component is given as:

$$T_{L,AC} = T_o + S_1\frac{\zeta_{AC}}{\alpha_{AC}} = T_o + 12S\frac{\zeta_{AC}}{\alpha_{AC}} \quad \text{(A.17)}$$

$$T_{L,PCC} = T_o + S_1\frac{z}{\alpha_{PCC}} = T_o + 12S\frac{z}{\alpha_{PCC}} \quad \text{(A.18)}$$

$$T_{L,Base} = T_o + S_1\frac{\zeta_{Base}}{\alpha_{Base}} = T_o + 12S\frac{\zeta_{Base}}{\alpha_{Base}} \quad \text{(A.19)}$$

where

$$S = \frac{\begin{aligned}\int_{-\frac{h_{AC}}{2}}^{\frac{h_{AC}}{2}} \alpha_{AC} E_{AC}\left[T(\zeta_{AC}) - T_{oAC}\right]\zeta_{AC}\, d\zeta_{AC} + \int_{-\frac{h_{PCC}}{2}}^{\frac{h_{PCC}}{2}} \alpha_{PCC} E_{PCC}\left[T(z) - T_o\right] z\, dz \\ + \int_{-\frac{h_{Base}}{2}}^{\frac{h_{Base}}{2}} \alpha_{Base} E_{Base}\left[T(\zeta_{Base}) - T_o\right]\zeta_{Base}\, d\zeta_{Base}\end{aligned}}{E_{AC} h_{AC}^3 + E_{PCC} h_{PCC}^3 + E_{Base} h_{Base}^3} \tag{A.20}$$

The thickness and the unit weight of an equivalent slab with Young's modulus E_{PCC} and coefficient of thermal expansion α_{PCC}, are given as:

$$h_{eff} = \sqrt[3]{\frac{E_{AC}}{E_{PCC}} h_{AC}^3 + h_{PCC}^3 + \frac{E_{Base}}{E_{PCC}} h_{Base}^3} \tag{A.21}$$

$$\gamma_{eff} = \frac{h_{AC}\gamma_{AC} + h_{PCC}\gamma_{PCC}}{h_{eff}} \tag{A.22}$$

Therefore, the linear strain-causing temperature in the equivalent slab can be written as:

$$T_{L,eff} = T_o + 12S\frac{z_{eff}}{\alpha_{PCC}} \tag{A.23}$$

Using equation (A.23), the linear strain-causing temperature at the top surface of the equivalent slab can be written as:

$$T_{L,eff,top} = T_o + 12S\frac{-h_{eff}/2}{\alpha_{PCC}} \tag{A.24}$$

and at the bottom surface as:

$$T_{L,eff,bot} = T_o + 12S\frac{h_{eff}/2}{\alpha_{PCC}} \tag{A.25}$$

Therefore, the linear temperature gradient in the equivalent slab can be derived as:

$$\Delta T_{L,eff} = T_{L,eff,top} - T_{L,eff,bot} = -12S\frac{h_{eff}}{\alpha_{PCC}} \tag{A.26}$$

or,

$$\Delta T_{L,eff} = \frac{-12}{h_{eff}^2}\left(\begin{array}{l}\dfrac{\alpha_{AC}E_{AC}}{\alpha_{PCC}E_{PCC}}\displaystyle\int_{-\frac{h_{AC}}{2}}^{\frac{h_{AC}}{2}}\left[T(\zeta_{AC})-T_{oAC}\right]\zeta_{AC}\,d\zeta_{AC} + \int_{-\frac{h_{PCC}}{2}}^{\frac{h_{PCC}}{2}}\left[T(z)-T_o\right]z\,dz \\ \qquad + \dfrac{\alpha_{Base}E_{Base}}{\alpha_{PCC}E_{PCC}}\displaystyle\int_{-\frac{h_{Base}}{2}}^{\frac{h_{Base}}{2}}\left[T(\zeta_{Base})-T_o\right]\zeta_{Base}\,d\zeta_{Base}\end{array}\right) \tag{A.27}$$

The Mechanistic Empirical Pavement Design Guide (MEPDG) assumes that the temperature distribution in the base layer is constant through its thickness and is equal to the temperature at the bottom of the PCC layer. Applying similar assumptions to the composite pavement, equation (A.27) can be rewritten as:

$$\Delta T_{L,eff} = \frac{-12}{h_{eff}^2}\left(\frac{\alpha_{AC}E_{AC}}{\alpha_{PCC}E_{PCC}}\int_{-\frac{h_{AC}}{2}}^{\frac{h_{AC}}{2}}\left[T(\zeta_{AC})-T_{oAC}\right]\zeta_{AC}\,d\zeta_{AC} + \int_{-\frac{h_{PCC}}{2}}^{\frac{h_{PCC}}{2}}\left[T(z)-T_o\right]z\,dz\right) \tag{A.28}$$

or,

$$\Delta T_{L,eff} = \frac{-12}{h_{eff}^2}\left(\frac{\alpha_{AC}E_{AC}}{\alpha_{PCC}E_{PCC}}\int_{-\frac{h_{AC}}{2}}^{\frac{h_{AC}}{2}}T(\zeta_{AC})\zeta_{AC}\,d\zeta_{AC} + \int_{-\frac{h_{PCC}}{2}}^{\frac{h_{PCC}}{2}}T(z)z\,dz\right) \tag{A.29}$$

The integrals of equation (A.29) can be approximated numerically as:

$$\Delta T_{L,eff} = \frac{-12}{h_{eff}^2}\left(\begin{array}{l}\frac{\alpha_{AC}E_{AC}}{\alpha_{PCC}E_{PCC}}\frac{h_{AC}}{24}\sum_{i=1}^{4}\left(\begin{array}{l}(T_i - T_{oACi})*\left((3i-2)*\frac{h_{AC}}{4} - 3\frac{h_{AC}}{2}\right)\\ +(T_{i+1} - T_{oACi+1})*\left((3i-1)*\frac{h_{AC}}{4} - 3\frac{h_{AC}}{2}\right)\end{array}\right)\\ +\frac{h_{PCC}}{60}\sum_{i=1}^{10}\left(\begin{array}{l}T_i*\left((3i-2)*\frac{h_{PCC}}{10} - 3\frac{h_{PCC}}{2}\right)\\ +T_{i+1}*\left((3i-1)*\frac{h_{PCC}}{10} - 3\frac{h_{PCC}}{2}\right)\end{array}\right)\end{array}\right) \quad \text{(A.30)}$$

Finally, using equations (A.17) to (A.19) and (A.30), the linear strain-causing temperature at the top and the bottom of all layers of the composite pavement can be written as:

$$T_{L,AC,top} - T_o = \frac{\Delta T_{L,eff}}{h_{eff}}\frac{h_{AC}}{2}\frac{\alpha_{PCC}}{\alpha_{AC}} \quad \text{(A.31)}$$

$$T_{L,AC,bot} - T_o = \frac{-\Delta T_{L,eff}}{h_{eff}}\frac{h_{AC}}{2}\frac{\alpha_{PCC}}{\alpha_{AC}} \quad \text{(A.32)}$$

$$T_{L,PCC,top} - T_o = \frac{\Delta T_{L,eff}}{h_{eff}}\frac{h_{PCC}}{2} \quad \text{(A.33)}$$

$$T_{L,PCC,bot} - T_o = \frac{-\Delta T_{L,eff}}{h_{eff}}\frac{h_{PCC}}{2} \quad \text{(A.34)}$$

$$T_{L,Base,top} - T_o = \frac{\Delta T_{L,eff}}{h_{eff}}\frac{h_{Base}}{2}\frac{\alpha_{PCC}}{\alpha_{Base}} \quad \text{(A.35)}$$

$$T_{L,Base,bot} - T_o = \frac{-\Delta T_{L,eff}}{h_{eff}}\frac{h_{Base}}{2}\frac{\alpha_{PCC}}{\alpha_{Base}} \quad \text{(A.36)}$$

2. Bonded AC-PCC and Bonded PCC-Base Interfaces

For this particular interface condition, the neutral axis (N.A.) of the composite pavement is given as follows:

$$x = \frac{\frac{E_{AC}}{E_{PCC}}\frac{h_{AC}^2}{2} + h_{PCC}\left(h_{AC} + \frac{h_{PCC}}{2}\right) + \frac{E_{Base}}{E_{PCC}}h_{Base}\left(h_{AC} + h_{PCC} + \frac{h_{Base}}{2}\right)}{\frac{E_{AC}}{E_{PCC}}h_{AC} + h_{PCC} + \frac{E_{Base}}{E_{PCC}}h_{Base}} \tag{A.37}$$

where

x is the distance of the NA from the top of the AC layer.

The thickness and the unit weight of an equivalent slab with Young's modulus E_{PCC} and coefficient of thermal expansion α_{PCC}, are given as:

$$h_{eff} = \sqrt[3]{\frac{E_{AC}}{E_{PCC}}h_{AC}^3 + h_{PCC}^3 + \frac{E_{Base}}{E_{PCC}}h_{Base}^3 + 12\left[\begin{array}{l}\frac{E_{AC}}{E_{PCC}}h_{AC}\left(x - \frac{h_{AC}}{2}\right)^2 + h_{PCC}\left(h_{AC} + \frac{h_{PCC}}{2} - x\right)^2 \\ + \frac{E_{Base}}{E_{PCC}}h_{Base}\left(h_{AC} + h_{PCC} + \frac{h_{Base}}{2} - x\right)^2\end{array}\right]} \tag{A.38}$$

$$\gamma_{eff} = \frac{h_{AC}\gamma_{AC} + h_{PCC}\gamma_{PCC} + h_{Base}\gamma_{Base}}{h_{eff}} \tag{A.39}$$

Using equation (A.1), the constant strain-causing temperature component in the PCC layer is given as:

$$T_c(z)-T_o=\frac{1}{\alpha(z)}\frac{\begin{array}{r}\int_{-x}^{h_{AC}-x}\alpha_{AC}E_{AC}\left[T(z)-T_{oAC}\right]dz+\int_{h_{AC}-x}^{h_{AC}+h_{PCC}-x}\alpha_{PCC}E_{PCC}\left[T(z)-T_o\right]dz\\ +\int_{h_{AC}+h_{PCC}-x}^{h_{AC}+h_{PCC}+h_{Base}-x}\alpha_{Base}E_{Base}\left[T(z)-T_o\right]dz\end{array}}{E_{AC}h_{AC}+E_{PCC}h_{PCC}+E_{Base}h_{Base}} \tag{A.40}$$

Equation (A.40) can be approximated numerically as follows:

$$T_c(z)-T_o=\frac{\begin{array}{l}\frac{\alpha_{AC}E_{AC}}{\alpha_{PCC}}\left(\frac{h_{AC}}{8}\left((T_{AC1}-T_{oAC1})+2*\sum_{i=2}^{4}(T_{ACi}-T_{oACi})+(T_{AC5}-T_{oAC5})\right)\right)\\ +E_{PCC}\left(\frac{h_{PCC}}{20}\left(T_1+2*\sum_{i=2}^{10}T_i+T_{11}\right)-T_oh_{PCC}\right)\end{array}}{E_{AC}h_{AC}+E_{PCC}h_{PCC}+E_{Base}h_{Base}} \tag{A.41}$$

The constant strain-causing temperature component in the AC and base layers can be written as:

$$T_{c,AC}(z)-T_o=(T_c(z)-T_o)*\frac{\alpha_{PCC}}{\alpha_{AC}} \tag{A.42}$$

$$T_{c,Base}(z)-T_o=(T_c(z)-T_o)*\frac{\alpha_{PCC}}{\alpha_{Base}} \tag{A.43}$$

Using equation (A.2), the linear strain-causing temperature component is given as:

$$T_L(z)=T_o+\frac{12z}{\alpha(z)}\frac{\begin{array}{r}\int_{-x}^{h_{AC}-x}\alpha_{AC}E_{AC}\left[T(z)-T_{oAC}\right]zdz+\int_{h_{AC}-x}^{h_{AC}+h_{PCC}-x}\alpha_{PCC}E_{PCC}\left[T(z)-T_o\right]zdz\\ +\int_{h_{AC}+h_{PCC}-x}^{h_{AC}+h_{PCC}+h_{Base}-x}\alpha_{Base}E_{Base}\left[T(z)-T_o\right]zdz\end{array}}{E_{AC}h_{AC}^3+E_{PCC}h_{PCC}^3+E_{Base}h_{Base}^3+12\left[\begin{array}{r}E_{AC}h_{AC}\left(x-\frac{h_{AC}}{2}\right)^2+E_{PCC}h_{PCC}\left(h_{AC}+\frac{h_{PCC}}{2}-x\right)^2\\ +E_{Base}h_{Base}\left(h_{AC}+h_{PCC}+\frac{h_{Base}}{2}-x\right)^2\end{array}\right]} \tag{A.44}$$

Therefore, the linear temperature gradient in the equivalent slab can be written as:

$$\Delta T_{L,eff} = \frac{-12h_{eff}}{\alpha_{PCC}} \left(\frac{\begin{array}{l} \int_{-x}^{h_{AC}-x} \alpha_{AC} E_{AC} [T(z) - T_{oAC}] z dz + \int_{h_{AC}-x}^{h_{AC}+h_{PCC}-x} \alpha_{PCC} E_{PCC} [T(z) - T_o] z dz \\ + \int_{h_{AC}+h_{PCC}-x}^{h_{AC}+h_{PCC}+h_{Base}-x} \alpha_{Base} E_{Base} [T(z) - T_o] z dz \end{array}}{E_{PCC} h_{eff}^3} \right) \quad \text{(A.45)}$$

or,

$$\Delta T_{L,eff} = \frac{-12}{h_{eff}^2} \left(\int_{-x}^{h_{AC}-x} \frac{\alpha_{AC} E_{AC}}{\alpha_{PCC} E_{PCC}} [T(z) - T_{oAC}] z dz + \int_{h_{AC}-x}^{h_{AC}+h_{PCC}-x} [T(z) - T_{11}] z dz \right) \quad \text{(A.46)}$$

Equation (A.46) can be approximated numerically as follows:

$$\Delta T_{L,eff} = \frac{-12}{h_{eff}^2} \left(\begin{array}{l} \frac{\alpha_{AC} E_{AC}}{\alpha_{PCC} E_{PCC}} \frac{h_{AC}}{24} \sum_{i=1}^{4} \left(\begin{array}{l} (T_i - T_{oACi}) * \left((3i-2) * \frac{h_{AC}}{4} - 3x \right) \\ + (T_{i+1} - T_{oACi+1}) * \left((3i-1) * \frac{h_{AC}}{4} - 3x \right) \end{array} \right) \\ + \frac{h_{PCC}}{60} \sum_{i=1}^{10} \left(\begin{array}{l} T_i * \left((3i-2) * \frac{h_{PCC}}{10} - 3(x - h_{AC}) \right) \\ + T_{i+1} * \left((3i-1) * \frac{h_{PCC}}{10} - 3(x - h_{AC}) \right) \end{array} \right) \\ - \frac{T_o}{2} h_{PCC} (h_{PCC} + 2h_{AC} - 2x) \end{array} \right) \quad \text{(A.47)}$$

Finally, the linear strain-causing temperature at the top and the bottom of all layers of the composite pavement can be written as:

$$T_{L,AC,top} - T_o = \frac{\Delta T_{L,eff}}{h_{eff}}(x) \frac{\alpha_{PCC}}{\alpha_{AC}} \quad \text{(A.48)}$$

$$T_{L,AC,bot} - T_o = \frac{\Delta T_{L,eff}}{h_{eff}}(x - h_{AC})\frac{\alpha_{PCC}}{\alpha_{AC}} \tag{A.49}$$

$$T_{L,PCC,top} - T_o = \frac{\Delta T_{L,eff}}{h_{eff}}(x - h_{AC}) \tag{A.50}$$

$$T_{L,PCC,bot} - T_o = \frac{-\Delta T_{L,eff}}{h_{eff}}(h_{PCC} + h_{AC} - x) \tag{A.51}$$

$$T_{L,Base,top} - T_o = \frac{-\Delta T_{L,eff}}{h_{eff}}(h_{PCC} + h_{AC} - x)\frac{\alpha_{PCC}}{\alpha_{Base}} \tag{A.52}$$

$$T_{L,Base,bot} - T_o = \frac{-\Delta T_{L,eff}}{h_{eff}}(h_{AC} + h_{PCC} + h_{Base} - x)\frac{\alpha_{PCC}}{\alpha_{Base}} \tag{A.53}$$

3. Unbonded AC-PCC and Bonded PCC-Base Interfaces

For this particular interface condition, the neutral axis (NA) for the bonded layers of the composite pavement and for the AC layer is given as follows:

$$x_{PB} = \frac{\frac{h_{PCC}^2}{2} + \frac{E_{Base}}{E_{PCC}}h_{Base}\left(h_{PCC} + \frac{h_{Base}}{2}\right)}{h_{PCC} + \frac{E_{Base}}{E_{PCC}}h_{Base}} \tag{A.54}$$

$$\zeta_{AC} = z + \left(\frac{h_{AC}}{2} + x_{PB}\right) \tag{A.55}$$

The thickness and the unit weight of an equivalent slab with Young's modulus E_{PCC} and coefficient of thermal expansion α_{PCC}, are given as:

$$h_{eff} = \sqrt[3]{\frac{E_{AC}}{E_{PCC}}h_{AC}^3 + h_{PCC}^3 + \frac{E_{Base}}{E_{PCC}}h_{Base}^3 + 12\left[\begin{array}{l} h_{PCC}\left(x_{PB} - \frac{h_{PCC}}{2}\right)^2 \\ + \frac{E_{Base}}{E_{PCC}}h_{Base}\left(h_{PCC} + \frac{h_{Base}}{2} - x_{PB}\right)^2 \end{array}\right]} \tag{A.56}$$

$$\gamma_{eff} = \frac{h_{AC}\gamma_{AC} + h_{PCC}\gamma_{PCC} + h_{Base}\gamma_{Base}}{h_{eff}} \tag{A.57}$$

Using equation (A.1), the constant strain-causing temperature components in the AC, PCC, and base layers are given as:

$$T_{c,AC} = T_o + \frac{\int_{-\frac{h_{AC}}{2}}^{\frac{h_{AC}}{2}} \alpha_{AC}E_{AC}\left[T(\zeta_{AC}) - T_{oAC}\right]d\zeta_{AC}}{\alpha_{AC}\int_{-\frac{h_{AC}}{2}}^{\frac{h_{AC}}{2}} E_{AC}d\zeta_{AC}} = \frac{1}{h_{AC}}\int_{-\frac{h_{AC}}{2}}^{\frac{h_{AC}}{2}} T(\zeta_{AC})d\zeta_{AC} \tag{A.58}$$

$$T_{c,PCC}(z) = T_o + \frac{1}{\alpha_{PCC}}\frac{\int_{-x_{PB}}^{h_{PCC}-x_{PB}} \alpha_{PCC}E_{PCC}\left[T(z) - T_o\right]dz + \int_{h_{PCC}-x_{PB}}^{h_{PCC}+h_{Base}-x_{PB}} \alpha_{Base}E_{Base}\left[T(z) - T_o\right]dz}{E_{PCC}h_{PCC} + E_{Base}h_{Base}} \tag{A.59}$$

$$T_{c,Base}(z) - T_o = (T_c(z) - T_o) * \frac{\alpha_{PCC}}{\alpha_{Base}} \tag{A.60}$$

Equations (A.58) and (A.59) can be approximated numerically as follows:

$$T_{c,AC} - T_o = \frac{1}{8}\left(T_{1AC} + 2 * \sum_{i=2}^{4} T_i + T_{5AC}\right) - T_o \tag{A.61}$$

$$T_{c,PCC} - T_o = \frac{E_{PCC}\left(\frac{h_{PCC}}{20}\left(T_1 + 2 * \sum_{i=2}^{10} T_i + T_{11}\right) - T_o h_{PCC}\right)}{E_{PCC}h_{PCC} + E_{Base}h_{Base}} \tag{A.62}$$

Using equation (A.2), the linear strain-causing temperature components are given as:

$$T_{L,AC} = T_o + 12S\frac{\zeta_{AC}}{\alpha_{AC}} \tag{A.63}$$

$$T_L(z) = T_o + 12S\frac{z}{\alpha(z)} \tag{A.64}$$

where

$$S = \frac{\begin{aligned}&\int_{-\frac{h_{AC}}{2}}^{\frac{h_{AC}}{2}} \alpha_{AC}E_{AC}\left[T(\zeta_{AC}) - T_{oAC}\right]\zeta_{AC}\,d\zeta_{AC} + \int_{-x_{PB}}^{h_{PCC}-x_{PB}} \alpha_{PCC}E_{PCC}\left[T(z) - T_o\right]z\,dz \\ &+ \int_{h_{PCC}-x_{PB}}^{h_{PCC}+h_{Base}-x_{PB}} \alpha_{Base}E_{Base}\left[T(z) - T_o\right]z\,dz\end{aligned}}{\begin{aligned}&E_{AC}h_{AC}^3 + E_{PCC}h_{PCC}^3 + E_{Base}h_{Base}^3 \\ &+12\left[E_{PCC}h_{PCC}\left(x_{PB} - \frac{h_{PCC}}{2}\right)^2 + E_{Base}h_{Base}\left(h_{PCC} + \frac{h_{Base}}{2} - x_{PB}\right)^2\right]\end{aligned}} \tag{A.65}$$

Therefore, the linear temperature gradient in the equivalent slab can be written as:

$$\Delta T_{L,eff} = \frac{-12h_{eff}}{\alpha_{PCC}}\left(\frac{\begin{aligned}&\int_{-\frac{h_{AC}}{2}}^{\frac{h_{AC}}{2}} \alpha_{AC}E_{AC}\left[T(\zeta_{AC}) - T_{oAC}\right]\zeta_{AC}\,d\zeta_{AC} \\ &+ \int_{-x_{PB}}^{h_{PCC}-x_{PB}} \alpha_{PCC}E_{PCC}\left[T(z) - T_o\right]z\,dz + \int_{h_{PCC}-x_{PB}}^{h_{PCC}+h_{Base}-x_{PB}} \alpha_{Base}E_{Base}\left[T(z) - T_o\right]z\,dz\end{aligned}}{E_{PCC}h_{eff}^3}\right) \tag{A.66}$$

or,

$$\Delta T_{L,eff} = \frac{-12}{h_{eff}^2}\left(\frac{\alpha_{AC}E_{AC}}{\alpha_{PCC}E_{PCC}}\int_{-\frac{h_{AC}}{2}}^{\frac{h_{AC}}{2}} T(\zeta_{AC})\zeta_{AC}\,d\zeta_{AC} + \int_{-x_{PB}}^{h_{PCC}-x_{PB}} T(z)z\,dz - T_o\int_{-x_{PB}}^{h_{PCC}-x_{PB}} z\,dz\right) \tag{A.67}$$

Equation (A.67) can be approximated numerically as follows:

$$\Delta T_{L,eff} = \frac{-12}{h_{eff}^2}\left(\begin{array}{l} \frac{\alpha_{AC}E_{AC}}{\alpha_{PCC}E_{PCC}}\frac{h_{AC}}{24}\sum_{i=1}^{4}\left(\begin{array}{l} T_i*\left((3i-2)*\frac{h_{AC}}{4}-3x_{AC}\right) \\ +T_{i+1}*\left((3i-1)*\frac{h_{AC}}{4}-3x_{AC}\right)\end{array}\right) \\ +\frac{h_{PCC}}{60}\sum_{i=1}^{10}\left(\begin{array}{l} T_i*\left((3i-2)*\frac{h_{PCC}}{10}-3x_{PB}\right) \\ +T_{i+1}*\left((3i-1)*\frac{h_{PCC}}{10}-3x_{PB}\right)\end{array}\right) \\ -\frac{T_{11}}{2}h_{PCC}\left(h_{PCC}-2x_{PB}\right)\end{array}\right) \tag{A.68}$$

Finally, the linear strain-causing temperature at the top and the bottom of all layers of the composite pavement can be written as:

$$T_{L,AC,top} - T_o = \frac{\Delta T_{L,eff}}{h_{eff}}\frac{h_{AC}}{2}\frac{\alpha_{PCC}}{\alpha_{AC}} \tag{A.69}$$

$$T_{L,AC,bot} - T_o = \frac{-\Delta T_{L,eff}}{h_{eff}}\frac{h_{AC}}{2}\frac{\alpha_{PCC}}{\alpha_{AC}} \tag{A.70}$$

$$T_{L,PCC,top} - T_o = \frac{\Delta T_{L,eff}}{h_{eff}}x_{PB} \tag{A.71}$$

$$T_{L,PCC,bot} - T_o = \frac{-\Delta T_{L,eff}}{h_{eff}}(h_{PCC} - x_{PB}) \tag{A.72}$$

$$T_{L,Base,top} - T_o = \frac{-\Delta T_{L,eff}}{h_{eff}}(h_{PCC} - x)\frac{\alpha_{PCC}}{\alpha_{Base}} \tag{A.73}$$

$$T_{L,Base,bot} - T_o = \frac{-\Delta T_{L,eff}}{h_{eff}}(h_{PCC} + h_{Base} - x)\frac{\alpha_{PCC}}{\alpha_{Base}} \tag{A.74}$$

4. Bonded AC-PCC and Unbonded PCC-Base Interfaces

For this particular interface condition, the neutral axes (NA) of the bonded layers of the composite pavement and of the base layer are given as follows:

$$x_{AP} = \frac{\frac{E_{AC}}{E_{PCC}}\frac{h_{AC}^2}{2} + h_{PCC}\left(h_{AC} + \frac{h_{PCC}}{2}\right)}{\frac{E_{AC}}{E_{PCC}}h_{AC} + h_{PCC}} \tag{A.75}$$

$$\zeta_{Base} = z - \left(h_{AC} + h_{PCC} - x_{AP} + \frac{h_{Base}}{2}\right) \tag{A.76}$$

The thickness and the unit weight of an equivalent slab with Young's modulus E_{PCC} and coefficient of thermal expansion α_{PCC}, are given as:

$$h_{eff} = \sqrt[3]{\frac{E_{AC}}{E_{PCC}}h_{AC}^3 + h_{PCC}^3 + 12\left[\begin{array}{l}\frac{E_{AC}}{E_{PCC}}h_{AC}\left(x_{AP} - \frac{h_{AC}}{2}\right)^2 \\ + h_{PCC}\left(h_{AC} + \frac{h_{PCC}}{2} - x_{AP}\right)^2\end{array}\right] + \frac{E_{Base}}{E_{PCC}}h_{Base}^3} \tag{A.77}$$

$$\gamma_{eff} = \frac{h_{AC}\gamma_{AC} + h_{PCC}\gamma_{PCC}}{h_{eff}} \tag{A.78}$$

Using equation (A.1), the constant strain-causing temperature components in the AC, PCC, and base layers are given as:

$$T_{c,AC}(z) = T_o + \frac{1}{\alpha_{AC}} \frac{\int_{-x_{AP}}^{h_{AC}-x_{AP}} \alpha_{AC}E_{AC}\left[T(z) - T_{oAC}\right]dz + \int_{h_{AC}-x_{AP}}^{h_{AC}+h_{PCC}-x_{AP}} \alpha_{PCC}E_{PCC}\left[T(z) - T_o\right]dz}{E_{AC}h_{AC} + E_{PCC}h_{PCC}} \tag{A.79}$$

$$T_{c,PCC}(z) = T_o + \frac{1}{\alpha_{PCC}} \frac{\int_{-x_{AP}}^{h_{AC}-x_{AP}} \alpha_{AC}E_{AC}\left[T(z) - T_{oAC}\right]dz + \int_{h_{AC}-x_{AP}}^{h_{AC}+h_{PCC}-x_{AP}} \alpha_{PCC}E_{PCC}\left[T(z) - T_o\right]dz}{E_{AC}h_{AC} + E_{PCC}h_{PCC}} \tag{A.80}$$

$$T_{c,Base} = T_o + \frac{\int_{\frac{-h_{Base}}{2}}^{\frac{h_{Base}}{2}} \alpha_{Base} E_{Base} \left[T(\zeta_{Base}) - T_{oBase} \right] d\zeta_{Base}}{\alpha_{Base} \int_{\frac{-h_{Base}}{2}}^{\frac{h_{Base}}{2}} E_{Base} d\zeta_{Base}} = \frac{1}{h_{Base}} \int_{\frac{-h_{Base}}{2}}^{\frac{h_{Base}}{2}} T(\zeta_{Base}) d\zeta_{Base} \quad \text{(A.81)}$$

Equations (A.79) to (A.81) can be approximated numerically as follows:

$$T_{c,PCC}(z) - T_o = \frac{\frac{\alpha_{AC} E_{AC}}{\alpha_{PCC}} \left(\frac{h_{AC}}{8} \left(T_{AC1} + 2 * \sum_{i=2}^{4} T_{ACi} + T_{AC5} \right) - T_{oAC} h_{AC} \right) + E_{PCC} \left(\frac{h_{PCC}}{20} \left(T_1 + 2 * \sum_{i=2}^{10} T_i + T_{11} \right) - T_o h_{PCC} \right)}{E_{AC} h_{AC} + E_{PCC} h_{PCC}} \quad \text{(A.82)}$$

$$T_{c,AC}(z) - T_o = (T_{c,PCC}(z) - T_o) * \frac{\alpha_{PCC}}{\alpha_{AC}} \quad \text{(A.83)}$$

$$T_{c,Base} - T_o = \frac{1}{2}(T_{1Base} + T_{2Base}) - T_o \quad \text{(A.84)}$$

Using equation (A.2), the linear strain-causing temperature components are given as:

$$T_L(z) = T_o + 12S \frac{z}{\alpha(z)} \quad \text{(A.85)}$$

$$T_{L,Base} = T_o + 12S \frac{\zeta_{Base}}{\alpha_{Base}} \quad \text{(A.86)}$$

where:

$$S = \frac{\begin{array}{l}\int_{-x_{AP}}^{h_{AC}-x_{AP}} \alpha_{AC} E_{AC}\left[T(z)-T_{oAC}\right]zdz + \int_{h_{AC}-x_{AP}}^{h_{AC}+h_{PCC}-x_{AP}} \alpha_{PCC} E_{PCC}\left[T(z)-T_{o}\right]zdz \\ + \int_{-\frac{h_{Base}}{2}}^{\frac{h_{Base}}{2}} \alpha_{Base} E_{Base}\left[T\left(\zeta_{Base}\right)-T_{o}\right]\zeta_{Base} d\zeta_{Base}\end{array}}{E_{AC}h_{AC}^{3} + E_{PCC}h_{PCC}^{3} + 12\left[\begin{array}{l}E_{AC}h_{AC}\left(x_{AP}-\frac{h_{AC}}{2}\right)^{2} \\ + E_{PCC}h_{PCC}\left(h_{AC}+\frac{h_{PCC}}{2}-x_{AP}\right)^{2}\end{array}\right] + E_{Base}h_{Base}^{3}} \tag{A.87}$$

Therefore, the linear temperature gradient in the equivalent slab can be written as:

$$\Delta T_{L,eff} = \frac{-12h_{eff}}{\alpha_{PCC}}\left(\frac{\begin{array}{l}\int_{-x_{AP}}^{h_{AC}-x_{AP}} \alpha_{AC} E_{AC}\left[T(z)-T_{oAC}\right]zdz + \int_{h_{AC}-x_{AP}}^{h_{AC}+h_{PCC}-x_{AP}} \alpha_{PCC} E_{PCC}\left[T(z)-T_{o}\right]zdz \\ + \int_{-\frac{h_{Base}}{2}}^{\frac{h_{Base}}{2}} \alpha_{Base} E_{Base}\left[T\left(\zeta_{Base}\right)-T_{o}\right]\zeta_{Base} d\zeta_{Base}\end{array}}{E_{PCC}h_{eff}^{3}}\right) \tag{A.88}$$

Equation (A.88) can be approximated numerically as follows:

$$\Delta T_{L,eff} = \frac{-12}{h_{eff}^2}\left(\begin{array}{l} \dfrac{\alpha_{AC}E_{AC}}{\alpha_{PCC}E_{PCC}}\dfrac{h_{AC}}{24}\displaystyle\sum_{i=1}^{4}\left(\begin{array}{l} T_i*\left((3i-2)*\dfrac{h_{AC}}{4}-3x_{AP}\right) \\ +T_{i+1}*\left((3i-1)*\dfrac{h_{AC}}{4}-3x_{AP}\right)\end{array}\right) \\ -\dfrac{\alpha_{AC}E_{AC}}{\alpha_{PCC}E_{PCC}}\dfrac{T_{oAC}}{2}h_{AC}\left(h_{AC}-2x_{AP}\right) \\ +\dfrac{h_{PCC}}{60}\displaystyle\sum_{i=1}^{10}\left(\begin{array}{l} T_i*\left((3i-2)*\dfrac{h_{PCC}}{10}-3(x_{AP}-h_{AC})\right) \\ +T_{i+1}*\left((3i-1)*\dfrac{h_{PCC}}{10}-3(x_{AP}-h_{AC})\right)\end{array}\right) \\ -\dfrac{T_{11}}{2}h_{PCC}\left(h_{PCC}+2h_{AC}-2x_{AP}\right)\end{array}\right) \tag{A.89}$$

Finally, the linear strain-causing temperature at the top and the bottom of all layers of the composite pavement can be written as:

$$T_{L,AC,top}-T_o=\frac{\Delta T_{L,eff}}{h_{eff}}(x_{AP})\frac{\alpha_{PCC}}{\alpha_{AC}} \tag{A.90}$$

$$T_{L,AC,bot}-T_o=\frac{\Delta T_{L,eff}}{h_{eff}}(x_{AP}-h_{AC})\frac{\alpha_{PCC}}{\alpha_{AC}} \tag{A.91}$$

$$T_{L,PCC,top}-T_o=\frac{\Delta T_{L,eff}}{h_{eff}}(x_{AP}-h_{AC}) \tag{A.92}$$

$$T_{L,PCC,bot}-T_o=\frac{-\Delta T_{L,eff}}{h_{eff}}(h_{PCC}+h_{AC}-x_{AP}) \tag{A.93}$$

$$T_{L,Base,top}-T_o=\frac{\Delta T_{L,eff}}{h_{eff}}\frac{h_{Base}}{2}\frac{\alpha_{PCC}}{\alpha_{Base}} \tag{A.94}$$

$$T_{L,Base,bot}-T_o=\frac{-\Delta T_{L,eff}}{h_{eff}}\frac{h_{Base}}{2}\frac{\alpha_{PCC}}{\alpha_{Base}} \tag{A.95}$$